

MANY-BODY EFFECTS

MANY-BODY EFFECTS IN THE ELECTRON GAS
AND POSITRON ANNIHILATION

By

BRIAN BERTRAND JOHN HEDE, B.SC.

A Thesis

Submitted to the School of Graduate Studies
in Partial Fulfilment of the Requirements

for the Degree

Doctor of Philosophy

McMaster University

November 1972

DOCTOR OF PHILOSOPHY (1972)
(Physics)

McMASTER UNIVERSITY
Hamilton, Ontario.

TITLE: Many-Body Effects in the Electron Gas and
Positron Annihilation

AUTHOR: Brian Bertrand John Hede
B.Sc. (McMaster University)

SUPERVISOR: Professor J. P. Carbotte

NUMBER OF PAGES: vi, 150

SCOPE AND CONTENTS:

A number of questions are examined concerning many-body correlations in connection with the electron gas at metallic densities ($2 \lesssim r_s \lesssim 5.7$) and the annihilation of a positron in simple metals, by means of a technique involving the two-particle correlation Green's function. Estimates are made of low temperature contributions to angular correlation data, which describe the momentum distribution of annihilating electron-positron pairs, in the form of smearing at the sharp cutoff corresponding to the Fermi momentum from electron- and positron-phonon interactions, and in the form of broad tails beyond the cutoff resulting from the high-momentum components introduced into the electron wave function by the presence of a periodic crystal lattice.

Phonon effects are introduced into the perturbation expansion of the two-particle Green's function describing an electron-positron pair. A calculation of the lowest-order

phonon contribution seems to indicate that such effects do not explain the smearing at the Fermi momentum.

A Green's function calculation of the first-order enhancement of the lattice tails, due to the positron-electron correlation, is made by introducing particle-lattice interactions explicitly in a model based on a simple metal such as sodium. It considers a weak potential and treats as zero the lattice components corresponding to other than nearest-neighbours points in reciprocal lattice space. The enhancement for $r_s=4$, which is almost a constant, is very similar to that for the main part of angular correlation data. This indicates that, for simple metals at least, angular correlation data can be interpreted directly from a free-particle model.

Short-range correlations among opposite-spin electrons are examined by field-theoretic techniques as a step to obtaining a fundamental understanding of the correlations among electrons at metallic densities. A calculation of the p.d.f. for opposite-spin electrons is positive over a wide range of metallic densities and seems to account for short-range correlations of the Coulomb hole through the multiple scattering of particle-particle ladders.

ACKNOWLEDGEMENTS

I wish to thank my supervisor, Dr. J. P. Carbotte for the many beneficial discussions we shared, both with regard to the work which led to this thesis and in the broader frame of physics. His valuable suggestions and constant encouragement were gratefully received.

I wish to thank Dr. Paul Truant for his advice and innumerable conversations, and all my fellow students for sharing in my experience.

I gratefully acknowledge the support of the National Research Council of Canada for four years and thank the Theoretical Physics Group of McMaster University for their support during the final months in which this thesis was prepared.

I wish to express my appreciation to Miss Erie Long for her patience in typing this thesis.

Finally, I wish to thank my wife Myrna for her understanding and encouragement, which were most valuable of all.

TABLE OF CONTENTS

	<u>Page</u>
CHAPTER I: INTRODUCTION	
1.1 Historical Introduction	1
1.2 Scope of Thesis	8
CHAPTER II: PHONON EFFECTS IN POSITRON ANNIHILATION	
2.1 Theory of Positron Annihilation	12
2.2 Positron Motion	20
2.3 Electron-Phonon and Positron-Phonon Interactions	29
2.4 First-Order Phonon Smearing	37
2.5 Calculation of Various Contributions to $R(\underline{p})$	41
2.6 Discussion of Calculations	53
CHAPTER III: LATTICE TAILS IN POSITRON ANNIHILATION	
3.1 Lattice Effects in Positron Annihilation	55
3.2 Bloch States in Annihilation Rates	57
3.3 Enhancement of Lattice Tails From First-Order Ladders	65
3.4 Calculation of Enhancements	78

	<u>Page</u>
CHAPTER IV: SPIN UP SPIN DOWN PAIR DISTRIBUTION FUNCTION AT METALLIC DENSITIES	
4.1 Short-Range Correlations	87
4.2 Ladder Contributions to the Pair Distribution Function	93
4.3 Particle-Hole Scattering	103
4.4 Calculation of Pair Distribution Function	107
CHAPTER V: CONCLUSIONS	
5.1 Phonon Smearing of Angular Correlation Data	115
5.2 Enhancement of Lattice Tails in $R(p)$ for Simple Metals	118
5.3 Correlations in an Electron Gas	122
APPENDIX A: POSITRON-PHONON MATRIX ELEMENT	125
APPENDIX B: FIRST-ORDER LADDER ANNIHILATION RATE	131
APPENDIX C: PROPAGATOR EQUATIONS	135
APPENDIX D: BETHE-GOLDSTONE EQUATION	142
REFERENCES	146

CHAPTER I

INTRODUCTION

1.1 Historical Introduction

The many-body problem presented by a solid has found its solution in a variety of model approximations. One widely-employed technique has been to regard the system as a collection of interacting ions and electrons and to make further simplifying assumptions within that framework. Many of the properties of metals, for example, have been understood in terms of the free electron theory of Sommerfeld ⁽¹⁾. In this model, it was assumed that one could neglect the strong interactions among electrons and between electrons and ions. The Hartree-Fock ⁽²⁾ approximation replaced free particles by quasiparticles. It handled the interactions between electrons in an average way and, by taking account of the Pauli exclusion principle, led to the concept of an electron moving with an accompanying exchange hole. The exchange nature of the quasiparticle went part of the way towards explaining the binding of alkali metals ⁽³⁾.

Various attempts to account for Coulomb correlations through a second-order perturbation-theoretic calculation led to a divergent result related to the long range of the interaction. In the 1930's Wigner ⁽⁴⁾ proposed a solution based

on an interpolation between high- and low-density calculations of the energy. Then, in the early 1950's, Bohm and Pines^(5,6) developed a collective description of the electron gas as a quantum plasma which exhibited collective behaviour in the form of screening and long-wavelength oscillations or plasmons. Within the Bohm-Pines theory, the random phase approximation provided a nontrivial model of the interacting electron system. From RPA, also described in terms of dielectric response theory, it was possible to calculate various properties of the electron gas at high densities ($r_s \ll 1$)⁽³⁾ such as the ground state energy, plasmon effects and a more suitable quasiparticle picture. In 1957 the perturbation-theoretic approach was finally applied successfully by Gell-Mann and Brueckner⁽⁷⁾ who summed entire sets of divergent terms using the Feynman⁽⁸⁾ propagator method to obtain finite sums. Their result for the ground state energy confirmed the RPA calculation for high densities.

Nonetheless, RPA failed to give a proper description of the electron gas in the metallic density range ($2 \lesssim r_s \lesssim 5.7$)^(9,10) where interactions become important. In particular, the approximation ignored exchange in its treatment of correlations so that short-range effects were inadequately described. This large momentum difficulty was pointed out by Nozieres and Pines⁽¹¹⁾ and Hubbard⁽¹²⁾ who, in 1957, proposed alternative solutions to the problem.

Hubbard introduced a particular infinite set of exchange diagrams which he approximated. This led to a modified expression for the dielectric screening function which was equivalent to RPA for small momenta but which had the effect of cutting in half the contribution to the correlation energy from large momenta. A number of modifications of Hubbard's approximation have since been suggested by Heine and Falicov (13), Rice (14), Geldart and Vosko (15) and Geldart (16) which maintain the essential momentum dependence of the average potential used by Hubbard but adjust a parameter to satisfy some additional constraint.

In a series of publications (17-20) Singwi et al. introduced and refined a theory which improved upon the short-range aspect of Hubbard's approximation by accounting for the local-field correction associated with the Coulomb hole. They included the short-range correlations specifically, in an approximate way, by making the dielectric function a functional of the Fourier transform of the pair distribution function (p.d.f.) $g(r)$ which describes the probability that there is a particle at position r if there is one at the origin. Their approach was a semi-classical one, based on an ansatz relating the two-particle distribution function to the one-particle distribution function and the p.d.f. The effective field felt by a particle then involved a local part through the p.d.f. which was contained in the dielectric function. There resulted a set of equations involving $\epsilon(q, \omega)$

and $S(q)$, the Fourier transform of the p.d.f., which had to be solved self-consistently. This method led to a good description of the p.d.f. for small r and of the compressibility which is a long-wavelength phenomenon.

The annihilation of positrons in solids has become a major tool in the investigation of many-body effects in solids. The angular correlation technique first carried out by de Benedetti et al. ⁽²¹⁾ measured the momentum distribution of the photon pair resulting from the annihilation of a positron with an electron.

Lee-Whiting ⁽²²⁾ suggested that a high-energy positron incident on an electron gas quickly lost its energy to the electron system by the creation of electron-hole pairs and was thermalized at the time of annihilation; that is, at zero temperature it was in the lowest energy state possible and at finite temperature it was in thermal equilibrium with the electron gas. At low temperatures, then, the momentum of the annihilating pair could be assigned to the electron. In the case of a metal, it was argued by de Benedetti ⁽²¹⁾ and Ferrell ⁽²³⁾ that a thermalized positron would be excluded from the cores so that annihilation would occur only with the valence electrons. Indeed, extensive measurements of angular correlations by Stewart ⁽²⁴⁾, for example, agreed with a free-electron distribution, which took the form of a parabola with a sharp cutoff at an angle corresponding to the Fermi momentum.

The aforementioned arguments provided the basis for the analysis of positron annihilation experiments but they failed to account for a number of characteristic features of angular correlation data such as the broad tails, the smearing in the vicinity of the Fermi momentum and the large total annihilation rates. Ferrell ⁽²³⁾ showed that a consideration of the screened Coulomb interaction between a positron and an electron would enhance the electron density at the positron by an order of magnitude. Detailed calculations by Kahana ⁽²⁵⁾ and Carbotte and Kahana ⁽²⁶⁾ by means of a zero-temperature Green's function technique ^(27,28) which took into account the Pauli exclusion principle and positron-electron correlations led to an enhancement factor that was reasonably constant across the Fermi sea. The parabolic shape of Sommerfeld theory was left largely unchanged, but the corresponding increase in the total annihilation rate was more in line with experimental results ^(29,30).

The independent work of Daniel ⁽³¹⁾ and Berko and Plaskett ⁽³²⁾ on the positron wave function provided evidence that the major part of the broad experimental tails was due to annihilation of the positron with core electrons. Estimates have since been made of annihilation with core electrons, which included enhancement effects, by Carbotte and Salvadori ⁽³³⁾. More recently considerable attention has been given to a determination of the positron wave function in order to study core contributions ⁽³⁴⁾, as well as

anisotropies in angular correlation data ⁽³⁵⁾ and defects in metals ⁽³⁶⁾.

Part of the angular correlation tails has also been shown to come from high momentum components introduced into the conduction electron wave function by the periodic lattice. Most estimates ^(32,37,38) have neglected Coulomb correlations, which are necessary for a quantitative measure of this effect.

Angular correlation data has also been characterized by smearing at the Fermi cutoff. Measurements over a wide range of temperatures ^(39,40) showed that this smearing increased with temperature, an indication of increased positron motion. Now, Carbotte and Arora ⁽⁴¹⁾ pointed out that positrons were not always thermalized when they annihilated. This fact was borne out by Kim et al. ⁽⁴⁰⁾ who fitted angular correlation data with calculated curves based on a free-particle Boltzmann distribution for the positron into which was introduced a parameter T_{eff} , the effective positron temperature. At high temperatures, the effective temperature was linear with the sample temperature, suggesting thermalization. At lower temperatures, however, T_{eff} was larger than expected for a thermalized positron and had a non-zero value at $T=0$.

It can be seen that, since the positron perturbs the many-body system of a metal and obscures much of the information about the electrons, it is necessary to

understand the details of the problem. Certainly, there is also much valuable information such as the Fermi surface of a metal or alloy that is readily accessible in terms of even the simplest approximations (32).

1.2 Scope of Thesis

The work of this thesis falls into three separate parts. The first two parts, in Chapters II and III, deal with problems related to positron annihilation in simple metals. The third part, in Chapter IV, examines correlations in the electron gas at metallic densities.

Woll and Carbotte ⁽⁴²⁾ described the energy loss of a positron through interactions with the electron gas. Their estimate for the minimum ($T=0$) average positron energy was appreciably lower than interpretation of experimental evidence for metals ⁽⁴⁰⁾ would indicate. It seems that part of the smearing could represent an effect not described by that theory. For annihilation in a metal there is an additional feature to be considered, the presence of a system of vibrating ions. It has been pointed out ^(43,44) that positron-phonon correlations provide an additional mechanism for thermalization of the positron. However, phonons can also lead to smearing at the Fermi cutoff.

The positron annihilation rate can be related to the electron-positron Green's function G_{ep} , which describes the propagation of an electron-positron pair in the medium. G_{ep} has a perturbation expansion in terms of free-particle propagators described by Feynman diagrams, which can be extended

to include phonon effects through additional diagrams involving positron (electron)-phonon correlations. The smearing from the lowest-order diagrams is calculated in Chapter II.

A periodic lattice potential has the effect of destroying the simple picture, valid for an electron gas, of free electrons in plane wave states by introducing higher momentum components into the conduction electron wave function. This leads to tails in the angular correlation data. There have been a number of estimates of this effect based on an independent-particle model (32,37,38). The purpose of Chapter III is to calculate the enhancement of the lattice tails due to first-order positron-electron correlations for a model based on sodium. It involves an additional set of diagrams in the perturbation expansion which account for the lattice explicitly through electron-ion interaction lines.

The third part of the thesis examines correlations between opposite-spin electrons in an electron gas at metallic densities from a perturbation-theoretic approach. Various approximations based on such an approach have the problem of a negative value for the p.d.f. at small r (16). The difficulty is that they all assume a weak interaction and use the Born approximation in estimating Coulomb correlations, while at small r even a screened potential is large. A solution for opposite-spin electrons, which suggests itself from the analysis of positron annihilation (25) and from a

calculation by Carbotte ⁽⁴⁵⁾ of the charge environment of a light negative charge in an electron gas, is to sum the complete set of ladder diagrams in the perturbation expansion of the particle-particle Green's function G_{ee} . This quantity is simply related to the spin-up-spin-down p.d.f.

$g_{\uparrow\downarrow}(r)$.

In section 2.1 of Chapter II the positron partial annihilation rate is related to the positron-electron Green's function and the perturbation expansion for G_{ep} is discussed. In section 2.2 the motion of a positron in an electronic medium is described. Phonons are introduced and it is shown how they modify the thermalization rate, the momentum distribution and the perturbation expansion. In section 2.3 the electron-phonon and positron-phonon coupling constants are derived. In sections 2.4 and 2.5 the contribution to the smearing from three first-order phonon diagrams in the perturbation expansion is calculated. The experimental smearing is also recalculated from the experimental value for T_{eff} . A discussion of the results of the calculations is given in section 2.6.

In section 3.1 of Chapter III reference is made to previous work on lattice effects. Section 3.2 describes how the lattice can be included in the perturbation expansion for G_{ep} by introducing Bloch functions into the free-particle Green's functions and derives the contribution to $R(p)$ from the zeroth- and first-order ladders. An alternate derivation

in section 3.3 takes explicit account of the electron-ion interaction V_e by introducing an additional infinite set of diagrams. In section 3.4 a first-order enhancement factor is calculated and discussed.

Section 4.1 of Chapter IV relates the p.d.f. to the two-electron Green's function. In section 4.2 the RPA spin-up-spin-down p.d.f. $g_{\uparrow\downarrow}(r)$ is derived and the contribution $g_{\uparrow\downarrow}^{L2}(r)$ of the remaining ladder graphs is formulated in terms of a Bethe-Goldstone function ⁽⁴⁶⁾. Particle-hole contributions to this function are discussed in section 4.3. In section 4.4 the Bethe-Goldstone function and $g_{\uparrow\downarrow}^{L2}(r)$ are calculated by making an angle-averaged approximation and the resulting $g_{\uparrow\downarrow}(r)$ is compared with Singwi et al. ⁽²⁰⁾.

In section 5.1 of Chapter V conclusions are drawn about phonon smearing. In section 5.2 conclusions are drawn concerning enhancement of lattice annihilation rates. Conclusions about correlations in the electron gas are offered in section 5.3.

In Appendix A the positron-phonon matrix element is calculated. In Appendix B the first-order ladder contribution to $R(\underline{p})$ is derived in terms of electron Bloch states. A formulation of the equation for a Green's function propagator is given in Appendix C, which accounts for the lattice through electron-ion interaction lines. In Appendix D an equation for the angle-average of the Bethe-Goldstone function is derived.

CHAPTER II

PHONON EFFECTS IN POSITRON ANNIHILATION

2.1 Theory of Positron Annihilation

The partial annihilation rate of a low-energy positron in an electron gas has been shown by Ferrell (23) to be given by the expression

$$R(\underline{p}) \propto \int d^3 \underline{x} d^3 \underline{y} e^{-i\underline{p} \cdot (\underline{x} - \underline{y})} \langle \phi^\dagger(\underline{y}) \phi(\underline{x}) \psi^\dagger(\underline{y}) \psi(\underline{x}) \rangle, \quad (2.1)$$

where $\psi(\underline{x})$ and $\phi(\underline{x})$ are the electron and positron field operators, respectively, and the expectation value is taken in the fully-interacting ground state for the initial system of electrons and positron. In terms of the zero-temperature electron-positron Green's function defined as

$$G_{ep}(\underline{x}, \underline{y}; \underline{x}', \underline{y}') = i^2 \langle T(\psi(\underline{x}) \phi(\underline{y}) \phi^\dagger(\underline{y}') \psi^\dagger(\underline{x}')) \rangle, \quad (2.2)$$

where T is the Wick (47) time-ordering operator, the partial annihilation rate can be written (23) as

$$R(\underline{p}) = \frac{\lambda}{\Omega} (-i)^2 \int d^3 \underline{x} d^3 \underline{y} e^{-i\underline{p} \cdot (\underline{x} - \underline{y})} G_{ep}(\underline{x}t, \underline{x}t; \underline{y}t^+, \underline{y}t^+). \quad (2.3)$$

The constant λ is given by the spin-averaged positronium annihilation rate λ_0 divided by the electron density, n_0 , at the positron in singlet positronium. It can be seen from equation (2.1) that the total annihilation rate is proportional to the electron density at the positron, averaged over all positron positions.

The Hamiltonian for the system of electrons and positron in the Heisenberg picture is

$$\begin{aligned}
 H = & \int d^3\underset{\sim}{x} \psi^\dagger(\underset{\sim}{x}) (-\nabla^2) \psi(\underset{\sim}{x}) + \int d^3\underset{\sim}{x} \phi^\dagger(\underset{\sim}{x}) (-\nabla^2) \phi(\underset{\sim}{x}) \\
 & + \frac{1}{2} \int d^3\underset{\sim}{x} d^3\underset{\sim}{x}' \psi^\dagger(\underset{\sim}{x}') \psi^\dagger(\underset{\sim}{x}) v(\underset{\sim}{x}; \underset{\sim}{x}') \psi(\underset{\sim}{x}) \psi(\underset{\sim}{x}') \\
 & + \frac{1}{2} \int d^3\underset{\sim}{x} d^3\underset{\sim}{x}' \phi^\dagger(\underset{\sim}{x}') \phi^\dagger(\underset{\sim}{x}) v(\underset{\sim}{x}; \underset{\sim}{x}') \phi(\underset{\sim}{x}) \phi(\underset{\sim}{x}') \\
 & - \int d^3\underset{\sim}{x} d^3\underset{\sim}{x}' \psi^\dagger(\underset{\sim}{x}') \phi^\dagger(\underset{\sim}{x}) v(\underset{\sim}{x}; \underset{\sim}{x}') \phi(\underset{\sim}{x}) \psi(\underset{\sim}{x}') \quad , \quad (2.4)
 \end{aligned}$$

where $v(\underset{\sim}{x}; \underset{\sim}{x}')$ is the Coulomb potential. In order to set up the perturbation series for a propagator, one derives the equation of motion for the propagator and then solves this equation by making a perturbation expansion in powers of the potential. Such a formulation has been carried out by Carbotte ⁽³⁷⁾, for example, and a similar derivation is presented in Appendix C. The latter involves the additional complication of a periodic crystal lattice but is otherwise the same.

The electron-positron Green's function G_{ep} satisfies the equation

$$\begin{aligned}
 G_{ep}(x_1, x_2; x'_1, x'_2) &= G_e^0(x_1; x'_1) G_p(x_2; x'_2) \\
 &\quad - i \int d^4 z d^4 z' v(z; z') G_e^0(x_1; z) \\
 &\quad \times [G_{eep}(\tilde{z}' t_z, z, x_2; \tilde{z}' t_z^+, x'_1, x'_2) \\
 &\quad - G_{pep}(\tilde{z}' t_z, z, x_2; \tilde{z}' t_z^+, x'_1, x'_2)] .
 \end{aligned}
 \tag{2.5}$$

The positron Green's function G_p and the three-particle Green's functions G_{eep} and G_{pep} satisfy similar equations; in fact, the general n -particle Green's function $G_{p_1 p_2 \dots p_n}$, where the subscript p_i can be either "e" or "p", satisfies an integral equation relating it to $(n-1)$ - and $(n+1)$ -particle Green's functions.

If interactions are neglected, G_{ep} reduces to

$$G_{ep}(x_1, x_2; x'_1, x'_2) = G_e^0(x_1; x'_1) G_p^0(x_2; x'_2) , \tag{2.6}$$

where G_e^0 and G_p^0 represent electron and positron free-particle propagators, respectively, which can be expanded in terms of plane waves as

$$\begin{pmatrix} G_e^0(x; x') \\ G_p^0(x; x') \end{pmatrix} = \frac{1}{\Omega} \sum_{\tilde{k}} e^{i\tilde{k} \cdot (\tilde{x} - \tilde{x}')} \int \frac{d\omega}{2\pi} e^{-i\omega(t-t')} \begin{pmatrix} G_e^0(\tilde{k}; \omega) \\ G_p^0(\tilde{k}; \omega) \end{pmatrix}, \quad (2.7)$$

where

$$G_e^0(\tilde{k}; \omega) = \frac{\theta(k - p_F)}{k^2 - \omega - i0^+} + \frac{\theta(p_F - k)}{k^2 - \omega + i0^+} \quad (2.8a)$$

and

$$G_p^0(\tilde{k}; \omega) = \frac{\theta(k)}{k^2 - \omega - i0^+} + \frac{\theta(-k)}{-\omega + i0^+}. \quad (2.8b)$$

With the expression (2.6) for G_{ep} , the annihilation rate reduces to the form

$$R(\tilde{p}) = \frac{\lambda}{\Omega} \sum_{\substack{\tilde{k} \\ k < p_F}} \delta_{\tilde{k}, \tilde{p}}. \quad (2.9)$$

In this approximation, then, the partial annihilation rate is proportional to the free-electron momentum distribution.

The quantity that is usually measured by the angular correlation technique is the number of photon pairs having a particular momentum p_z in some fixed (z-) direction; that is, to within a proportionality constant one measures

$$R(p_z) = \sum_{p_x p_y} R(\tilde{p}). \quad (2.10)$$

In the limit of infinite volume the annihilation rate described by equations (2.9) and (2.10) can be written as

$$\begin{aligned}
 R(p_z) &= 0 && \text{for } p_z > p_F \\
 &= \frac{\lambda \cdot 2\pi}{(2\pi)^3} (p_F^2 - p_z^2) && \text{for } p_z < p_F, \quad (2.11)
 \end{aligned}$$

which includes a factor of 2 to account for spin. The result of equation (2.11) is illustrated in figure (2.1) and is essentially the shape of experimental correlation data.

For a fully-interacting system the equation (2.5) for G_{ep} couples G_{ep} to Green's functions having fewer and greater numbers of particles which satisfy similar equations. The solution of the resultant infinite set of equations leads to a perturbation expansion for G_{ep} in terms of the potential $v(x;x')$ and the free-particle propagators G_e^0 and G_p^0 . Kahana (25) and Carbotte and Kahana (26) have shown that the major contribution to the annihilation rate comes from the infinite series of ladder diagrams of figure (2.2), represented by the equation

$$\begin{aligned}
 G_{ep}(x_1, x_2; x'_1, x'_2) &= G_e^0(x_1; x'_1) G_p^0(x_2; x'_2) \\
 &\quad - i \int d^4z d^4z' u(z; z') G_e^0(x_1; z) G_p^0(x_2; z') \\
 &\quad \times G_{ep}(z, z'; x'_1, x'_2), \quad (2.12)
 \end{aligned}$$

Figure 2.1 Sommerfeld positron partial annihilation rate as a function of the electron-positron momentum p_z in a fixed (z-) direction.

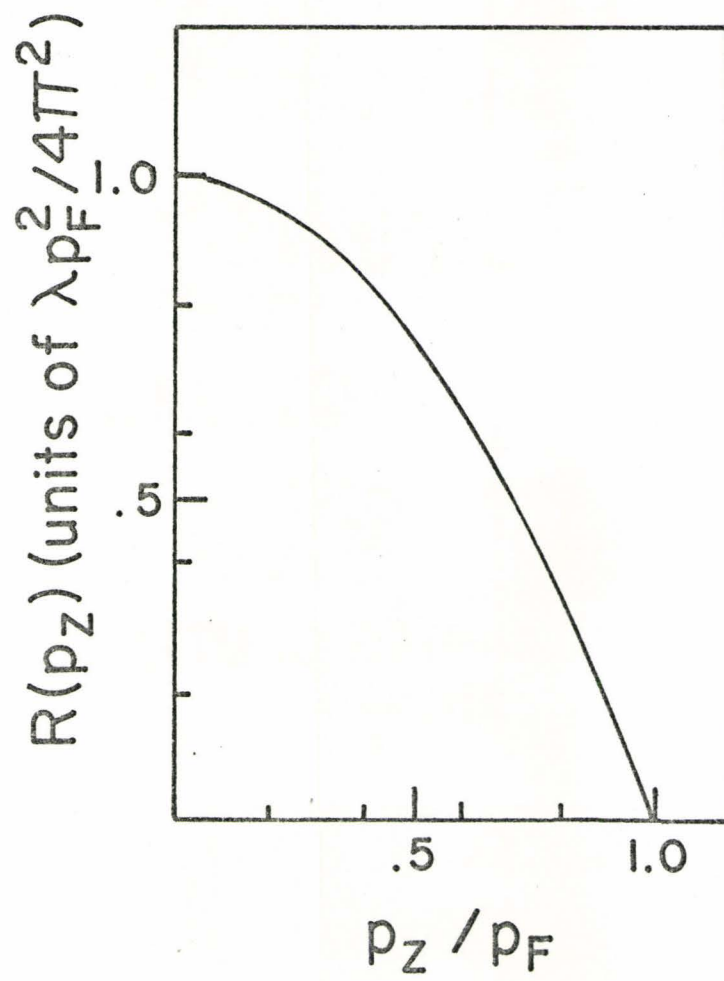
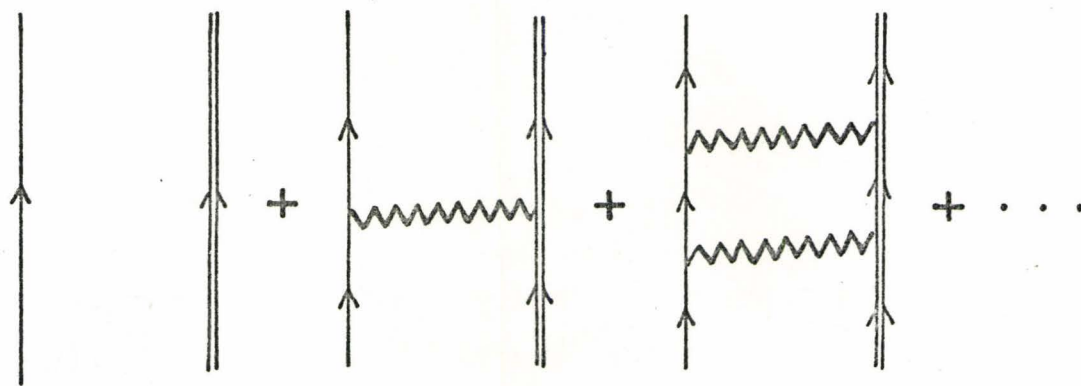


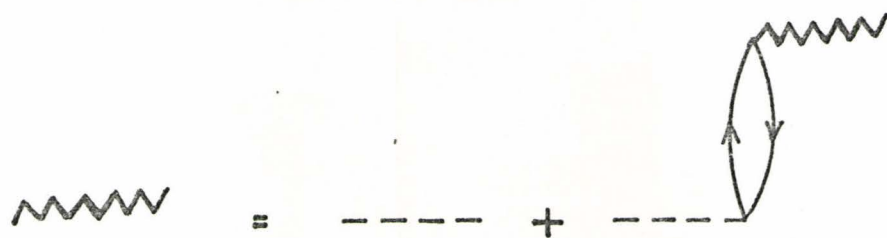
Figure 2.1

Figure 2.2

(a) Infinite set of ladder diagrams in the perturbation expansion for the electron-positron Green's function G_{ep} . The single lines represent the free-electron propagators G_e^0 and the double lines represent the free-positron propagators G_p^0 . The interaction line describes the static limit of the effective potential in the random phase approximation. (b) The effective potential in the random phase approximation.



(a)



(b)

Figure 2.2

where $u(z; z')$ represents an effective electron-positron potential, taken in the static limit, that takes into account the effect of the medium on the Coulomb interaction between an electron and a positron. The correlations lead to an enhancement of the partial annihilation rate (25,26) but do not modify appreciably the parabolic shape described by equation (2.11) and figure (2.1).

The interpretation of angular correlation data for metals in terms of the electron momentum distribution is obscured by a number of features. There are, for instance, broad tails superimposed on the "parabolic" shape. Carbotte and Kahana (26) have examined the tails introduced into the electron and positron momentum distributions by the inclusion of interactions with the medium and have found a strong cancellation between these self-energy contributions and ladder contributions. The experimental tails must come from the presence of the crystal lattice. The lattice, in fact, introduces tails through annihilation with core electrons. It also leads to higher momentum components in the conduction electron single-particle wave functions, which form the subject of Chapter III.

2.2 Positron Motion

Angular correlation data is characterized by smearing at the Fermi cutoff. Extensive measurements over a wide range of temperatures by Kim ⁽⁴⁰⁾ show that the smearing increases with the temperature of the sample. Thermal smearing can be readily estimated. The smearing of the electron momentum distribution, Δk , is described by

$$(k_F \pm \Delta k)^2 \approx E_F \pm k_B T \quad , \quad (2.13)$$

which gives

$$\frac{\Delta k}{k_F} \approx \frac{k_B T}{2E_F} \quad . \quad (2.14)$$

At room temperatures in sodium, for example, this is negligible. Thermal smearing due to positron motion is of the order k_+ , given by

$$k_+^2 \approx \frac{3}{2} k_B T \quad , \quad (2.15)$$

which, in the same system, yields

$$\frac{k_+}{k_F} \approx \left(\frac{3k_B T}{2E_F} \right)^{1/2} \approx .1 \quad . \quad (2.16)$$

This effect is observable.

A high-energy positron entering a metal loses its energy essentially by collisions with valence electrons. The first estimate of the energy loss by Lee-Whiting ⁽²²⁾ suggests that the positron is thermalized at the time of annihilation. Carbotte and Arora ⁽⁴¹⁾ have applied Green's function techniques in order to calculate the rate of energy loss in terms of the imaginary part of the positron self-energy operator $M(\underline{k};\omega)$ defined by the Dyson equation ^(48,49),

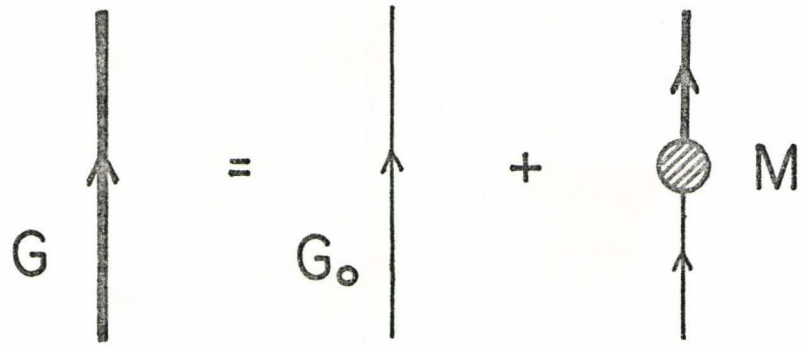
$$G_p(\underline{k};\omega) = G_p^0(\underline{k};\omega) + G_p^0(\underline{k};\omega)M(\underline{k};\omega)G_p(\underline{k};\omega) \quad , \quad (2.17)$$

illustrated in figure (2.3a). The calculation took into account the simple self-energy diagram of figure (2.3b), with the effective potential taken in both the random phase and Hubbard approximations. The results of Carbotte and Arora indicate that the positron is not always thermalized on annihilation. On the other hand, estimates by Perkins and Carbotte ⁽⁴³⁾ and Mikeska ⁽⁴⁴⁾ of an additional mechanism for energy loss, phonon excitation, indicate that it becomes significant at lower positron energies, resulting in a shortening of the thermalization time.

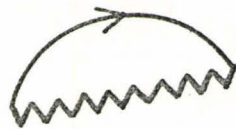
Experiments designed to examine positron motion have been carried out by Stewart ⁽³⁹⁾ and Kim ⁽⁴⁰⁾. Kim assumed a free-particle Boltzmann distribution for the positron in terms of a parameter T_{eff} , the effective positron

Figure 2.3

(a) Dyson equation for a positron (electron) Green's function propagator. The heavy lines represent true propagators, the light lines represent free-particle propagators and the shaded circle stands for the self-energy operator. (b) The lowest-order positron (electron) self-energy operator with the interaction given by an effective potential.



(a)



(b)

Figure 2.3

temperature, which he fit to experiments. This involved a comparison of the slope of the angular correlation data with calculated curves which were convolutions of an enhanced free-electron distribution, the optical resolution and the function

$$e^{-\hbar^2 k^2 / 2m k_B T_{\text{eff}}}$$

describing the positron motion. At high temperatures, the effective temperature was linear with the sample temperature, as shown in figure (2.4). This was taken to signify that the positron was thermalized, with a Boltzmann momentum distribution

$$e^{-\hbar^2 k^2 / 2m^* k_B T}$$

where m^* is the positron effective mass. The effective mass obtained in this way from the slope of the curve plotting effective temperature vs sample temperature was considerably larger than theoretical estimates of the effective mass (50,51). Mikeska (44) and Bergersen and Pajanne (52) have since argued that the positron-phonon interaction leads to an additional contribution to the momentum distribution. If the real distribution is replaced by a Boltzmann distribution, the Boltzmann distribution has an apparent effective mass greater than m^* , one which fits the experiments of

Figure 2.4 Variation of positron effective temperature with specimen temperature for positrons in Na (from Kim et al. (40)).

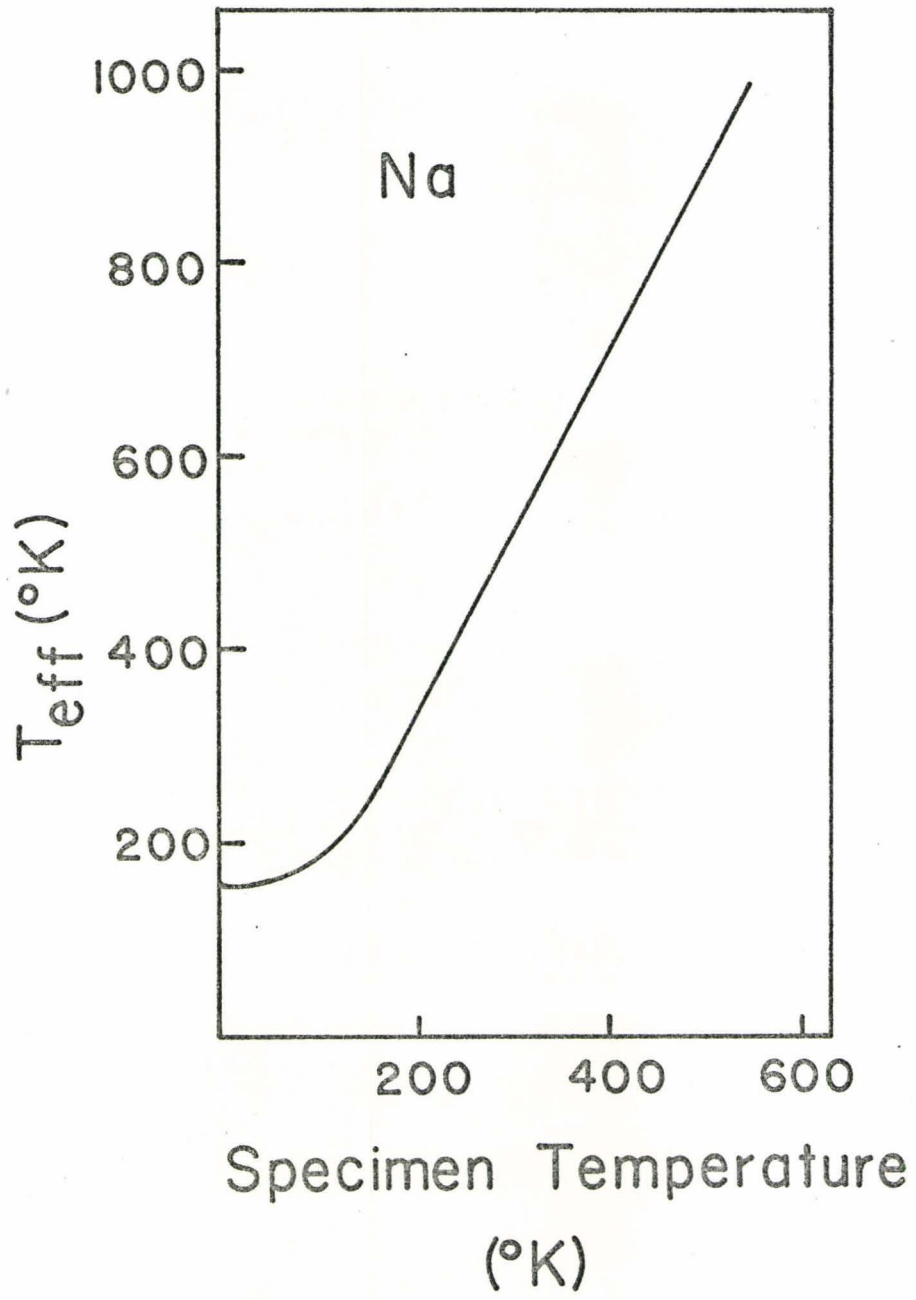


Figure 2.4

Kim (40) and Stewart and Shand (39,53) to within the experimental limits.

As the temperature of the sample was lowered, the effective temperature was no longer linear with the temperature. Thermalization was apparently incomplete, and at $T=0$ the positron still had some minimum non-zero energy on annihilation, which in sodium corresponded to 160°K motion. A theoretical calculation of the minimum T_{eff} from a Boltzmann equation approach by Woll and Carbotte (42) described the positron decay in terms of its screened Coulomb interactions with the electrons and yielded a considerably lower value. It would seem that part of the experimental smearing may represent a temperature-independent effect not described by the theory outlined thus far.

Smearing at the Fermi surface can result from positron (electron)-phonon effects. As in the case of thermal smearing of the electron momentum distribution, the smearing due to electron-phonon interactions is quite small. Written as Δk , it is given by

$$(k_F \pm \Delta k)^2 = E_F \pm \hbar\omega \quad , \quad (2.18)$$

so that for sodium

$$\frac{\Delta k}{k_F} \approx \frac{\hbar\omega}{2E_F} \approx .002 \quad . \quad (2.19)$$

The positron-phonon interaction, on the other hand, leads to smearing, say k_+ , given by

$$\frac{k_+}{k_F} \approx \left(\frac{\hbar\omega}{E_F}\right)^{1/2} \approx .1 \quad . \quad (2.20)$$

This is roughly the extent of the smearing that is of interest at $T=0$.

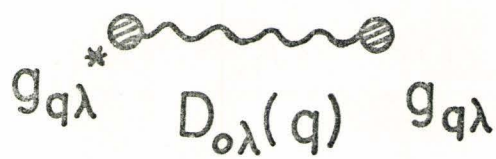
The perturbation expansion for the electron-positron Green's function propagator can be easily extended to include positron (electron)-phonon interactions, as shown, for example, by Schrieffer ⁽⁵⁴⁾. A new set of Feynman diagrams results from replacing Coulomb interaction lines by phonon propagators with positron (electron)-phonon coupling constants at the vertices. This is illustrated in figure (2.5). Carbotte and Kahana ⁽²⁶⁾ found a strong cancellation of tails from the lowest-order self-energy and ladder diagrams in the perturbation expansion for an electron gas. However, in the case of the lowest-order phonon diagrams of figure (2.6), such a cancellation is not expected since the extent of smearing is quite different. A more detailed analysis appears in the remaining sections of Chapter II, based on the results of a paper by Hede and Carbotte ⁽⁵⁵⁾.

Figure 2.5

(a) Coulomb potential. (b) Phonon propagator with positron (electron)-phonon coupling constants at the vertices. It can replace the element (a) in a perturbation diagram in G_{ep} for a system that includes phonons.

 $v(q)$

(a)



$g_{q\lambda}^*$ $D_{0\lambda}(q)$ $g_{q\lambda}$

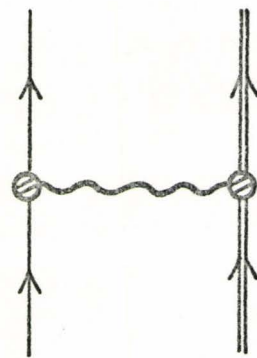
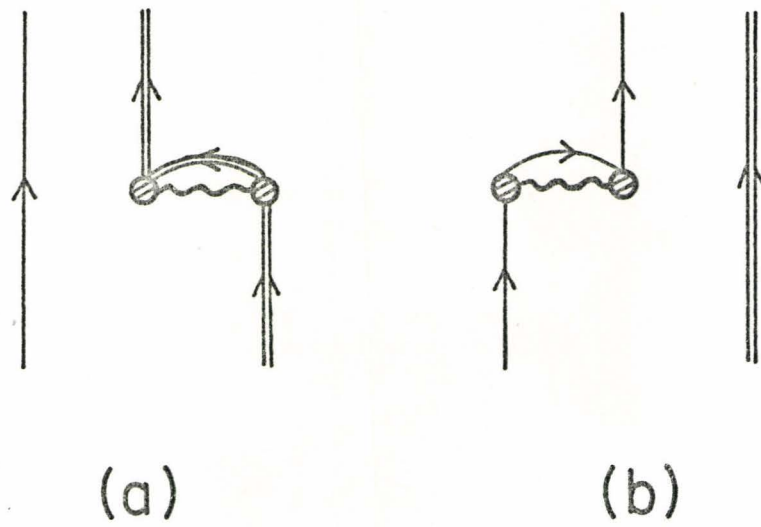
(b)

Figure 2.5

Figure 2.6

Lowest-order diagrams in the phonon

propagator in the perturbation expansion for G_{ep} . The single lines represent electron propagators, the double lines represent positron propagators, the wavy lines represent phonon propagators and the shaded circles represent positron (electron)-phonon coupling constants. (a) Positron self-energy diagram. (b) Electron self-energy diagram. (c) Ladder diagram.



(c)

Figure 2.6

2.3 Electron-Phonon and Positron-Phonon Interactions

In this section, the positron- and electron-phonon interactions are formulated. The rigid ion model ⁽⁵⁶⁾ is assumed and the potential seen by a positron (electron) is written as a sum over ionic potentials as

$$\sum_{\ell} V(\underline{r} - \underline{R}_{\ell}) \quad , \quad (2.21)$$

where \underline{r} is the positron (electron) location and \underline{R}_{ℓ} is the position of the ℓ th ion. Expanding the potential about the ion equilibrium position \underline{R}_{ℓ}^0 , one has, to first order in the displacement $\underline{U}_{\ell} = \underline{R}_{\ell} - \underline{R}_{\ell}^0$,

$$\begin{aligned} V(\underline{r} - \underline{R}_{\ell}) &= V(\underline{r} - \underline{R}_{\ell}^0) + \sum_{\ell} \underline{U}_{\ell} \cdot \frac{\partial}{\partial \underline{R}_{\ell}} V(\underline{r} - \underline{R}_{\ell}) \Big|_{\underline{R}_{\ell} = \underline{R}_{\ell}^0} \\ &= V(\underline{r} - \underline{R}_{\ell}^0) - \underline{U}_{\ell} \cdot \nabla V(\underline{r} - \underline{R}_{\ell}^0) \quad . \end{aligned} \quad (2.22)$$

The first term leads to the crystal potential for a perfect lattice, while the second term leads to the positron (electron)-phonon interaction described by the Hamiltonian

$$H_{\text{pos(el)-ph}} = - \sum_{i\ell} \underline{U}_{\ell} \cdot \nabla V(\underline{r}_i - \underline{R}_{\ell}^0) \quad , \quad (2.23)$$

where the subscript i refers to the i th positron (electron).

In second-quantized notation this becomes

$$\begin{aligned}
 H_{\text{pos}(el)\text{-ph}} = & -\sum_{\underline{k}\underline{q}} \sum_{\sigma} \langle \underline{k}+\underline{q} | \sum_{\underline{l}} U_{\underline{l}} \cdot \nabla V(\underline{r}-\underline{R}_{\underline{l}}^0) | \underline{k} \rangle \\
 & \times c_{\underline{k}+\underline{q}\sigma}^{\dagger} c_{\underline{k}\sigma} .
 \end{aligned} \tag{2.24}$$

c^{\dagger} , c are the positron (electron) creation and annihilation operators and the complete set of states $|\underline{k}\rangle$ is taken to be the set of Bloch states defined by

$$|\underline{k}\rangle = \frac{1}{\sqrt{\Omega}} u_{\underline{k}}(\underline{r}) e^{i\underline{k}\cdot\underline{r}} , \tag{2.25}$$

where Ω is the crystal volume and $u_{\underline{k}}(\underline{r})$ has the periodicity of the perfect lattice.

$U_{\underline{l}}$ can be expanded in terms of the normal coordinates $Q(\underline{k},\lambda)$ as

$$U_{\underline{l}} = \frac{1}{\sqrt{MN}} \sum_{\underline{k}'} \sum_{\lambda} Q(\underline{k}',\lambda) \underline{\varepsilon}_{\lambda}(\underline{k}') e^{i\underline{k}'\cdot\underline{R}_{\underline{l}}^0} , \tag{2.26}$$

where the sum on \underline{k}' extends over the first Brillouin zone (FBZ). $\underline{\varepsilon}_{\lambda}(\underline{k}')$ is the polarization vector for a phonon of polarization λ and wavevector \underline{k}' , M is the ionic mass and N is the total number of ions. From the periodicity of the function $u_{\underline{k}}$ and the relationship

$$\frac{1}{N} \sum_{\ell} e^{i\mathbf{k} \cdot \mathbf{R}_{\ell}^0} = \sum_{\mathbf{g}} \delta_{\mathbf{k}, \mathbf{g}} \quad , \quad (2.27)$$

where \mathbf{g} is a reciprocal lattice vector, the positron (electron)-phonon Hamiltonian (2.24) can be seen to reduce to

$$H_{\text{pos(el)-ph}} = -\sqrt{\frac{N}{M}} \sum_{\mathbf{k}\mathbf{q}} \sum_{\sigma\lambda} Q(\mathbf{q}, \lambda) \underline{\underline{\epsilon}}_{\lambda}(\mathbf{q}) \cdot \langle \mathbf{k} + \mathbf{q} | \nabla V | \mathbf{k} \rangle \times c_{\mathbf{k} + \mathbf{q}\sigma}^{\dagger} c_{\mathbf{k}\sigma} \quad . \quad (2.28)$$

The \mathbf{q} -vector appearing in the normal coordinate Q and the polarization vector $\underline{\underline{\epsilon}}$ is the reduced value of \mathbf{q} , which is permissible since phonons are described in the first Brillouin zone. The Kronecker delta is non-zero for only one value of the reciprocal lattice vector \mathbf{g} , given by $\mathbf{k}' = \mathbf{q} + \mathbf{g}$, which reduces \mathbf{q} to the FBZ. If the normal coordinate is expressed in terms of phonon creation and annihilation operators $a_{\mathbf{q}\lambda}^{\dagger}$, $a_{\mathbf{q}\lambda}$ in the form

$$Q(\mathbf{k}, \lambda) = \frac{1}{\sqrt{\omega_{\lambda}(\mathbf{q})}} (a_{-\mathbf{q}\lambda}^{\dagger} + a_{\mathbf{q}\lambda}) \quad , \quad (2.29)$$

where $\omega_{\lambda}(\mathbf{q})$ is the frequency of a phonon of polarization λ and wavevector \mathbf{q} , equation (2.28) can finally be written in the form

$$H_{\text{pos (el)-ph}} = \sum_{\underline{k}\underline{q}} \sum_{\sigma\lambda} g_{\underline{k}+\underline{q},\underline{k},\lambda} c_{\underline{k}+\underline{q}\sigma}^{\dagger} c_{\underline{k}\sigma} (a_{-\underline{q}\lambda}^{\dagger} + a_{\underline{q}\lambda}) \quad (2.30)$$

$g_{\underline{k}+\underline{q},\underline{k},\lambda}$, called the positron (electron)-phonon coupling constant, is given by

$$g_{\underline{k}+\underline{q},\underline{k},\lambda} = -(\hbar N/2M\omega_{\lambda}(\underline{q}))^{1/2} \varepsilon_{\lambda}(\underline{q}) \cdot \langle \underline{k}+\underline{q} | \nabla V | \underline{k} \rangle \quad (2.31)$$

and can be seen to satisfy the condition

$$g_{\underline{k}+\underline{q},\underline{k},\lambda}^* = g_{\underline{k},\underline{k}+\underline{q},\lambda} \quad (2.32)$$

In the vicinity of an ion a valence electron experiences a strong Coulomb potential. It is also restricted by the Pauli principle to states that are orthogonal to the core states so that the wavefunction has rapid oscillations which are manifested as a large kinetic energy in the core region. The net effect of these various contributions to the valence electron energy is equivalent to a weak potential, called a pseudopotential, acting on the electron. It allows one to use perturbation theory and a plane wave basis for the electron wavefunction. In the medium of all the other conduction electrons this bare pseudopotential seen by an electron undergoes screening which can be described in terms of a dielectric function, by analogy with the screening of a bare charge in an electron gas.

The electron-phonon matrix element $M_e(\underline{q})$ is given in the plane wave approximation by

$$\begin{aligned} M_e(\underline{q}) &= - \langle \underline{k} + \underline{q} | \nabla V_e | \underline{k} \rangle \\ &= - \frac{i}{\Omega} \underline{q} \int e^{-i\underline{q} \cdot \underline{r}} V_e(\underline{r}) d^3 \underline{r} \\ &= \frac{-i}{N} \underline{q} V_e(\underline{q}) \quad , \end{aligned} \quad (2.33)$$

assuming the electron-ion potential $V_e(\underline{r})$ vanishes at large r .

The effective electron-ion interaction is represented here by a one-parameter model pseudopotential proposed by Ashcroft (57), which is zero out to a core radius R_c and is the Coulomb potential beyond R_c . The potential is screened and the parameter R_c is determined by a fit to experimental band gaps. The screened pseudopotential form factor takes the form

$$V_e(q) = - \frac{4\pi n e^2}{q^2} \cos qR_c / (1 + \frac{4\pi n e^2}{q^2} f(q)) \quad , \quad (2.34)$$

where $f(q)$, the static limit of the Lindhard (58) polarization part given by

$$f(q) = \left(\frac{1}{2} + \frac{4p_F^2 - q^2}{8p_F q} \ln \left| \frac{2p_F + q}{2p_F - q} \right| \right) / \frac{2}{3} E_F \quad (2.35)$$

describes screening in the random phase approximation. The screened electron-phonon coupling constant $\bar{g}_{\vec{k}+\vec{q},\vec{k},\lambda}^e$ shown in figure (2.7) can then be written as

$$\bar{g}_{\vec{k}+\vec{q},\vec{k},\lambda}^e = -i(\hbar/2MN\omega_\lambda(\vec{q}))^{1/2} \underline{\epsilon}_\lambda(\vec{q}) \cdot \vec{q} V_e(\vec{q}) \quad . \quad (2.36)$$

Evaluation of the positron-phonon matrix element is based on a self-consistent calculation of the electron-phonon matrix element by Bardeen (59). It explicitly accounts for the shift of conduction electrons due to the ion displacement and the resultant screening of the ions. A derivation of the positron-phonon matrix element $M_p(\vec{q})$ given in Appendix A yields a result similar to equations (2.33) and (2.34), namely

$$M_p(\vec{q}) = \frac{-i}{N} \vec{q} V_p(\vec{q}) \quad , \quad (2.37)$$

where $V_p(\vec{q})$ is given by

$$V_p(\vec{q}) = G(qr_0) \left(\frac{4\pi n e^2}{q^2} + E_0 - w(r_0) / \left(1 + \frac{4\pi n e^2}{q^2} f(q) \right) \right) , \quad (2.38)$$

with the function G defined as

$$G(x) = \frac{3}{x^3} (\sin x - x \cos x) \quad . \quad (2.39)$$

Figure 2.7 Positron (electron)-phonon coupling
constant with the interaction screened in the
random phase approximation.

$$\bar{g}_{q\lambda} = \text{●} + \text{●} \begin{array}{c} \nearrow \\ \text{---} \\ \searrow \end{array} \text{●}$$

$g_{q\lambda}$

Figure 2.7

r_0 in equation (2.38) is the radius of a Wigner-Seitz sphere about the ion, $w(r)$ is the effective positron-ion potential of equation (A.2) and E_0 is the energy of the $\underline{k}=0$ positron state. The screened positron-phonon coupling constant $\overline{g}_{\underline{k}+\underline{q},\underline{k},\lambda}^p$ then takes the form

$$\overline{g}_{\underline{k}+\underline{q},\underline{k},\lambda}^p = -i (\hbar/2MN\omega_\lambda(q))^{1/2} \underline{\epsilon}_\lambda(\underline{q}) \cdot \underline{q} V_p(q) \quad . \quad (2.40)$$

2.4 First-Order Phonon Smearing

If positron-electron correlations are ignored, the electron-positron Green's function G_{ep} can be written as the simple product of single-particle Green's functions

$$G_{ep}(x_1, x_2; x_1', x_2') = G_e(x_1; x_1') G_p(x_2; x_2') \quad . \quad (2.41)$$

The contribution to the positron annihilation rate of equation (2.3) from the uncorrelated product (2.41) has the form

$$R(\underline{p}) = \frac{\lambda}{\Omega} \sum_{\underline{k}} P_e(\underline{p}-\underline{k}) P_p(\underline{k}) \quad , \quad (2.42)$$

where $P_e(\underline{k})$ and $P_p(\underline{k})$ are, respectively, the electron and positron probability of occupation of a state $|\underline{k}\rangle$, given by

$$P_e(\underline{k}) = i \int \frac{d\Omega}{2\pi} G_e(\underline{k}; \omega) e^{i\omega 0^+} \quad (2.43a)$$

and

$$P_p(\underline{k}) = i \int \frac{d\Omega}{2\pi} G_p(\underline{k}; \omega) e^{i\omega 0^+} \quad . \quad (2.43b)$$

The first-order terms in the expansion of the product (2.42) represent the self-energy effects described by figures (2.6a) and (2.6b). For the positron self-energy diagram of figure (2.6a) one can write

$$P_e(\underline{p}-\underline{k}) = i \int \frac{d\omega}{2\pi} G_e^0(\underline{p}-\underline{k}; \omega) e^{i\omega 0^+} \quad (2.44a)$$

and

$$P_p(\underline{k}) = \sum_{\underline{q}} \sum_{\lambda} \int \frac{d\omega}{2\pi} \frac{d\varepsilon}{2\pi} [G_p^0(\underline{k}; \omega)]^2 G_p^0(\underline{k}-\underline{q}; \omega-\varepsilon) \\ \times D_{0\lambda}(\underline{q}; \varepsilon) (-i)^2 |\bar{g}_{\underline{k}, \underline{k}-\underline{q}, \lambda}^p|^2, \quad (2.44b)$$

where $D_{0\lambda}(\underline{q}; \varepsilon)$ is the phonon Green's function defined by

$$D_{0\lambda}(\underline{q}; \varepsilon) = \frac{2\omega_{\lambda}(\underline{q})}{\varepsilon^2 - \omega_{\lambda}^2(\underline{q}) + i0^+} \\ = \frac{1}{\varepsilon - \omega_{\lambda}(\underline{q}) + i0^+} - \frac{1}{\varepsilon + \omega_{\lambda}(\underline{q}) - i0^+}. \quad (2.45)$$

$P_e(\underline{p}-\underline{k})$ reduces by contour integration to $\theta(p_F - |\underline{p}-\underline{k}|)$. The ω - and ε -integrations in equation (2.44b) can also be performed by contour integration to give the contribution to $R(\underline{p})$,

$$R^{pse}(\underline{p}) = \frac{\lambda}{\Omega} \sum_{\underline{k}\underline{q}} \sum_{\lambda} \theta(p_F - |\underline{p}-\underline{k}|) |\bar{g}_{\underline{k}, \underline{k}-\underline{q}, \lambda}^p|^2 \\ \times \left[\frac{\theta(k)\theta(-|\underline{k}-\underline{q}|)}{(k^2 + \omega_{\lambda}(\underline{q}))^2} - \frac{\theta(-k)\theta(|\underline{k}-\underline{q}|)}{(|\underline{k}-\underline{q}|^2 + \omega_{\lambda}(\underline{q}))^2} \right]. \quad (2.46)$$

The sum over \underline{k} yields two terms. The second is negative and contributes only for $p < p_F$. It represents a decrease in the probability of finding a positron of momentum $\underline{k}=0$ as a result of interactions between the positron and phonons.

The first term is positive and contributes for arbitrary p . It represents the probability of finding a non-thermalized positron with momentum $k \neq 0$. The contribution for momentum p greater than p_F , written $R_{>}^{pse}(p)$, is then given by

$$R_{>}^{pse}(p) = \frac{\lambda}{\Omega} \sum_{\underline{q}} \sum_{\lambda} \frac{\theta(p-p_F) \theta(p_F - |\underline{p}-\underline{q}|) \theta(q)}{(q^2 + \omega_{\lambda}(q))^2} |\bar{g}_{\underline{q},0,\lambda}^p|^2. \quad (2.47)$$

For the electron self-energy diagram of figure (2.6b), $P_p(k)$ is simply

$$\begin{aligned} P_p(k) &= i \int \frac{d\omega}{2\pi} G_p^0(k; \omega) e^{i\omega 0^+} \\ &= \theta(-k) \quad , \end{aligned} \quad (2.48)$$

so that the contribution to $R(p)$ from this diagram reduces to

$$\begin{aligned} R^{ese}(p) &= \frac{\lambda}{\Omega} P_e(p) \\ &= \frac{\lambda}{\Omega} \sum_{\underline{q}} \sum_{\lambda} \int \frac{d\omega}{2\pi} \frac{d\varepsilon}{2\pi} [G_e^0(p; \omega)]^2 G_e^0(\underline{p}-\underline{q}; \omega-\varepsilon) \\ &\quad \times D_{0\lambda}(q; \varepsilon) (-i)^2 |\bar{g}_{\underline{p},\underline{p}-\underline{q},\lambda}^e|^2 \\ &= \sum_{\underline{q}} \sum_{\lambda} |\bar{g}_{\underline{p},\underline{p}-\underline{q},\lambda}^e|^2 \left[\frac{\theta(p-p_F) \theta(p_F - |\underline{p}-\underline{q}|)}{(p^2 - |\underline{p}-\underline{q}|^2 + \omega_{\lambda}(q))^2} \right. \\ &\quad \left. - \frac{\theta(p_F-p) \theta(|\underline{p}-\underline{q}| - p_F)}{(p^2 - |\underline{p}-\underline{q}|^2 - \omega_{\lambda}(q))^2} \right]. \end{aligned} \quad (2.49)$$

The contribution, $R_{>}^{\text{ese}}(\underline{p})$, for $p > p_F$ is given by

$$R_{>}^{\text{ese}}(\underline{p}) = \frac{\lambda}{\Omega} \sum_{\underline{q}} \sum_{\lambda} \frac{\theta(p-p_F) \theta(p_F - |\underline{p}-\underline{q}|) \theta(q) |\bar{g}_{\underline{p}, \underline{p}-\underline{q}, \lambda}^e|^2}{(p^2 - |\underline{p}-\underline{q}|^2 + \omega_{\lambda}(\underline{q}))^2}. \quad (2.50)$$

In addition to the two phonon self-energy diagrams discussed, there is another diagram of first order in the phonon propagator. This is the ladder diagram of figure (2.6c) in which the positron and electron scatter off one another by exchanging a phonon. Its contribution to the positron partial annihilation rate is given by

$$\begin{aligned} R_{>}^{\text{lad}}(\underline{p}) &= i \frac{\lambda}{\Omega} \sum_{\underline{k}, \underline{q}} \sum_{\lambda} \int \frac{d\omega}{2\pi} \frac{d\omega'}{2\pi} \frac{d\varepsilon}{2\pi} G_{\underline{p}}^0(\underline{k}; \omega) \\ &\times G_{\underline{p}}^0(\underline{k}-\underline{q}; \omega-\varepsilon) G_e^0(\underline{p}-\underline{k}; \omega') G_e^0(\underline{p}+\underline{q}-\underline{k}; \omega'+\varepsilon) \\ &\times D_{0\lambda}(\underline{q}; \varepsilon) (-i)^2 \bar{g}_{\underline{k}, \underline{k}-\underline{q}, \lambda}^p \bar{g}_{\underline{p}-\underline{k}, \underline{p}+\underline{q}-\underline{k}, \lambda}^e. \quad (2.51) \end{aligned}$$

On performing the angular integrations, one obtains the contribution for $p > p_F$, $R_{>}^{\text{lad}}(\underline{p})$, given by

$$\begin{aligned} R_{>}^{\text{lad}}(\underline{p}) &= \frac{\lambda}{\Omega} \sum_{\underline{q}} \sum_{\lambda} \frac{\theta(p-p_F) \theta(q)}{q^2 + \omega_{\lambda}(\underline{q})} \\ &\times \left[\frac{\theta(p_F - |\underline{p}-\underline{q}|) \bar{g}_{\underline{q}, 0, \lambda}^p \bar{g}_{\underline{p}-\underline{q}, \underline{p}, \lambda}^e}{p^2 - |\underline{p}-\underline{q}|^2 + \omega_{\lambda}(\underline{q})} \right. \\ &\left. + \frac{\theta(p_F - |\underline{p}+\underline{q}|) \bar{g}_{0, -\underline{q}, \lambda}^p \bar{g}_{\underline{p}, \underline{p}+\underline{q}, \lambda}^e}{p^2 - |\underline{p}+\underline{q}|^2 + \omega_{\lambda}(\underline{q})} \right]. \quad (2.52) \end{aligned}$$

2.5 Calculation of Various Contributions to $R(\underline{p})$

In order to calculate the quantities of equations (2.47), (2.50) and (2.52) it is necessary to go to the limit of infinite volume where it is possible to replace the sum over \underline{q} by an integration. The angular integration is complicated by the presence of the reduced wavevector \underline{q} in the phonon frequency $\omega_\lambda(\underline{q})$ and the polarization vector $\underline{\epsilon}_\lambda(\underline{q})$ which appear in the coupling constants. The integrand then contains quantities which involve the angle between \underline{q} and \underline{g} , as well as the angle between \underline{q} and \underline{p} . Furthermore, for \underline{q} outside the FBZ both longitudinal and transverse phonon modes contribute to scattering of positrons and electrons.

Reciprocal lattice space is illustrated in figure (2.8). For \underline{p} near the Fermi surface, \underline{q} can have a magnitude extending out to about $2p_F$ which, in terms of the lattice constant a , is given by $1.24 \times 2\pi/a$. The region of \underline{q} -values contributing to umklapp processes is of the same order of magnitude as for normal processes. However, it is important to notice that \underline{q} does not extend as far as a reciprocal lattice point, which means that the frequency denominator $\omega_\lambda(\underline{q})$ is never small for \underline{q} outside the FBZ. On the other hand, frequencies become small in the region of small \underline{q} . Certainly, umklapp processes do not contribute disproportionately to the quantities expressed by equations (2.47), (2.50)

Figure 2.8 x-y plane in fcc reciprocal lattice
space showing the FBZ and a sphere at $2p_F$. \underline{q}'
is a vector in the FBZ. \underline{q} is a vector outside
the FBZ which reduces to the FBZ as \underline{q}_{red} .

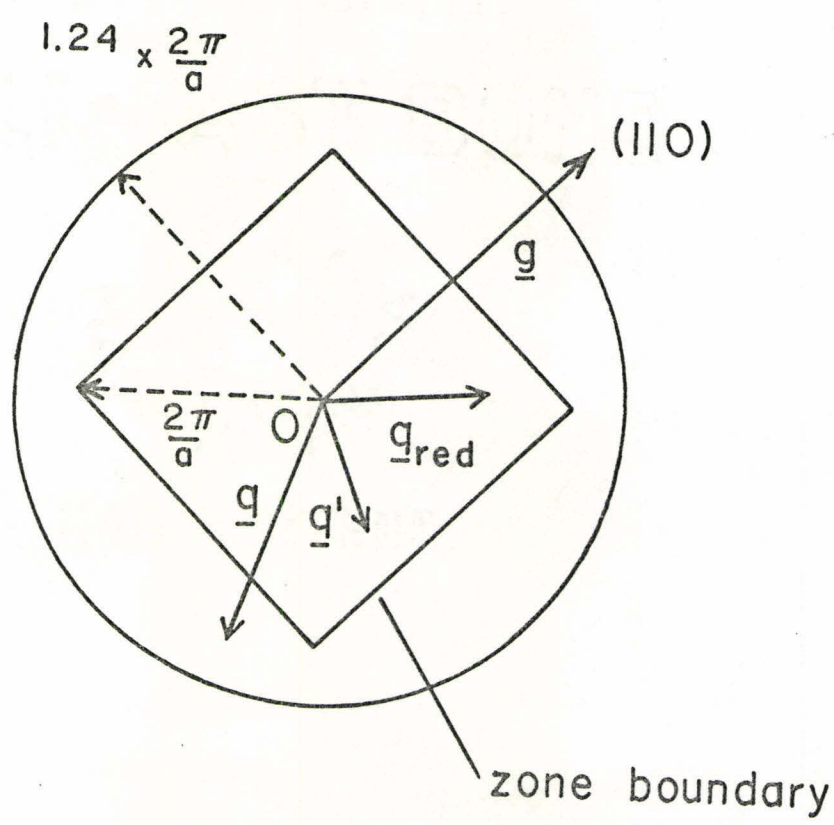


Figure 2.8

and (2.52) and it should not be a serious approximation to replace $\omega_\lambda(\underline{q})$ by an isotropic longitudinal mode frequency $\omega(\underline{q})$. The phonon frequency $\omega(\underline{q})$ is approximated by a representative sine function which reduces at small q to the screened jellium frequency vq , where v is the longitudinal sound velocity given by

$$v = (m/3M)^{1/2} v_F , \quad (2.53)$$

where m is the electron mass and v_F is the velocity at the Fermi surface. $\omega(\underline{q})$ has the form

$$\omega(\underline{q}) = c \sin qb , \quad (2.54)$$

where b is chosen such that the phonon frequency goes to zero at the nearest-neighbour reciprocal lattice point; that is,

$$\omega(\underline{q}) = \frac{2\sqrt{2}}{a} v \sin \frac{qa}{2\sqrt{2}} . \quad (2.55)$$

The sum over the polarization λ then takes the form

$$\sum_{\lambda} |\epsilon_{\lambda}(\underline{q}) \cdot \underline{q}|^2 = q^2 . \quad (2.56)$$

Taking the q_z -direction along the direction of \underline{p} , the equations (2.47), (2.50) and (2.52) reduce, respectively, to the expressions

$$R_{>}^{pse}(p) = \frac{\lambda}{(2\pi)^3} \int_{p-p_F}^{p+p_F} \int_{\mu_F}^1 \int_0^{2\pi} \frac{|\bar{g}_{\underline{q},0}^p|^2 q^2 dq d\mu d\phi}{(q^2 + \omega(q))^2}, \quad (2.57)$$

$$R_{>}^{ese}(p) = \frac{\lambda}{(2\pi)^3} \int_{p-p_F}^{p+p_F} \int_{\mu_F}^1 \int_0^{2\pi} \frac{|\bar{g}_{\underline{p},\underline{p}-\underline{q}}^e|^2 q^2 dq d\mu d\phi}{(2pq\mu - q^2 + \omega(q))^2}, \quad (2.58)$$

$$R_{>}^{lad}(p) = \frac{2\lambda}{(2\pi)^3} \int_{p-p_F}^{p+p_F} \int_{\mu_F}^1 \int_0^{2\pi} \frac{\bar{g}_{\underline{q},0}^p \bar{g}_{\underline{p},\underline{p}-\underline{q}}^{e*} q^2 dq d\mu d\phi}{(q^2 + \omega(q))(2pq\mu - q^2 + \omega(q))}. \quad (2.59)$$

The quantity μ_F is the value of μ determined by the condition that $\underline{p}-\underline{q}$ lies on the Fermi surface, as shown in figure (2.9), and is given by

$$\mu_F = (p^2 + q^2 - p_F^2)/2pq. \quad (2.60)$$

The quantities $\bar{g}_{\underline{q},0}^p$ and $\bar{g}_{\underline{p},\underline{p}-\underline{q}}^e$ have the forms

$$\bar{g}_{\underline{q},0}^p = -i(\hbar/2MN\omega(q))^{1/2} q V_p(q) \quad (2.61a)$$

and

Figure 2.9 \underline{q} -space showing the limit μ_F for the
 μ -integration of equations (2.56) through (2.58).

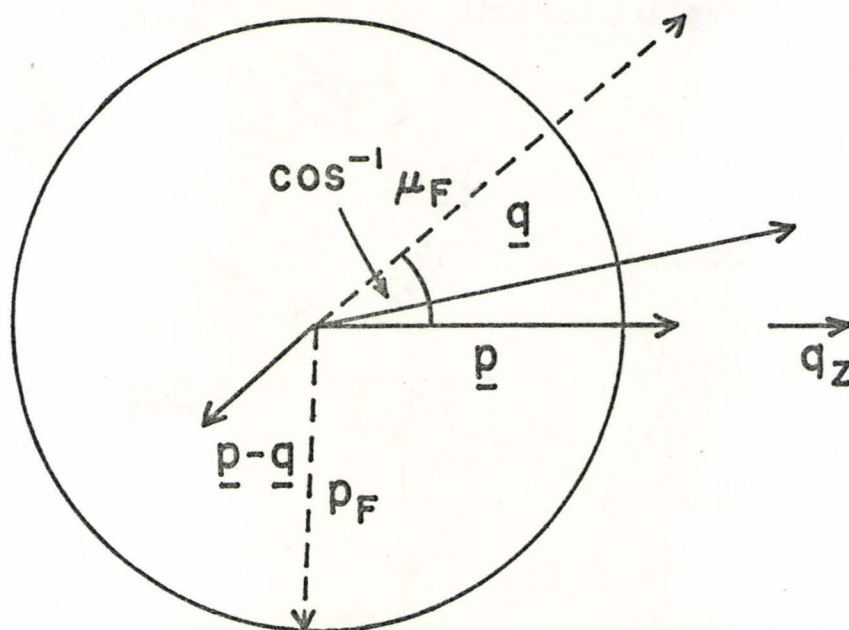


Figure 2.9

$$\bar{g}_{p, p-q}^e = -i (\hbar/2M\Omega\omega(q))^{1/2} q V_e(q) \quad . \quad (2.61b)$$

Performing the angular integrations in equations (2.57) to (2.59) yields the quantities

$$R_{>}^{pse}(p) = \frac{\lambda}{\Omega} \frac{\hbar}{16\pi^2 Mnp} \int_{p-p_F}^{p+p_F} dq q^3 \frac{|V_p(q)|^2 (p_F^2 - (p-q)^2)}{\omega(q) (q^2 + \omega(q))^2} \quad (2.62)$$

$$R_{>}^{ese}(p) = \frac{\lambda}{\Omega} \frac{\hbar}{16\pi^2 Mnp} \int_{p-p_F}^{p+p_F} dq q^3 \frac{|V_e(q)|^2}{\omega(q)} \times \frac{(p_F^2 - (p-q)^2)}{(p^2 - p_F^2 + \omega(q)) (2pq - q^2 + \omega(q))} \quad , \quad (2.63)$$

$$R_{>}^{lad}(p) = \frac{\lambda}{\Omega} \frac{\hbar}{8\pi^2 Mnp} \int_{p-p_F}^{p+p_F} dq q^3 \frac{V_p(q)V_e(q)}{\omega(q) (q^2 + \omega(q))} \times \ln \left[\frac{2pq - q^2 + \omega(q)}{p^2 - p_F^2 + \omega(q)} \right] \quad . \quad (2.64)$$

A simpler approximation to the positron-ion and electron-ion interactions than is described by the form factors of equations (2.34) and (2.38) is the screened Coulomb potential. Taking the static long-wavelength limit of the RPA screening function $f(q)$, the form factor $V(q)$ can be written

$$V(q) = \pm 4\pi n e^2 / (q^2 + \lambda^2) \quad , \quad (2.65)$$

where λ is the Fermi-Thomas screening parameter given by

$$\lambda^2 = 4p_F / \pi a_0 \quad . \quad (2.66)$$

The various form factors are plotted in figure (2.10) in units of Rydbergs. The value of R_c in the electron pseudo-potential is taken to be $0.82089 \text{ \AA}^{\circ}$ (60).

In order to make a direct comparison of the quantities of equations (2.62), (2.63) and (2.64) with the smearing described by a positron effective temperature, the results of Kim (40) and Woll and Carbotte (42) are reformulated. The smearing at the Fermi cutoff due to positron motion can be described by a partial annihilation rate, $R^{\text{eff}}(\underline{p})$, of the form

$$R^{\text{eff}}(\underline{p}) = \frac{\lambda}{\Omega} \sum_{\underline{k}} P_e(\underline{p}-\underline{k}) P_p(\underline{k}) \quad . \quad (2.67)$$

$P_e(\underline{p}-\underline{k})$ represents an enhanced free-electron distribution, and can be described by the function $\varepsilon\theta(p_F - |\underline{p}-\underline{k}|)$. $P_p(\underline{k})$ is described by a Boltzmann distribution for free particles at an effective temperature T_{eff} , given by

$$F(k) = c e^{-\hbar^2 k^2 / 2mk_B T_{\text{eff}}} \quad . \quad (2.68)$$

Figure 2.10 Comparison of the Ashcroft pseudopotential form factor (dashed curve) and the Bardeen "form factor" for the positron (solid curve) with the Coulomb form factor in the Fermi-Thomas approximation (dotted curve) (for Na). The vertical scale is to be read as positive for the Bardeen form factor.

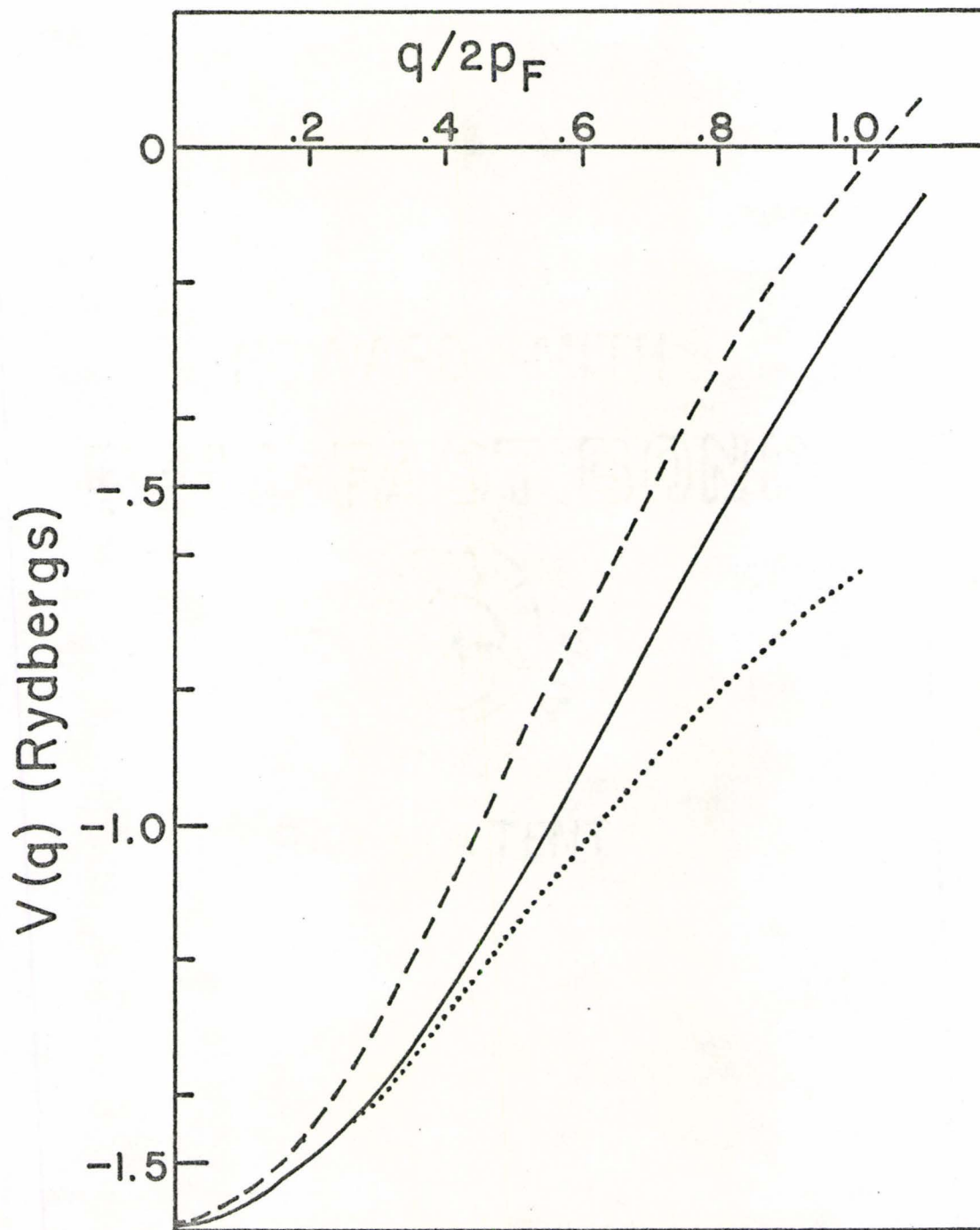


Figure 2.10

The normalization constant c is determined by the condition

$$\sum_{\tilde{k}} P_{\tilde{p}}(\tilde{k}) = 1 \quad , \quad (2.69)$$

which yields

$$c = \frac{(2\pi)^3}{\Omega} \left(\frac{\hbar^2}{2\pi m k_B T_{\text{eff}}} \right)^{3/2} \quad . \quad (2.70)$$

Since positron-electron correlations have not been included in the analysis of phonon effects, for purposes of comparison the unenhanced free-electron distribution is used in equation (2.67). The contribution for $p > p_F$ is then given by

$$R_{>}^{T_{\text{eff}}}(\tilde{p}) = \frac{\lambda}{\Omega} \sum_{\tilde{k}} \theta(p - p_F) \theta(p_F - |\tilde{p} - \tilde{k}|) F(\tilde{k}) \quad . \quad (2.71)$$

This reduces in the limit of infinite volume to the form

$$R_{>}^{T_{\text{eff}}}(p) = \frac{\lambda}{\Omega} \left(\frac{\hbar^2}{2m k_B T_{\text{eff}}} \right)^{3/2} \frac{1}{\pi^{1/2} p} \int_{p-p_F}^{p+p_F} dk k \\ \times e^{-\hbar^2 k^2 / 2m k_B T_{\text{eff}}} (p_F^2 - (p-k)^2) \quad . \quad (2.72)$$

The integrals in equations (2.62), (2.63), (2.64) and (2.72) were solved for sodium using a six-point gauss integration for a number of values of p greater than the

Fermi momentum and for the theoretical and experimental values of T_{eff} . The results of the two self-energy terms are compared in figure (2.11). In figure (2.12) the sum of the three phonon contributions is compared with the difference between experimental and theoretical positron smearing.

Figure 2.11 Smearing of the positron partial
annihilation rate in Na from the phonon self-
energy effects of figure (2.6). The solid curve
is for the positron self-energy and the dashed
curve is for the electron self-energy.

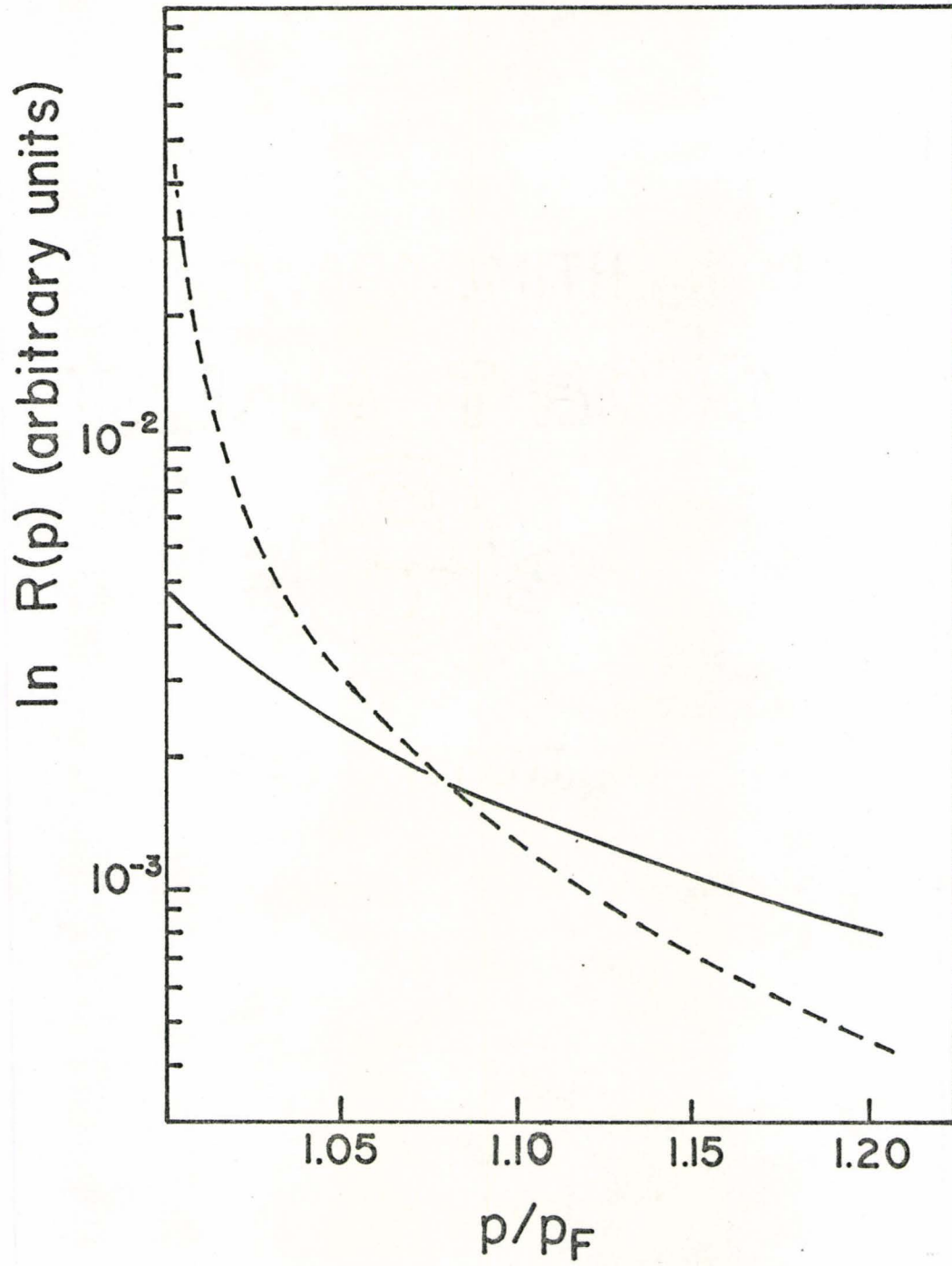


Figure 2.11

Figure 2.12

Comparison of first-order phonon smearing of the positron partial annihilation rate at the Fermi momentum with the difference between experimental smearing (Kim ⁽⁴⁰⁾) and theoretical smearing (Woll and Carbotte ⁽⁴²⁾) (for Na). The upper dashed curve representing phonon smearing is based on a screened Coulomb interaction while the lower dashed curve includes the Ashcroft pseudopotential and the Bardeen-type formulation. The upper solid curve gives the difference between smearing from positron motion corresponding to 160°K and that for 110°K. The lower solid curve gives the difference between 110°K and 49°K motion.

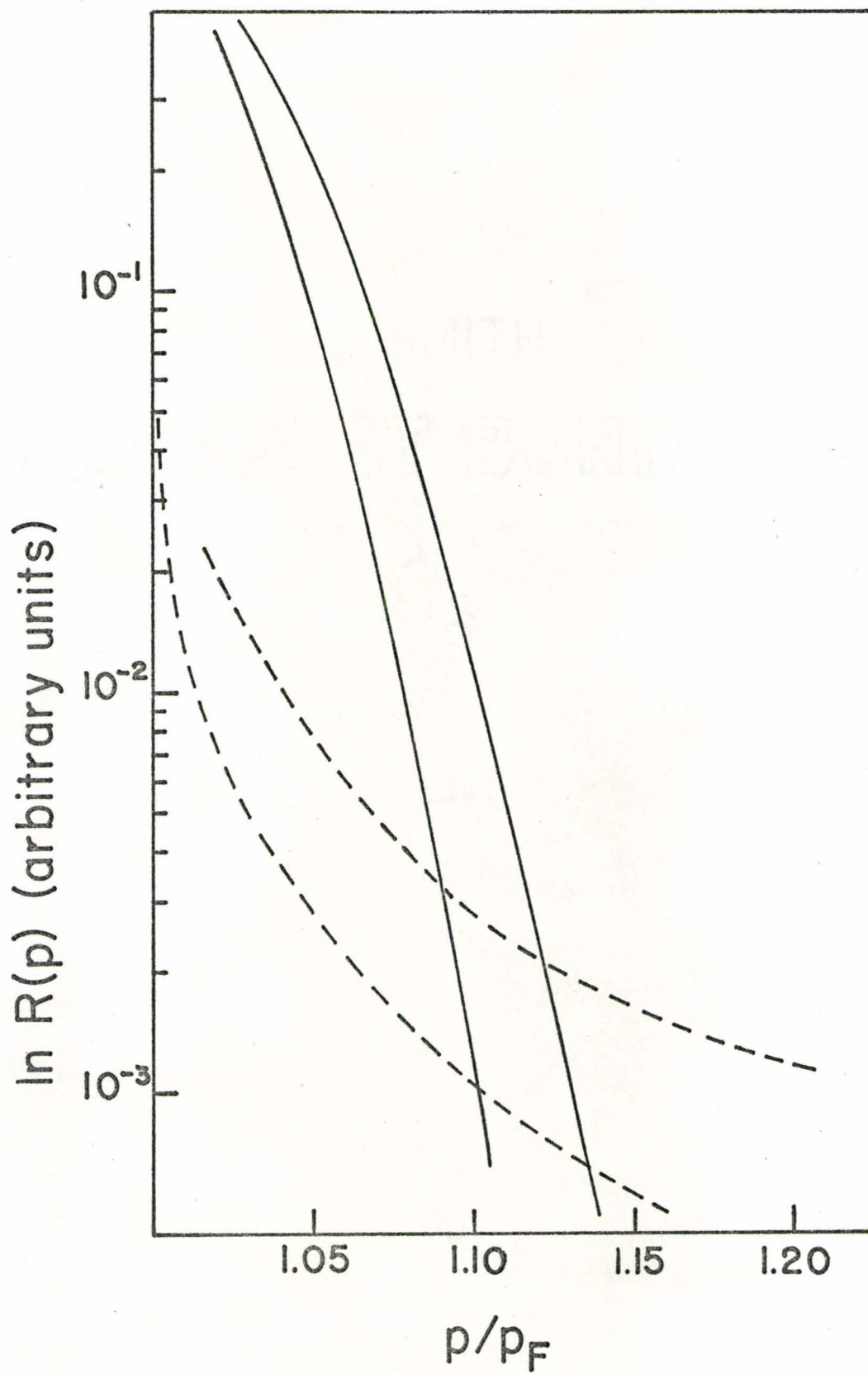


Figure 2.12

2.6 Discussion of Calculations

In evaluating the positron-phonon interaction, careful account was taken of the scattering of the conduction electrons by a displacement of the ions and the resultant enhancement of the screening of the ion from the positron. The weakness of this repulsive interaction which tends to exclude the positron from the vicinity of the cores can be seen from figure (2.10) by comparing the positron-ion interaction obtained in the Bardeen approach with the simple Coulomb potential screened in the Fermi-Thomas approximation.

Figure (2.11) gives the contributions to the partial annihilation rate from the positron and electron self-energy terms describing the smearing of the respective momentum distributions by phonons. It can be seen that the electron smearing is less than that for positrons, as expected. However, the electron self-energy diagram cannot be ignored in spite of its short tails. The sum of these two contributions and that from the first-order phonon ladder diagram, employing the screened Coulomb potential to represent the positron- and electron-ion interactions, is an order of magnitude smaller than the effect we are looking for. When the improved form of the positron-ion interaction and the model pseudopotential are used, the results become even less significant.

All of the calculations depend on the plane wave approximation to positron states and conduction electron states, thereby ignoring their Bloch character. In the case of simple metals, where the pseudopotential and screened positron-ion potential are weak, this should not be a serious limitation.

CHAPTER III

LATTICE TAILS IN POSITRON ANNIHILATION

3.1 Lattice Effects in Positron Annihilation

When a positron enters a real metal, it sees more than just the simple medium consisting of an electron gas, as has already been indicated in Chapter II. In addition to the phonon effects described there, the situation is complicated by the presence of core electrons with which the positron can annihilate. This leads to broad tails in the angular correlation data. The periodic lattice also means that the picture of conduction electrons as free electrons in plane wave states is no longer valid. By introducing higher momentum components into the conduction electron wave function, it leads to further tails in the annihilation data.

A number of estimates have been made of this effect for simple metals, based on an independent-particle model which includes Coulomb correlations only in an average way (32,37,38). The result is additional weighted contributions associated with Fermi surfaces about each of the reciprocal lattice points. A paper by Fujiwara (61) goes further than these by introducing a many-body theory which treats the effect of a periodic field on the basis of nearly-free electron theory and which includes electron-positron correlations. It deals with models based on metals whose

Fermi surfaces intersect a zone face and restricts itself to a treatment of the vicinity of a zone face.

3.2 Bloch States in Annihilation Rates

When the lattice potential is included, the Hamiltonian for the positron-electron system is given by

$$\begin{aligned}
 H = & \int d^3 \underline{x} \psi^\dagger(\underline{x}) [-\nabla^2 + H_e(\underline{x})] \psi(\underline{x}) \\
 & + \int d^3 \underline{x} \phi^\dagger(\underline{x}) [-\nabla^2 + H_p(\underline{x})] \phi(\underline{x}) \\
 & + \frac{1}{2} \int d^3 \underline{x} d^3 \underline{x}' \psi^\dagger(\underline{x}', t) \psi^\dagger(\underline{x}) v(\underline{x}; \underline{x}') \psi(\underline{x}) \psi(\underline{x}', t) \\
 & + \frac{1}{2} \int d^3 \underline{x} d^3 \underline{x}' \phi^\dagger(\underline{x}', t) \phi^\dagger(\underline{x}) v(\underline{x}; \underline{x}') \phi(\underline{x}) \phi(\underline{x}', t) \\
 & - \int d^3 \underline{x} d^3 \underline{x}' \psi^\dagger(\underline{x}', t) \phi^\dagger(\underline{x}) v(\underline{x}; \underline{x}') \phi(\underline{x}) \psi(\underline{x}', t) \quad ,
 \end{aligned} \tag{3.1}$$

where H_e and H_p represent some average potential seen by the electron and positron, respectively. The equation for the electron-positron Green's function G_{ep} takes a form equivalent to equation (2.5) in terms of zeroth-order electron and positron Green's functions that satisfy an equation

$$\left(-i \frac{\partial}{\partial t} + H_{e(p)}(\underline{x}) \right) G_{e(p)}^0(\underline{x}; \underline{x}') = \delta^4(\underline{x} - \underline{x}') \quad . \tag{3.2}$$

The system is no longer invariant under an arbitrary displacement but has the periodicity of the lattice, so that the propagator satisfies the weaker symmetry described by

$$G_{e(p)}^0(\tilde{x}+R_{\tilde{l}}^0, t; \tilde{x}'+R_{\tilde{l}}^0, t') = G_{e(p)}^0(\tilde{x}; \tilde{x}') \quad . \quad (3.3)$$

It is concluded that the propagator can be written in terms of Bloch functions. In particular, the zeroth-order propagators can be expanded in the forms

$$G_e^0(\tilde{x}; \tilde{x}') = \frac{1}{\Omega} \sum_{\tilde{k}} e^{i\tilde{k} \cdot (\tilde{x} - \tilde{x}')} u_{\tilde{k}}(\tilde{x}) u_{\tilde{k}}^*(\tilde{x}') \\ \times \int \frac{d\omega}{2\pi} e^{-i\omega(t-t')} G_e^0(\tilde{k}; \omega) \quad (3.4a)$$

and

$$G_p^0(\tilde{x}; \tilde{x}') = \frac{1}{\Omega} \sum_{\tilde{k}} e^{i\tilde{k} \cdot (\tilde{x} - \tilde{x}')} v_{\tilde{k}}(\tilde{x}) v_{\tilde{k}}^*(\tilde{x}') \\ \times \int \frac{d\omega}{2\pi} e^{-i\omega(t-t')} G_p^0(\tilde{k}; \omega) \quad , \quad (3.4b)$$

where $u_{\tilde{k}}$ and $v_{\tilde{k}}$ are periodic functions. $G_e^0(\tilde{k}; \omega)$ and $G_p^0(\tilde{k}; \omega)$ are given by

$$G_e^0(\tilde{k}; \omega) = \frac{\theta(k-p_F)}{E_{\tilde{k}}^e - \omega - i0^+} + \frac{\theta(p_F - k)}{E_{\tilde{k}}^e - \omega + i0^+} \quad (3.5a)$$

and

$$G_p^0(\tilde{k}; \omega) = \frac{\theta(k)}{E_{\tilde{k}}^p - \omega - i0^+} + \frac{\theta(-k)}{E_{\tilde{k}}^p - \omega + i0^+} \quad , \quad (3.5b)$$

where $E_{\tilde{k}}^e$ and $E_{\tilde{k}}^p$ represent the energy of the electron and positron, respectively, in the Bloch states

$$\begin{pmatrix} \psi_{\tilde{k}}(\tilde{x}) \\ \phi_{\tilde{k}}(\tilde{x}) \end{pmatrix} = \frac{1}{\sqrt{\Omega}} e^{i\tilde{k} \cdot \tilde{x}} \begin{pmatrix} u_{\tilde{k}}(\tilde{x}) \\ v_{\tilde{k}}(\tilde{x}) \end{pmatrix} . \quad (3.6)$$

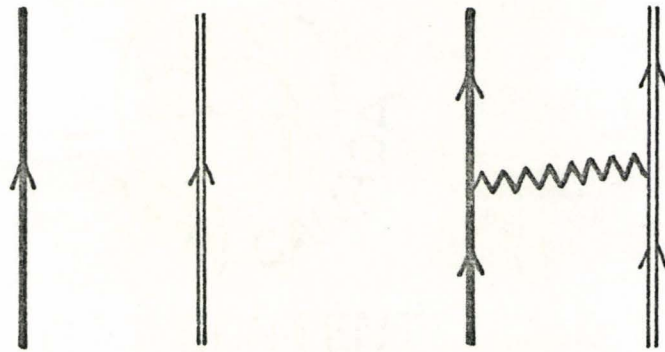
From equation (2.5) it can be seen that, if all correlations are neglected, the positron partial annihilation rate is given by

$$\begin{aligned} R(\tilde{p}) &= \frac{\lambda}{\Omega} (-i)^2 \int d^3\tilde{x} d^3\tilde{x}' e^{-i\tilde{p} \cdot (\tilde{x} - \tilde{x}')} G_e^0(\tilde{x}; \tilde{x}' t^+) \\ &\quad \times G_p^0(\tilde{x}; \tilde{x}' t^+) . \end{aligned} \quad (3.7)$$

This describes the contribution of the diagram of figure (3.1a). For simplicity it is assumed that the positron is in a plane wave state, so that G_p^0 is given by equation (2.7), while G_e^0 is given by equation (3.4a). If the Bloch function $u_{\tilde{k}}(\tilde{x})$ is expanded in terms of Fourier components, it takes the form

$$u_{\tilde{k}}(\tilde{x}) = \sum_{\tilde{g}} u_{\tilde{k}}(\tilde{g}) e^{i\tilde{g} \cdot \tilde{x}} , \quad (3.8)$$

Figure 3.1 Lowest-order ladder diagrams in the perturbation expansion of G_{ep} with a periodic lattice taken into account through Bloch states in the propagators. The heavy lines represent electron propagators and the double lines positron propagators. The interaction line in (b) represents the dynamic effective potential.



(a)

(b)

Figure 3.1

where \underline{g} is a reciprocal lattice vector. The partial annihilation rate described by equation (3.7) then reduces to

$$R(\underline{p}) = \frac{\lambda}{\Omega} \sum_{\substack{\underline{k} \\ k < p_F}} \sum_{\underline{g}} |u_0(\underline{g})|^2 \delta_{\underline{p}, \underline{k} + \underline{g}} \quad , \quad (3.9)$$

where the \underline{k} -dependence of $u_{\underline{k}}(\underline{g})$ has been ignored. This equation is very similar to the Sommerfeld result of equation (2.9). If $R(\underline{p})$ is summed over p_x and p_y , however, the p_z -plane no longer intersects just the Fermi sphere centred about the origin, giving rise to the parabolic shape of equation (2.11). It also intersects a number of spheres situated at reciprocal lattice points, as shown in figure (3.2). This leads to parabolic contributions centred about these reciprocal lattice points weighted by the corresponding factor $|u_0(\underline{g})|^2$. The annihilation rate is now non-zero for momenta greater than the Fermi momentum, as illustrated in figure (3.3).

The effect of including the first-order electron-positron correlation described by the ladder diagram of figure (3.1b) is the contribution

$$R(\underline{p}) = \frac{\lambda}{\Omega} (-i)^2 (-i) \int d^3 \underline{x} d^3 \underline{x}' d^4 z d^4 z' e^{-i \underline{p} \cdot (\underline{x} - \underline{x}')} u(z; z') \\ \times G_e^0(x; z) G_e^0(z; \underline{x}' t^+) G_p^0(x; z') G_p^0(z'; \underline{x}' t^+) \quad , \quad (3.10)$$

Figure 3.2 Projection onto the yz-plane of fcc
reciprocal lattice space with Fermi spheres
about reciprocal lattice points and a plane at
 p_z .

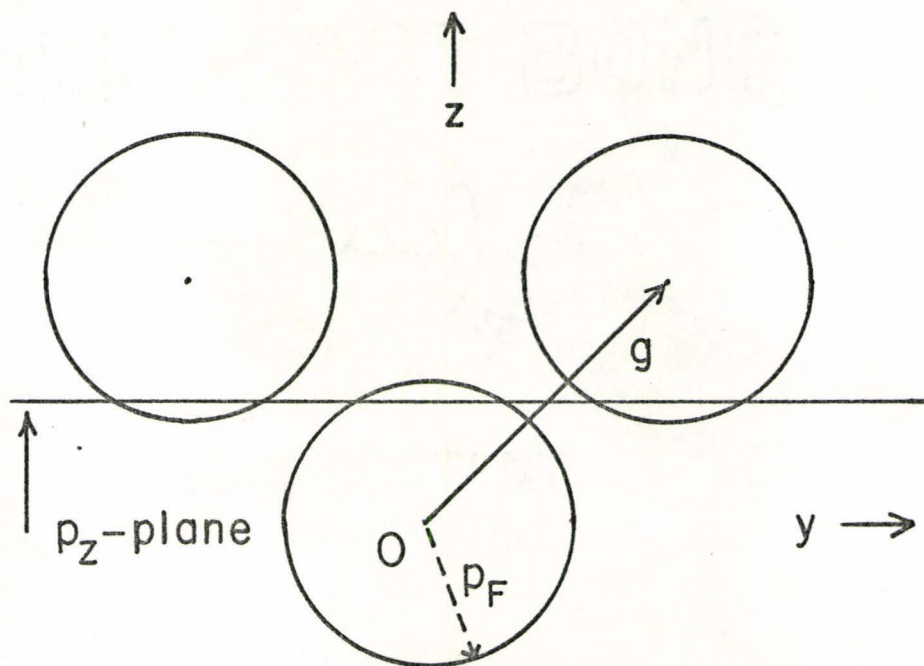


Figure 3.2

Figure 3.3 Positron annihilation rate as a function of electron-positron momentum component p_z for an independent-particle model in a periodic lattice. The respective parabolic contributions centred about the reciprocal points at \underline{g} are weighted by the factors $|u_0(\underline{g})|^2$.

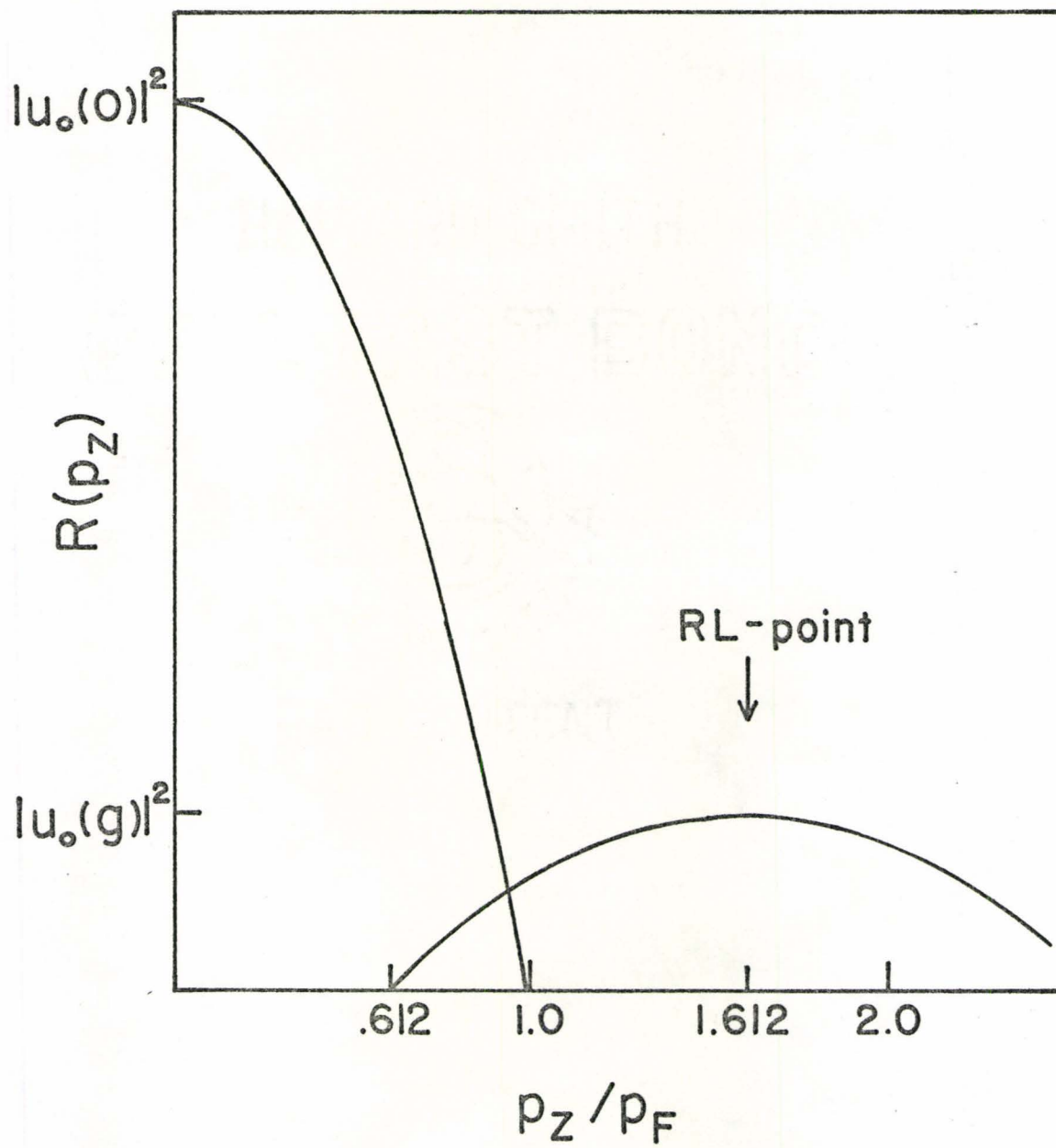


Figure 3.3

where $u(z; z')$ is the dynamic effective electron-positron potential. G_p^0 is again described by plane waves. Equation (3.10) is calculated in Appendix B to be given, in the limit of a static potential, by

$$R(\underline{p}) = \frac{2\lambda}{\Omega} \sum_{\substack{\underline{k} \\ k < p_F}} \sum_{\substack{\underline{k}' \\ k' > p_F}} \sum_{\underline{g}, \underline{G}, \underline{G}'} \frac{u(\underline{k} - \underline{k}' + \underline{G}'; 0)}{E_{\underline{k}'} - E_{\underline{k}} + |\underline{k} - \underline{k}' + \underline{G}'|^2} \\ \times u_0(\underline{g}) u_0^*(\underline{G} + \underline{g}') u_0(\underline{G}) u_0^*(\underline{g} - \underline{G}') \delta_{\underline{p}, \underline{k} + \underline{g}} \quad (3.11)$$

The sums on \underline{g} , \underline{G} and \underline{G}' represent sums over reciprocal lattice vectors. Again the \underline{k} -dependence of $u_{\underline{k}}(\underline{g})$'s is ignored.

When one takes correlations into account through a term such as equation (3.10), one must be careful not to include these same correlations in the average field H_e of equation (3.1) seen by an electron; that is, H_e must be taken to be the bare ion potential. It leads to electron Bloch states $\psi_{\underline{k}}$ of energy $E_{\underline{k}}$ which are not the same as the Bloch states calculated, for example, by Callaway (62), who used a Hartree-Fock type of potential. Furthermore, it appears that the triple sum over reciprocal lattice vectors does not readily converge. An alternative approach to handling the lattice, first presented in a paper by Hede and Carbotte (63), is discussed in the following sections.

3.3 Enhancement of Lattice Tails From First-Order Ladders

It is possible to account for the effect of a periodic lattice on the positron partial annihilation rate by handling the electron (positron)-lattice interaction explicitly rather than by employing Bloch states for the wave functions. In the absence of a crystal lattice, the electron-positron Green's function G_{ep} has the well-known perturbation expansion in terms of Feynman diagrams (37). The crystal field leads to additional diagrams which are modifications of the previous diagrams containing one or more electron (positron)-lattice interaction lines. A detailed derivation of the new perturbation expansion is given by Appendix C. The lattice diagrams actually replace the usual diagrams representing a uniform positive background included to ensure charge neutrality. The latter cancel against the set of bubble diagrams of figure (3.4), which correspond to an electron (positron) interacting with the electron gas.

The major contribution to the partial annihilation rate in an electron gas is given by the infinite set of ladder diagrams of figure (2.2) (25,26). The set of ladder diagrams with modified electron lines is shown in figure (3.5). If the plane wave approximation is made for positrons,

Figure 3.4 Infinite set of bubble diagrams which describe an electron (positron) interacting with the electronic medium. The single lines stand for electron propagators and the double lines stand for positron propagators.

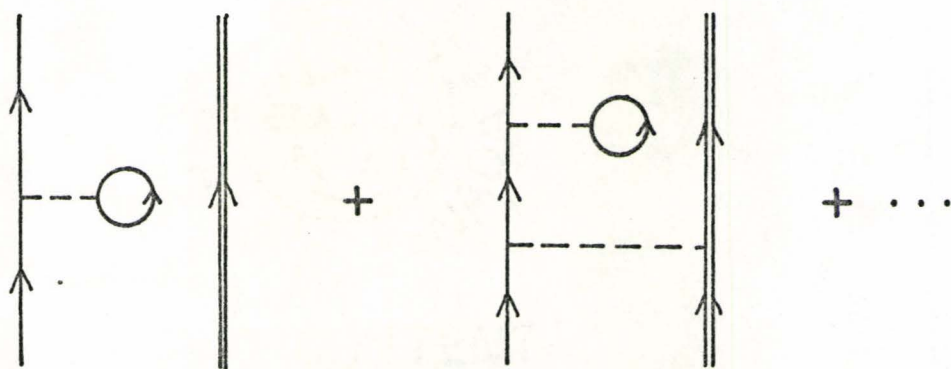


Figure 3.4

Figure 3.5 Infinite set of ladder diagrams with electron lines modified by the presence of a crystal lattice. The single lines represent electron propagators, the double lines represent positron propagators and the dotted lines ending in a cross represent the electron-lattice interaction.

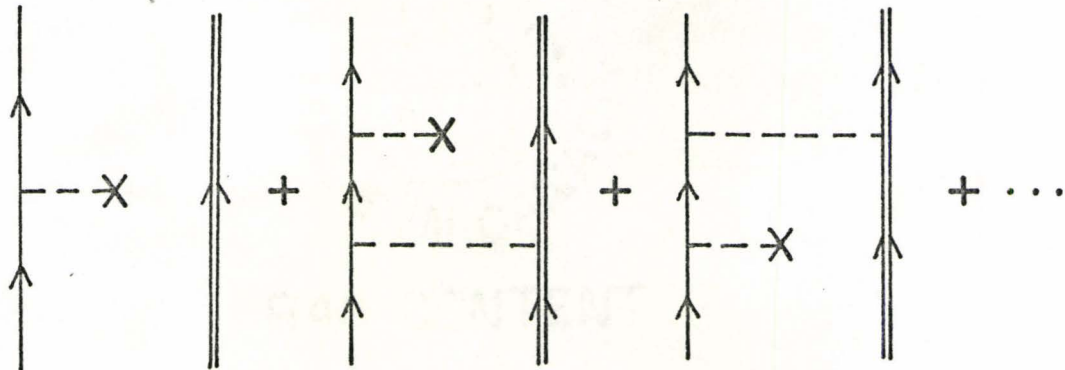


Figure 3.5

as in section 3.2, it is just these diagrams that should make the greatest lattice contribution to $R(\underline{p})$, by analogy with the electron gas. The lattice is considered to be a weak perturbation, which is the case for metals such as sodium, so that only the lowest-order diagrams in the lattice potential V need be included. If, for simplicity, a calculation is made just of the enhancement from first-order correlations, there are but a very limited number of diagrams to be considered.

It is assumed that the potential field about an ion is rigidly attached to it. The average crystal potential seen by an electron is written as the sum of ionic potentials about the equilibrium positions \underline{R}_ℓ^0 ; that is,

$$\begin{aligned}
 V(\underline{x}) &= \sum_{\ell} W(\underline{x} - \underline{R}_\ell^0) \\
 &= \frac{1}{\Omega} \sum_{\ell} \sum_{\underline{q}} e^{i\underline{q} \cdot (\underline{x} - \underline{R}_\ell^0)} W(\underline{q}) \\
 &= n \sum_{\underline{q}} \sum_{\underline{g}} e^{i\underline{q} \cdot \underline{x}} W(\underline{q}) \delta_{\underline{q}, \underline{g}} .
 \end{aligned} \tag{3.12}$$

The contribution to the partial annihilation rate from the uncorrelated diagram of figure (3.6a) is given by

$$\begin{aligned}
 R(\underline{p}) &= \frac{\lambda}{\Omega} (-i)^2 \int d^3 \underline{x} d^3 \underline{x}' e^{-i\underline{p} \cdot (\underline{x} - \underline{x}')} G_e(\underline{x}; \underline{x}' t^+) \\
 &\quad \times G_p(\underline{x}; \underline{x}' t^+) ,
 \end{aligned} \tag{3.13}$$

Figure 3.6 Ladder diagrams with a single electron-
lattice interaction line. These cancel against
bubble diagrams.

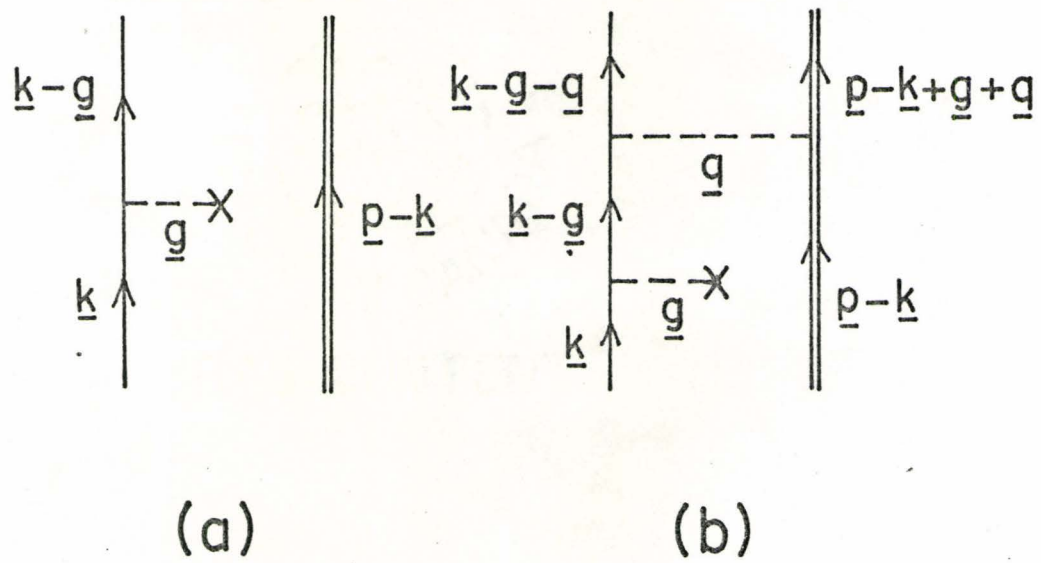


Figure 3.6

where G_p is simply the free positron propagator G_p^0 , while G_e is given by

$$G_e(x; x') = \int d^4z V(z) G_e^0(x; z) G_e^0(z; x') \quad . \quad (3.14)$$

On doing the space- and time-integrations, $R(\underline{p})$ reduces to

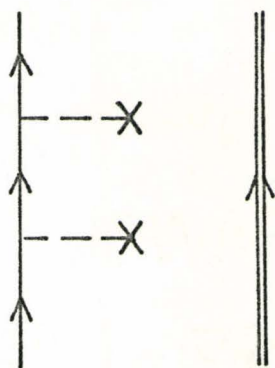
$$R(\underline{p}) = \frac{\lambda}{\Omega} nW(0) \sum_{\underline{k}} \int \frac{d\omega}{2\pi} \frac{d\omega'}{2\pi} [G_e^0(\underline{k}; \omega)]^2 G_p^0(\underline{p}-\underline{k}; \omega') \quad . \quad (3.15)$$

$W(0)$ is the $g=0$ component of the lattice potential. It can be seen from figure (3.6a) that g is actually zero, by noting that the total electron-positron momentum coming out and the total momentum going in are both equal to \underline{p} . Such a term cancels the equivalent bubble diagram. Similarly, a correlation diagram modified to first order in the lattice, such as that of figure (3.6b), leads to the $g=0$ component of W and cancels against a bubble diagram. The lowest-order lattice diagrams which have a contribution to $R(\underline{p})$ are those of second order in V shown in figure (3.7).

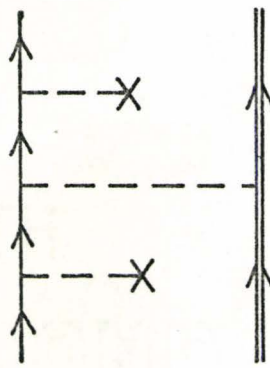
The contribution to the partial annihilation rate from the uncorrelated diagram of figure (2.2a), which is referred to as $R^{(0)}(\underline{p})$, is given by equation (2.9) as

$$R^{(0)}(\underline{p}) = \frac{\lambda}{\Omega} \sum_{\substack{\underline{k} \\ k < p_F}} \delta_{\underline{k}, \underline{p}} \quad . \quad (2.9)$$

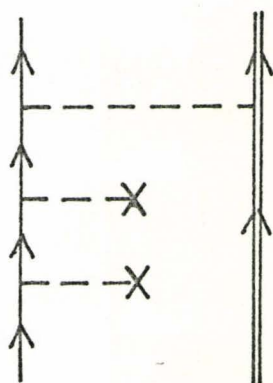
Figure 3.7 Ladder diagrams of second order in the
electron-lattice interaction and up to first
order in the electron-positron interaction.



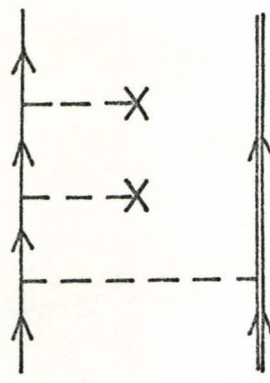
(a)



(b)



(c)



(d)

Figure 3.7

$R^{(0)}(\underline{p})$ is zero for $p > p_F$. The first-order correlation diagram of figure (2.2a) contributes the rate

$$\begin{aligned}
 R^{(c)}(\underline{p}) &= \frac{i\lambda}{\Omega} \sum_{\underline{k}\underline{q}} \int \frac{d\omega}{2\pi} \frac{d\omega'}{2\pi} \frac{d\varepsilon}{2\pi} u(\underline{q}; \varepsilon) \\
 &\quad \times G_e^0(\underline{k}; \omega) G_e^0(\underline{k}-\underline{q}; \omega-\varepsilon) \\
 &\quad \times G_p^0(\underline{p}-\underline{k}; \omega') G_p^0(\underline{p}-\underline{k}+\underline{q}; \omega'+\varepsilon) \quad . \quad (3.16)
 \end{aligned}$$

Taking the static limit for the Fourier transform of the effective potential $u(\underline{q}; \varepsilon)$, $R^{(c)}(\underline{p})$ can be reduced quite easily to

$$R^{(c)}(\underline{p}) = \frac{2\lambda}{\Omega^2} \sum_{\underline{q}} \frac{\theta(p_F - p) \theta(|\underline{p}-\underline{q}| - p_F) u(\underline{q}; 0)}{q^2 + |\underline{p}-\underline{q}|^2 - p^2} \quad , \quad (3.17)$$

or, alternatively,

$$R^{(c)}(\underline{p}) = \frac{2\lambda}{\Omega^2} \sum_{\substack{\underline{k} \\ k < p_F}} \sum_{\substack{\underline{k}' \\ k' > p_F}} \frac{u(\underline{k}-\underline{k}'; 0) \delta_{\underline{k}, \underline{p}}}{k'^2 + |\underline{k}-\underline{k}'|^2 - k^2} \quad . \quad (3.18)$$

Like equation (2.9) it is zero for momenta $p > p_F$. Its contribution to an enhancement factor $\varepsilon(\underline{p})$ is given by

$$\varepsilon(\underline{p}) = R^{(c)}(\underline{p}) / R^{(0)}(\underline{p}) \quad . \quad (3.19)$$

The lattice contribution to the partial annihilation rate is mainly from diagrams of second order in the electron-lattice interaction V . For the uncorrelated diagram of figure (3.7a), the contribution can be shown to be

$$R^{(0')}(\underline{p}) = \frac{\lambda}{\Omega} (-i)^2 \sum_{\underline{k}} \sum_{\underline{g} \neq 0} W(\underline{g}) W(-\underline{g}) \int \frac{d\omega}{2\pi} \frac{d\omega'}{2\pi} \\ \times [G_e^0(\underline{k}; \omega)]^2 G_e^0(\underline{k}-\underline{g}; \omega) G_p^0(\underline{p}-\underline{k}; \omega') \quad . \quad (3.20)$$

The $\underline{g}=0$ term cancels against a bubble diagram. In the region $p < p_F$, $R^{(0')}(\underline{p})$ is negligible compared to $R^{(0)}(\underline{p})$ since V is a weak potential and this part of $R^{(0')}(\underline{p})$ is neglected. The contribution for $p > p_F$, referred to as $R_{>}^{(0')}(\underline{p})$, reduces on doing the angular integrations to

$$R_{>}^{(0')}(\underline{p}) = \frac{\lambda}{\Omega} \sum_{\underline{g} \neq 0} \frac{\theta(p-p_F) \theta(p_F - |\underline{p}-\underline{g}|) |W(\underline{g})|^2}{(p^2 - |\underline{p}-\underline{g}|^2)^2} \\ = \frac{\lambda}{\Omega} \sum_{\substack{\underline{k} \\ k < p_F \\ |\underline{k}+\underline{g}| > p_F}} \frac{|W(\underline{g})|^2 \delta_{\underline{p}, \underline{k}+\underline{g}}}{(|\underline{k}+\underline{g}|^2 - k^2)^2} \quad . \quad (3.21)$$

The lowest-order lattice ladder diagrams involving correlations are shown in figures (3.7b), (3.7c) and (3.7d). Figure (3.7b) gives, on introducing an effective potential

in place of the Coulomb potential, a contribution, $R^{(1')}(p)$, of the form

$$\begin{aligned}
 R^{(1')}(p) &= \frac{i\lambda}{\Omega^2} \sum_{\underline{k}\underline{q}} \sum_{\underline{g} \neq 0} W(\underline{g})W(-\underline{g}) \int \frac{d\omega}{2\pi} \frac{d\omega'}{2\pi} \frac{d\varepsilon}{2\pi} \\
 &\times u(\underline{q}; \varepsilon) G_e^0(\underline{k}; \omega) G_e^0(\underline{k}-\underline{g}; \omega) \\
 &\times G_e^0(\underline{k}-\underline{q}-\underline{g}; \omega-\varepsilon) G_p^0(\underline{p}-\underline{k}; \omega') \\
 &\times G_p^0(\underline{p}-\underline{k}+\underline{q}; \omega'+\varepsilon) \quad . \quad (3.22)
 \end{aligned}$$

The angular integrations can be performed, on taking the static limit for $u(\underline{q}; \varepsilon)$, to give the result for $p > p_F$ as

$$\begin{aligned}
 R_{>}^{(1')}(p) &= \frac{2\lambda}{\Omega^2} \sum_{\underline{g} \neq 0} |W(\underline{g})|^2 \sum_{\underline{q}} \frac{\theta(p-p_F)\theta(p_F - |\underline{p}-\underline{g}|)}{p^2 - |\underline{p}-\underline{g}|^2} \\
 &\times u(\underline{q}; 0) \left[\frac{\theta(|\underline{p}-\underline{q}| - p_F)\theta(|\underline{p}-\underline{q}-\underline{g}| - p_F)}{(|\underline{p}-\underline{q}|^2 + q^2 - |\underline{p}-\underline{g}|^2)(|\underline{p}-\underline{q}-\underline{g}|^2 + q^2 - |\underline{p}-\underline{g}|^2)} \right. \\
 &- \frac{\theta(|\underline{p}-\underline{q}-\underline{g}| - p_F)\theta(p_F - |\underline{p}-\underline{q}|)}{(|\underline{p}-\underline{q}-\underline{g}|^2 + q^2 - |\underline{p}-\underline{g}|^2)(|\underline{p}-\underline{q}-\underline{g}|^2 - |\underline{p}-\underline{q}|^2)} \\
 &\left. - \frac{\theta(|\underline{p}-\underline{q}| - p_F)\theta(p_F - |\underline{p}-\underline{q}-\underline{g}|)}{(|\underline{p}-\underline{q}|^2 + q^2 - |\underline{p}-\underline{g}|^2)(|\underline{p}-\underline{q}|^2 - |\underline{p}-\underline{q}-\underline{g}|^2)} \right] \quad . \quad (3.23)
 \end{aligned}$$

The two diagrams (3.7c) and (3.7d) contribute equally to the partial annihilation, so that it is necessary to calculate just the contribution from figure (3.7c). The rate,

$R^{(1'')}(\underline{p})$, from these diagrams, with an effective electron-positron potential, is given by

$$\begin{aligned}
 R^{(1'')}(\underline{p}) &= \frac{2i\lambda}{\Omega^2} \sum_{\underline{k}\underline{q}} \sum_{\underline{g} \neq 0} W(\underline{g})W(-\underline{g}) \int \frac{d\omega}{2\pi} \frac{d\omega'}{2\pi} \frac{d\varepsilon}{2\pi} \\
 &\quad \times u(\underline{q};\varepsilon) [G_e^0(\underline{k};\omega)]^2 G_e^0(\underline{k}-\underline{g};\omega) \\
 &\quad \times G_e^0(\underline{k}-\underline{q};\omega-\varepsilon) G_p^0(\underline{p}-\underline{k};\omega') G_p^0(\underline{p}-\underline{k}+\underline{q};\omega'+\varepsilon) \quad .
 \end{aligned} \tag{3.24}$$

For $p > p_F$ there is the contribution, called $R_{>}^{(1'')}(\underline{p})$, which has the reduced form

$$\begin{aligned}
 R_{>}^{(1'')}(\underline{p}) &= \frac{2\lambda}{\Omega^2} \sum_{\underline{g} \neq 0} |W(\underline{g})|^2 \sum_{\underline{q}} u(\underline{q};0) \\
 &\quad \times \frac{\theta(p-p_F)\theta(p_F - |\underline{p}-\underline{q}|)\theta(|\underline{p}-\underline{q}| - p_F)}{(p^2 - |\underline{p}-\underline{q}|^2)^2 (q^2 + |\underline{p}-\underline{q}|^2 - |\underline{p}-\underline{q}|^2)} \quad . \tag{3.25}
 \end{aligned}$$

The sum of equations (3.23) and (3.25) can then be written in the form

$$\begin{aligned}
R_{>}^{(c')}(\underline{p}) &= \frac{2\lambda}{\Omega^2} \sum_{\underline{g} \neq 0} |W(\underline{g})|^2 \sum_{\substack{\underline{k} \\ k < p_F \\ |\underline{k} + \underline{g}| > p_F}} \frac{1}{|\underline{k} + \underline{g}|^2 - k^2} \\
&\times \left[\sum_{\substack{\underline{k}' \\ k' > p_F \\ |\underline{k}' + \underline{g}| > p_F}} \frac{u(\underline{k} - \underline{k}'; 0)}{(k'^2 + |\underline{k} - \underline{k}'|^2 - k^2) (|\underline{k}' + \underline{g}|^2 + |\underline{k} - \underline{k}'|^2 - k^2)} \right. \\
&- \sum_{\substack{\underline{k}' \\ k' > p_F \\ |\underline{k}' + \underline{g}| < p_F}} \frac{u(\underline{k} - \underline{k}'; 0)}{(k'^2 + |\underline{k} - \underline{k}'|^2 - k^2) (k'^2 - |\underline{k}' + \underline{g}|^2)} \\
&- \sum_{\substack{\underline{k}' \\ k' < p_F \\ |\underline{k}' + \underline{g}| > p_F}} \frac{u(\underline{k} - \underline{k}'; 0)}{(|\underline{k}' + \underline{g}|^2 + |\underline{k} - \underline{k}'|^2 - k^2) (|\underline{k}' + \underline{g}|^2 - k'^2)} \\
&\left. + \sum_{\substack{\underline{k}' \\ |\underline{k}' + \underline{g}| > p_F}} \frac{u(\underline{k} - \underline{k}'; 0)}{(|\underline{k} + \underline{g}|^2 - k^2) (|\underline{k}' + \underline{g}|^2 + |\underline{k} - \underline{k}'|^2 - k^2)} \right] \delta_{\underline{p}, \underline{k} + \underline{g}}. \quad (3.26)
\end{aligned}$$

It is convenient, in the second term, to make the transformation of variable $\underline{k}' \rightarrow \underline{k}' - \underline{g}$ in order to express the term in the form

$$\begin{aligned}
& - \frac{2\lambda}{\Omega^2} \sum_{\underline{g} \neq 0} |W(\underline{g})|^2 \sum_{\substack{\underline{k} \\ k < p_F \\ |\underline{k} + \underline{g}| > p_F}} \frac{\delta_{\underline{p}, \underline{k} + \underline{g}}}{|\underline{k} + \underline{g}|^2 - k^2} \sum_{\substack{\underline{k}' \\ k' < p_F \\ |\underline{k}' - \underline{g}| > p_F}} \\
& \times \frac{u(\underline{k} - \underline{k}' + \underline{g}; 0)}{(|\underline{k}' - \underline{g}|^2 - k'^2) (|\underline{k} - \underline{k}' + \underline{g}|^2 + |\underline{k}' - \underline{g}|^2 - k^2)}. \quad (3.27)
\end{aligned}$$

It is also convenient to expand the last term in equation (3.26) into a part for which the variable $k' < p_F$ and a part for which $k' > p_F$.

In the present approximation the annihilation rate and, hence, any enhancement in the region outside the Fermi momentum is due to the effect of the lattice. The contribution to the enhancement of the uncorrelated rate of equation (3.21) from the modified first-order ladder graphs, denoted by $\varepsilon'(\underline{p})$, is given by

$$\varepsilon'(\underline{p}) = R_{>}^{(c')}(\underline{p}) / R_{>}^{(0')}(\underline{p}) \quad . \quad (3.28)$$

3.4 Calculation of Enhancements

The various quantities of section 3.3 are calculated by replacing the sums by integrals. An additional sum over p_x and p_y means an integration in the p_z -plane. For $R^{(0)}(\underline{p})$ and $R^{(c)}(\underline{p})$ the integration is over an area in the p_z -plane subtended by a Fermi sphere at the origin. As a result, there is no contribution for $p_z > p_F$. When the lattice is included, as it is in equations (3.21) and (3.26), the p_z -plane intersects spheres located at a number of reciprocal lattice points at $g \neq 0$. This can occur for values of p_z greater than the Fermi momentum. A model calculation is made which considers only nearest-neighbour reciprocal lattice points. For a face-centred cubic reciprocal lattice, these occur at $2\pi/a(\pm 1, 0, 1)$ and $2\pi/a(0, \pm 1, 1)$ (ignoring those RL points with negative z -component). These RL points are equivalent in the present calculation, so that the sum on g merely introduces a factor of 4.

The quantities which are actually calculated are

$$R^{(0)}(p_z) = \frac{1}{(2\pi)^3} \int_{k < p_F} d^3 \underline{k} \delta(k_z - p_z) \quad , \quad (3.29)$$

$$R^{(c)}(p_z) = \frac{2}{(2\pi)^6} \int_{k < p_F} d^3 \underline{k} \int_{k' > p_F} d^3 \underline{k}' \frac{u(\underline{k} - \underline{k}'; 0) \delta(k_z - p_z)}{k'^2 + |\underline{k} - \underline{k}'|^2 - k^2} \quad , \quad (3.30)$$

$$R^{(0')} (p_z) = \frac{|W(g)|^2}{(2\pi)^3} \int_{\substack{k < p_F \\ |\underline{k} + \underline{g}| > p_F}} d^3 \underline{k} \frac{\delta(k_z + g_z - p_z)}{(|\underline{k} + \underline{g}|^2 - k^2)^2}, \quad (3.31)$$

$$R^{(c')} (p_z) = \frac{2|W(g)|^2}{(2\pi)^6} \int_{\substack{k < p_F \\ |\underline{k} + \underline{g}| > p_F}} d^3 \underline{k} \frac{\delta(k_z + g_z - p_z)}{|\underline{k} + \underline{g}|^2 - k^2}$$

$$\times \left[\int_{\substack{k' > p_F \\ |\underline{k}' + \underline{g}| > p_F}} \frac{d^3 \underline{k}' u(\underline{k} - \underline{k}'; 0)}{(k'^2 + |\underline{k} - \underline{k}'|^2 - k^2) (|\underline{k}' + \underline{g}|^2 + |\underline{k} - \underline{k}'|^2 - k^2)} \right.$$

$$- \int_{\substack{k' < p_F \\ |\underline{k}' - \underline{g}| > p_F}} \frac{d^3 \underline{k}' u(\underline{k} - \underline{k}' + \underline{g}; 0)}{(|\underline{k}' - \underline{g}|^2 - k'^2) (|\underline{k} - \underline{k}' + \underline{g}|^2 + |\underline{k}' - \underline{g}|^2 - k^2)}$$

$$- \int_{\substack{k' < p_F \\ |\underline{k}' + \underline{g}| > p_F}} \frac{d^3 \underline{k}' u(\underline{k} - \underline{k}'; 0)}{(|\underline{k}' + \underline{g}|^2 + |\underline{k} - \underline{k}'|^2 - k^2) (|\underline{k}' + \underline{g}|^2 - k'^2)}$$

$$+ \int_{\substack{k' < p_F \\ |\underline{k}' + \underline{g}| > p_F}} \frac{d^3 \underline{k}' u(\underline{k} - \underline{k}'; 0)}{(|\underline{k} + \underline{g}|^2 - k^2) (|\underline{k}' + \underline{g}|^2 + |\underline{k} - \underline{k}'|^2 - k^2)}$$

$$\left. + \int_{\substack{k' > p_F \\ |\underline{k}' + \underline{g}| > p_F}} \frac{d^3 \underline{k}' u(\underline{k} - \underline{k}'; 0)}{(|\underline{k} + \underline{g}|^2 - k^2) (|\underline{k}' + \underline{g}|^2 + |\underline{k} - \underline{k}'|^2 - k^2)} \right], \quad (3.32)$$

where the effective electron-positron interaction is expressed in terms of the Fermi-Thomas screening parameter of equation (2.65); that is,

$$u(q;0) = 4\pi e^2 / (q^2 + \lambda^2) \quad . \quad (3.33)$$

The overlap in the p_z direction of the Fermi spheres located at the origin and at g means that there is an overlap of the main central contribution and the lattice contribution which extends from $0.612 p_F$ to $2.612 p_F$. The enhancement factor for the region $p_z > p_F$ corresponds to equation (3.28), and is given by

$$\epsilon'(p_z) = R^{(c')} (p_z) / R^{(0')} (p_z) \quad . \quad (3.34)$$

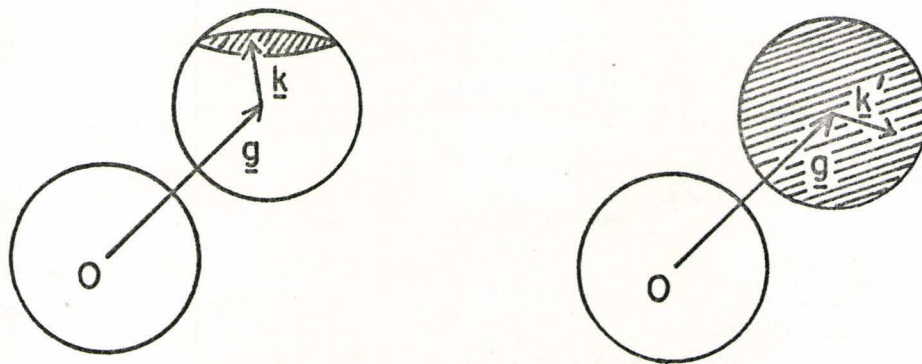
Since lattice effects are small, the enhancement factor for the region $p_z < p_F$ is essentially given by

$$\epsilon(p_z) = R^{(c)} (p_z) / R^{(0)} (p_z) \quad . \quad (3.35)$$

However, it is helpful to calculate the quantity $\epsilon'(p_z)$ for $p_z < p_F$. This quantity describes the enhancement due to positron-electron correlations of the contribution to the partial annihilation resulting from the presence of a crystal lattice and associated with the Fermi sphere at g .

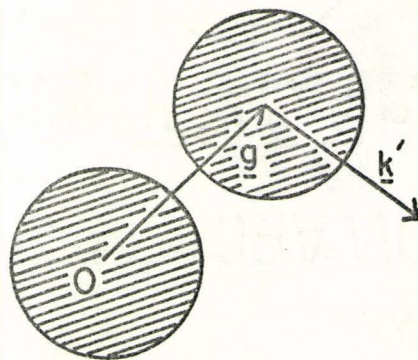
The regions of the \underline{k} - and \underline{k}' -integrations are described in figure (3.8). The \underline{k} -integration is actually an integration over a plane rather than a volume integral. All but the simplest integrations in equations (3.29) through

Figure 3.8 Regions of various \tilde{k} - and \tilde{k}' - integrations in equations (3.29) to (3.32). The shaded area in (a) is the area subtended in the Fermi sphere by a plane. The shaded regions of (a) and (b) represent regions of integration. The shaded areas in (c) represent the region of \tilde{k}' -space excluded from integration.



(a)

(b)



(c)

Figure 3.8

(3.32) were done by means of the Monte Carlo technique described, for example, by Shreider ⁽⁶⁴⁾. This method, which is useful for a multi-dimensional calculation, samples at random a region of n-dimensional space which contains the region of integration. An integral can be approximated by the product of the average value of the integrand and the volume of integration. Now, in the limit of a large sample,

$$\frac{n}{N} = \frac{V_R}{V} , \quad (3.36)$$

where n and N are the numbers of sampled points in the region of integration V_R and the sampled region V, respectively. Therefore, the integral is given approximately by

$$\begin{aligned} \int_R d^n x f(x) &= \bar{f} V_R \\ &= \frac{V}{N} \sum_{i=1}^n f(x_i) . \end{aligned} \quad (3.37)$$

For those terms in which the \tilde{k}' -integration extends to infinity, it is convenient to split the integration up into two regions. For $k' > 10 p_F$ it is assumed that k' is much larger than quantities such as k and λ , so that it is possible to do the \tilde{k}' -integration analytically. The enhancement factors ϵ and ϵ' are plotted in figures (3.9) and (3.10), respectively, for various values of p_z and $r_s = 4$.

Figure 3.9 First-order enhancement factor ϵ as a function of electron-positron momentum p_z for annihilation in an electron gas ($r_s=4$). The error bars describe the uncertainties associated with the Monte Carlo integration.

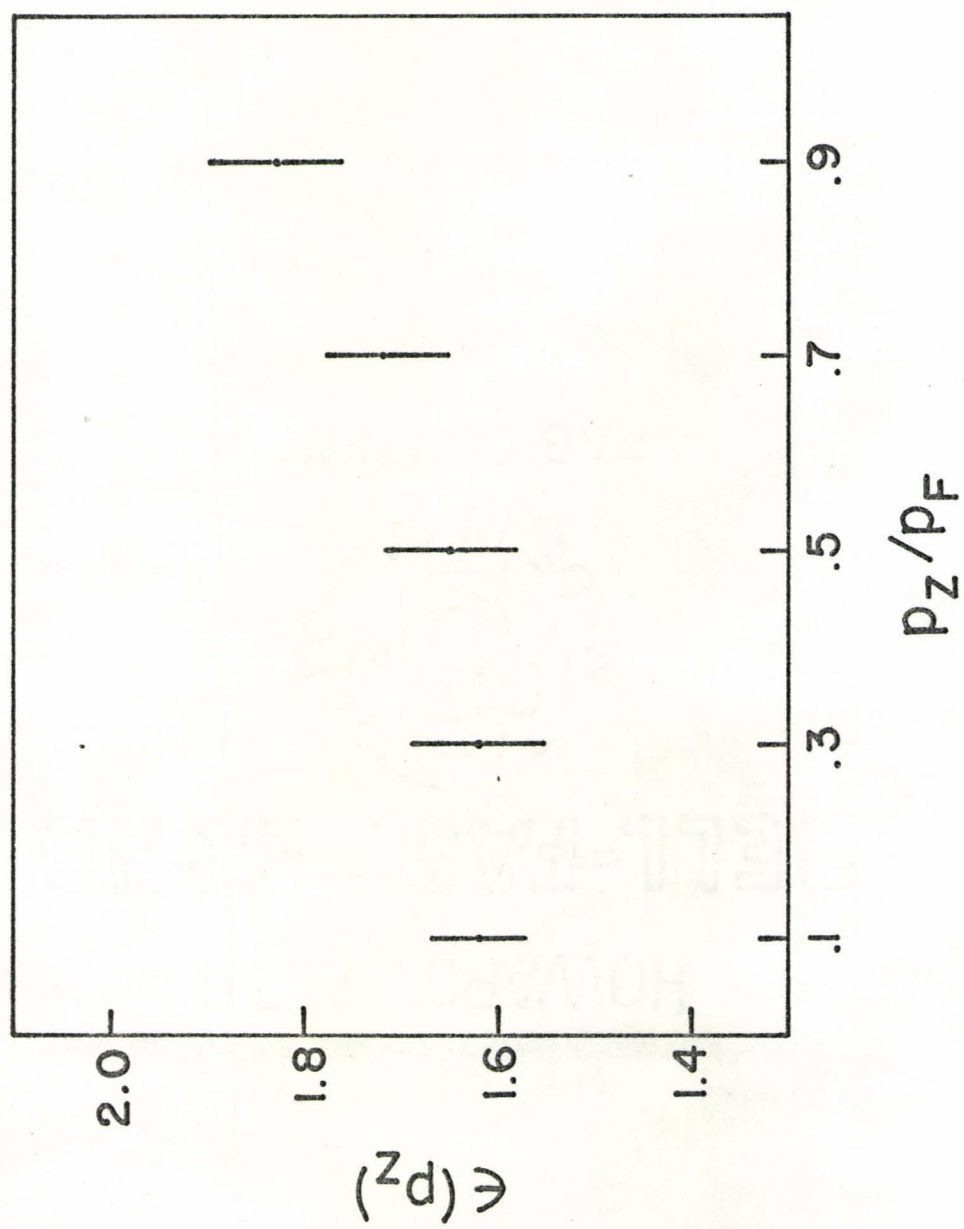


Figure 3.9

Figure 3.10

Variation with electron-positron

momentum component p_z of the first-order lattice enhancement factor ϵ' associated with contributions to the positron annihilation rate centred about the reciprocal lattice point at \underline{g} ($r_s=4$). The error bars give the uncertainties in the Monte Carlo integration.

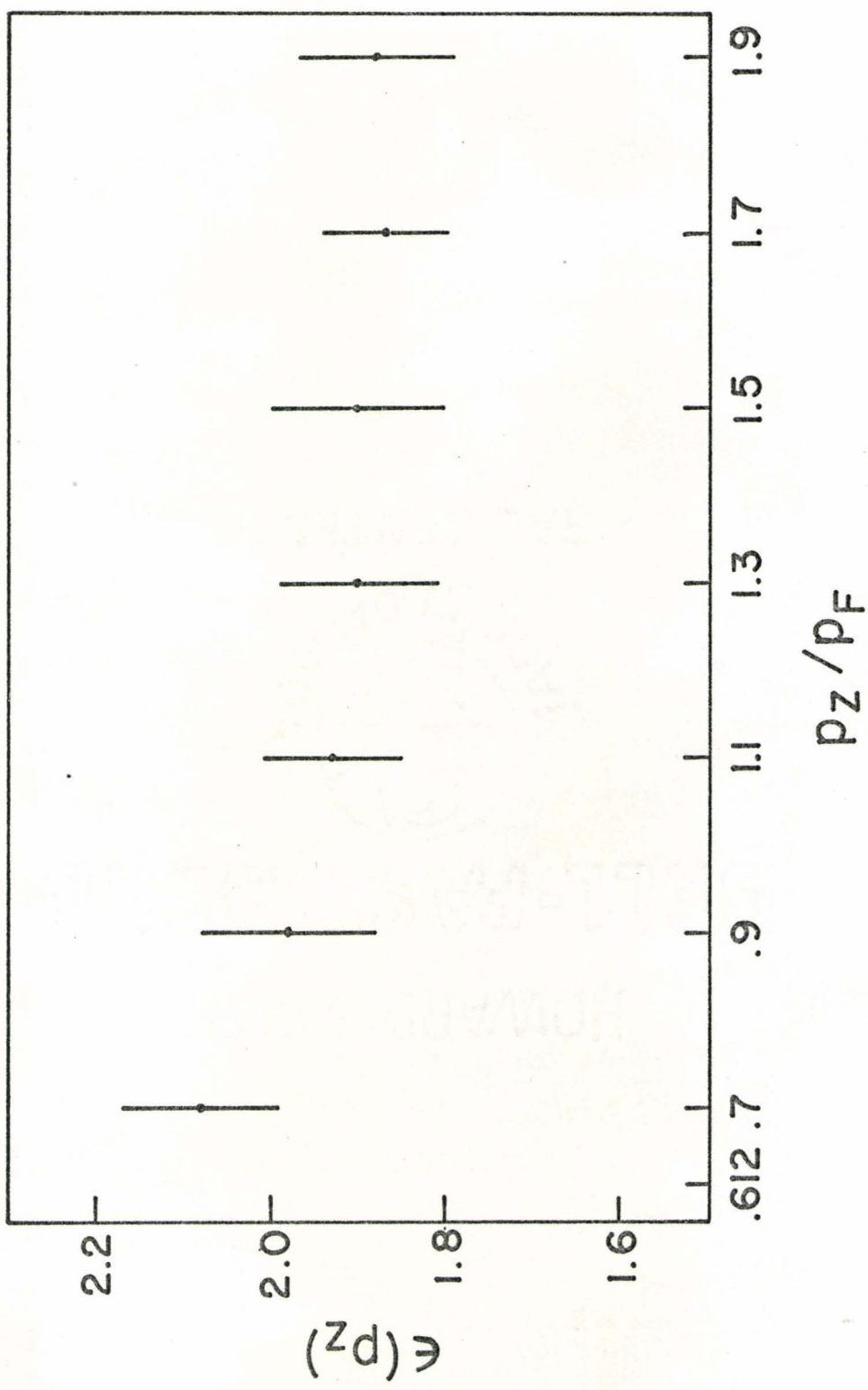


Figure 3.10

The positron partial annihilation rate in the absence of all interactions is the inverted parabola of equation (2.11) and figure (2.1). The effect of electron-positron correlations is to multiply this parabola by an enhancement factor. The enhancement factor due to the first-order ladder correlation, shown in figure (3.9) for a static potential and calculated by Carbotte and Kahana ⁽²⁶⁾ to include plasmons, has a slight momentum dependence. This results in a slightly distorted parabola that bulges out from a true parabolic shape. Such an effect is explained by the fact that electrons near the Fermi surface are more highly correlated with the positron. It is easier to scatter an electron near the Fermi surface. If all orders in the ladder diagrams are included, the momentum dependence and the distortion become slightly more pronounced ⁽²⁶⁾. The main difference, however, is just a greater enhancement. Experimental observations have been made of the momentum dependence for metals such as sodium ⁽⁶⁵⁾.

The lattice introduces a contribution to the annihilation rate that is connected with the Fermi spheres about reciprocal lattice points, in particular those about the nearest-neighbour R-L points, which extend from $0.612 p_F$ to $2.612 p_F$. The effect of correlations is to enhance this quantity in essentially the same way as the central parabola. There is an overall difference of about 15% from the magnitude

of the enhancement factor ϵ , but the momentum dependence near the edge of the Fermi sphere is very similar.

CHAPTER IV
SPIN-UP-SPIN-DOWN PAIR DISTRIBUTION FUNCTION AT
METALLIC DENSITIES

4.1 Short-range Correlations

The properties of the many-body system of an interacting electron gas at high densities ($r_s \ll 1$) have been adequately described by the random phase approximation. An outline of the properties is given by Pines (3,66), for example. At metallic densities, however, the RPA is no longer satisfactory, particularly in describing short-range phenomena (9,10), and it is not hard to see why. For instance, RPA ignores exchange effects in its treatment of correlations. Since correlations due to exchange act to keep electrons of parallel spin apart, they are an important feature of the small- r regime. Various attempts (13-16) to correct this deficiency of RPA are based on an approximation due to Hubbard (12) of a particular set of exchange diagrams in the perturbation expansion describing particle-particle interactions. However, these estimates all possess the feature of RPA at metallic densities of an unphysical negative value for the pair distribution function $g(\underline{r})$.

The spin-dependent p.d.f. $g_{\sigma\sigma}(\underline{x}-\underline{x}')$ describes the probability that, if there is an electron of spin σ at

position \underline{x} and time t , there is also an electron of spin σ' at position \underline{x}' and the same time t . It is defined by

$$g_{\sigma\sigma'}(\underline{x}-\underline{x}') = \langle \psi_{\sigma}^{\dagger}(\underline{x}, t) \psi_{\sigma}(\underline{x}, t) \psi_{\sigma'}^{\dagger}(\underline{x}', t) \psi_{\sigma'}(\underline{x}', t) \rangle , \quad (4.1)$$

where $\psi_{\sigma}(\underline{x}, t)$ is the field operator for an electron of spin σ and the expectation value is taken in the fully-interacting ground state of the electron system. The two-particle electron Green's function G_{ee} , which describes the propagation of a pair of electrons, is defined as

$$G_{ee}(x\sigma, x'\sigma'; y\sigma, y'\sigma') = (-i)^2 \langle T(\psi_{\sigma}(x) \times \psi_{\sigma'}(x') \psi_{\sigma'}^{\dagger}(y') \psi_{\sigma}^{\dagger}(y)) \rangle . \quad (4.2)$$

In terms of G_{ee} , the p.d.f. takes the form

$$g_{\sigma\sigma'}(\underline{x}-\underline{x}') = (-i)^2 G_{ee}(\underline{x}t\sigma, \underline{x}'t\sigma'; \underline{x}t^+\sigma, \underline{x}'t^+\sigma') . \quad (4.3)$$

The plus sign indicates the proper ordering of equal-time operators. The two-particle Green's function has the well-known perturbation expansion ⁽²⁷⁾ in terms of the free-electron propagator G_e^0 defined by equations (2.7) and (2.8a).

The difficulty with Hubbard's approximation is that it includes only local-field effects due to the exchange hole, while continuing to ignore the local-field correction

associated with the Coulomb hole. Similarly, RPA not only neglects exchange correlations but also ignores the Coulomb hole by treating the interaction in the Born approximation, which assumes the potential is small. It can be seen, however, that in the small- r limit even a screened potential such as the simple Fermi-Thomas potential $e^{-\lambda r}/r$ becomes very large. At metallic densities, where correlations are important and, in fact, interaction energies are comparable with kinetic energies, it becomes necessary to consider these correlations much more carefully than in RPA.

For a positron in an electron gas of metallic density, there is a considerable improvement in the electron density at the positron and, hence, in the total annihilation rate, if higher orders are included in addition to the first-order ladder correlation (25,26,67). These consist essentially of the remaining terms in the set of particle-particle ladder diagrams of figure (2.2). Such diagrams describe the repeated scattering of the charged particle off an electron in the presence of all the other electrons. In the problem of a light negatively-charged impurity in an electron gas examined by Carbotte (45), the Coulomb hole in the RPA resembles that found by Ueda (68) for the spin-up-spin-down p.d.f. $g_{\uparrow\downarrow}(\underline{r})$ in the same approximation. This reflects the fact that it is the Coulomb repulsion and not the Pauli principle which keeps opposite-spin electrons apart. When the full set of ladder diagrams is included, the Coulomb hole is much

improved over RPA. As shown in figure (4.1), the displaced electron density at the test charge is now reduced to a value less than the actual average charge density in the system over a wide range of the density parameter. It is expected that a similar procedure for opposite-spin electrons of including the complete set of particle-particle ladders of figure (4.2) would lead to a more adequate description of $g_{\uparrow\downarrow}(\tilde{r})$ at small r . The results of this problem, considered in the following sections, are to appear in a paper by Hede and Carbotte (69).

Figure 4.1 Displaced electron density at a light negative impurity as a function of electron gas density $\alpha = r_s / (1.919 \pi^2)$. The dashed curve is the RPA result. The solid curve is from the full ladder treatment. The vertical scale is read as negative for $\Delta n(0)$ and positive for n_{av} (from Carbotte (45)).

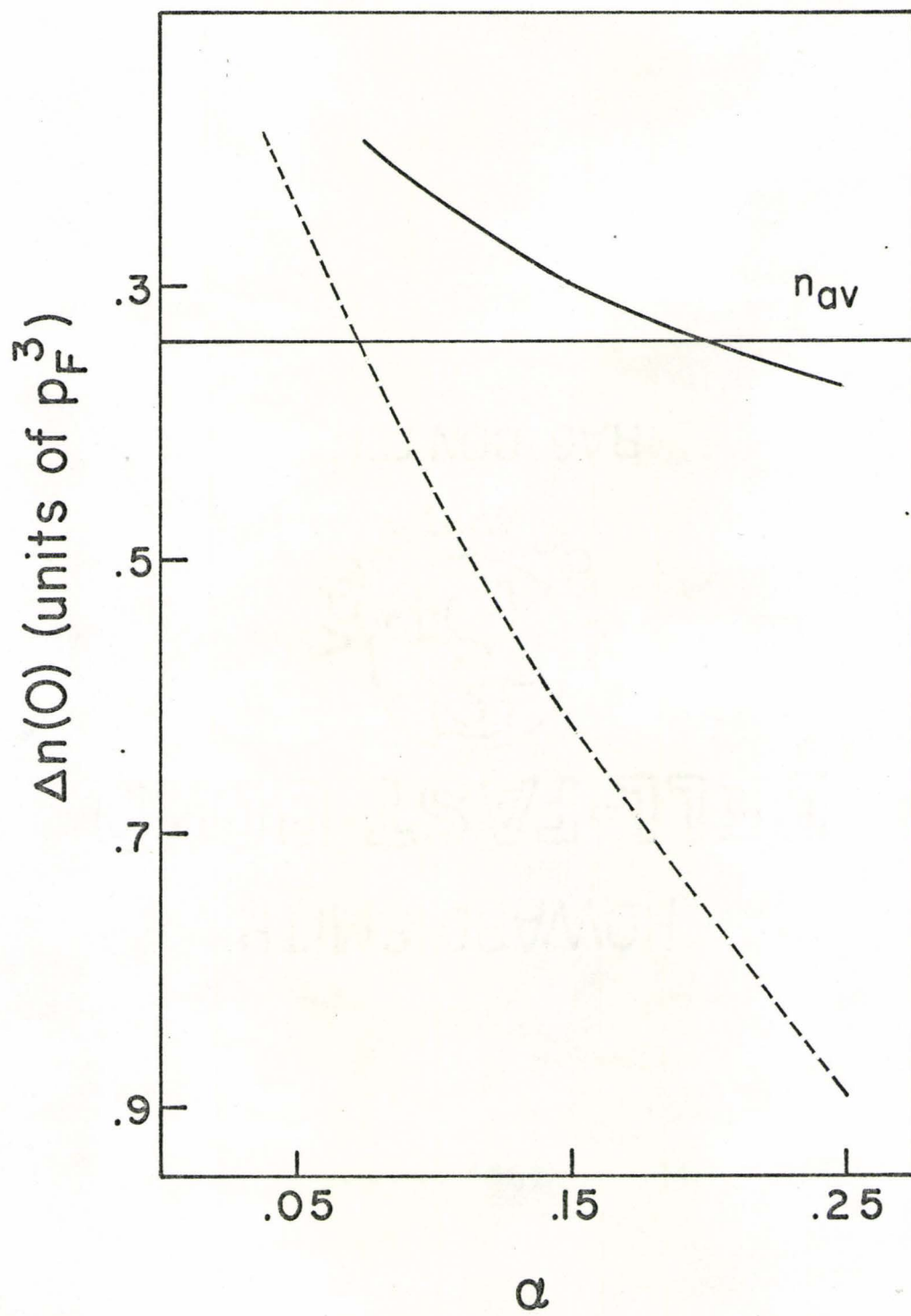
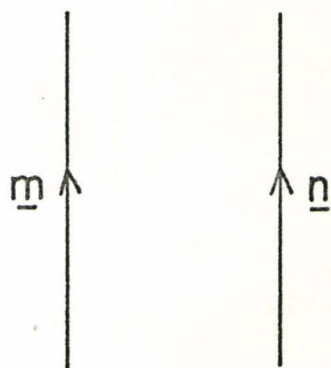
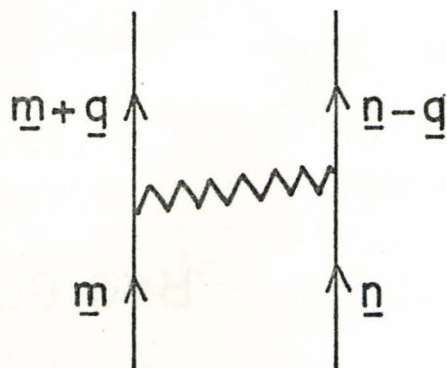


Figure 4.1

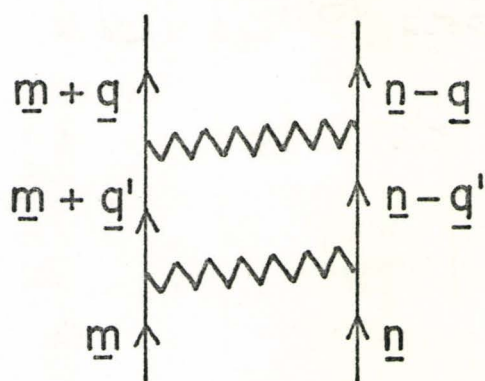
Figure 4.2 Members of the infinite set of ladder diagrams in the perturbation expansion for the electron-electron Green's function G_{ee} . The interaction lines represent the static limit of the effective potential in the random phase approximation.



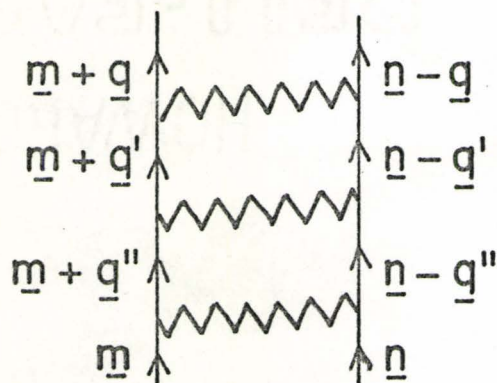
(a)



(b)



(c)



(d)

Figure 4.2

4.2 Ladder Contributions to the Pair Distribution Function

The lowest-order term in the perturbation expansion of the two-particle Green's function G_{ee} involves a simple product of G_e^0 's. Its contribution to the spin-up-spin-down p.d.f., denoted by $g_{\uparrow\downarrow}^0$, is simply

$$g_{\uparrow\downarrow}^0(\underline{x}-\underline{x}') = 2n^2, \quad (4.4)$$

where n is the average density of single-spin electrons and the factor of 2 accounts for the fact that $g_{\downarrow\uparrow}$ is the same as $g_{\uparrow\downarrow}$.

The higher-order terms in the expansion of G_{ee} describe correlations among the electrons; in particular, the first-order ladder graph leads to the RPA result. The contribution to $g(\underline{x}-\underline{x}')$ from such a term is

$$g_{\uparrow\downarrow}^{(1)}(\underline{x}-\underline{x}') = (-i)^2 (-i) \int d^4z d^4z' u(z; z') \\ \times G_e^0(\underline{x}t; z) G_e^0(\underline{x}'t; z') G_e^0(z; \underline{x}t^+) G_e^0(z'; \underline{x}'t^+). \quad (4.5)$$

$u(z; z')$ is the dynamic effective potential taken in the random phase approximation. Fourier transformation and integration over the space and time variables leads to the expression

$$g_{\uparrow\downarrow}^{(1)}(\underline{x}-\underline{x}') = \frac{-i}{V} \sum_{\underline{q}} e^{i\underline{q}\cdot(\underline{x}-\underline{x}')} \int \frac{d\varepsilon}{2\pi} u(\underline{q};\varepsilon) \times Q_0(\underline{q};\varepsilon) Q_0(-\underline{q};-\varepsilon) \quad , \quad (4.6)$$

where $Q_0(\underline{q};\varepsilon)$ is the polarization part given by

$$Q_0(\underline{q};\varepsilon) = \frac{i}{V} \sum_{\underline{k}} \int \frac{d\omega}{2\pi} G_e^0(\underline{k};\omega) G_e^0(\underline{k}-\underline{q};\omega-\varepsilon) \quad . \quad (4.7)$$

It can be seen from equation (4.7) that $Q_0(\underline{q};\varepsilon)$ satisfies the condition

$$Q_0(-\underline{q};-\varepsilon) = Q_0(\underline{q};\varepsilon) \quad . \quad (4.8)$$

Now, $u(\underline{q};\varepsilon)$ and $Q_0(\underline{q};\varepsilon)$ depend only on the magnitude of the vector \underline{q} . If the sum is changed to an integration, it is a simple matter to do the angular integration by letting the q_z -axis lie along the direction of $\underline{r} = \underline{x}-\underline{x}'$. Following the procedure outlined in the Appendix of reference (67), where the ε -integration is transformed to one along the imaginary axis, equation (4.6) reduces to

$$g_{\uparrow\downarrow}^{(1)}(r) = \frac{p_F^6}{32\pi^6} \int_0^\infty dq q^2 \frac{\sin qr}{r} \int_0^\infty \frac{d\varepsilon \alpha \bar{Q}_0(q;\varepsilon) \bar{Q}_0(q;\varepsilon)}{q^2 + \alpha \bar{Q}_0(q;\varepsilon)} \quad , \quad (4.9)$$

where

$$\begin{aligned} \bar{Q}_0(q; \epsilon) = 2\pi \left\{ 1 - \frac{1}{2q} \left[1 - \frac{1}{4}(q^2 - \epsilon^2) \ln \left(\frac{\epsilon^2 + (q-2)^2}{\epsilon^2 + (q+2)^2} \right) \right] \right. \\ \left. - \frac{\epsilon}{2} \left[\tan^{-1} \left(\frac{2-q}{\epsilon} \right) + \tan^{-1} \left(\frac{2+q}{\epsilon} \right) \right] \right\} . \end{aligned} \quad (4.10)$$

α is related to the parameter r_s according to

$$\alpha = r_s / 1.919 \pi^2 , \quad (4.11)$$

and all momenta in equations (4.9) and (4.10) are expressed in units of p_F .

It has been found that the infinite set of ladder diagrams in the perturbation of the particle-particle Green's function are of considerable importance in describing short-range correlations involving a charged impurity in an electron gas of metallic density. The ladder series of figure (4.2) describing repeated scattering between opposite-spin electrons is given by the integral equation

$$\begin{aligned} G_{ee}^L(x, x'; y, y') = G_e^0(x; y) G_e^0(x'; y') \\ - i \int d^4 z d^4 z' u(z; z') G_e^0(x; z) G_e^0(x'; z') \\ \times G_{ee}^L(z, z'; y, y') , \end{aligned} \quad (4.12)$$

where spin subscripts have been omitted. It should be noted that the potential is static, so that $t_{z'} = t_z$. In order to make the problem tractable, the dynamic potential, which is taken to be the RPA screened potential, is approximated by its static limit.

From the definition of equation (4.2), both $G_{ee}(\underline{x}t, \underline{x}'t; \underline{x}t^+, \underline{x}'t^+)$ and $g(\underline{x}-\underline{x}')$ are independent of time and depend only on the space variable $\underline{x}-\underline{x}'$. Denoting by g^L the ladder contribution to the p.d.f., its space Fourier transform can be expressed in terms of G_{ee}^L as

$$g^L(\underline{q}) = (-1) \int \frac{d\omega}{2\pi} e^{i\omega 0^+} G_{ee}^L(\underline{q}; \omega) \quad (4.13)$$

It is convenient to introduce a new amplitude Ω^L according to

$$\begin{aligned} G_{ee}^L(\underline{x}t, \underline{x}'t; \underline{x}t^+, \underline{x}'t^+) &= \int d^4z d^3z' \\ &\times \Omega^L(\underline{x}t, \underline{x}'t; z, z') G_e^0(z; \underline{x}t^+) G_e^0(z'; \underline{x}'t^+) \quad (4.14) \end{aligned}$$

This definition is consistent with equation (4.12). Ω^L can be shown to satisfy the integral equation

$$\begin{aligned} \Omega^L(\underline{x}, \underline{x}'; \underline{y}, \underline{y}') &= \delta^4(\underline{x}-\underline{y}) \delta^3(\underline{x}'-\underline{y}') - i \int d^4z d^3z' u(z; z') \\ &\times G_e^0(\underline{x}; z) G_e^0(\underline{x}'; z') \Omega^L(z, z'; \underline{y}, \underline{y}') \quad (4.15) \end{aligned}$$

and its Fourier transform satisfies the equation

$$\begin{aligned} \Omega_{\tilde{m}, \tilde{n}; \tilde{m}', \tilde{n}'}^L(\omega) &= \delta_{\tilde{m}, \tilde{m}'} \delta_{\tilde{n}, \tilde{n}'} + [p_{\tilde{m}, \tilde{n}}^+(\omega) + p_{\tilde{m}, \tilde{n}}^-(\omega)] \\ &\times \sum_{\tilde{k}, \tilde{k}'} u_{\tilde{m}, \tilde{n}; \tilde{k}, \tilde{k}'} \Omega_{\tilde{k}, \tilde{k}'; \tilde{m}', \tilde{n}'}^L(\omega) \quad , \quad (4.16) \end{aligned}$$

where the quantities $p_{\tilde{m}, \tilde{n}}^+(\omega)$ and $p_{\tilde{m}, \tilde{n}}^-(\omega)$ are given, respectively, by

$$p_{\tilde{m}, \tilde{n}}^+(\omega) = \frac{\theta(m-p_F) \theta(n-p_F)}{m^2 + n^2 - \omega - i0^+} \quad (4.17a)$$

and

$$p_{\tilde{m}, \tilde{n}}^-(\omega) = \frac{-\theta(p_F-m) \theta(p_F-n)}{m^2 + n^2 - \omega + i0^+} \quad . \quad (4.17b)$$

This leads to the expression

$$\begin{aligned} g^L(\underline{q}) &= \frac{-i}{V} \sum_{\tilde{m}, \tilde{n}} \int \frac{d\omega}{2\pi} e^{i\omega 0^+} \Omega_{\tilde{m}+\underline{q}, \tilde{n}-\underline{q}; \tilde{m}, \tilde{n}}^L(\omega) \\ &\times [p_{\tilde{m}, \tilde{n}}^+(\omega) + p_{\tilde{m}, \tilde{n}}^-(\omega)] \quad . \quad (4.18) \end{aligned}$$

In order to do the ω -integration in equation (4.18), the product $\Omega^L(p^+ + p^-)$ is expanded to obtain terms in the integrand which have the symbolic form

$$e^{i\omega 0^+} (P^+ + P^-) U(P^+ + P^-) \dots U(P^+ + P^-) \quad . \quad (4.19)$$

In the case of the term involving only a single factor $(P^+ + P^-)$, just P^- contributes through contour integration in the upper half plane. For the other terms a further expansion leads, in the case of n factors $(P^+ + P^-)$, to a sum of 2^n products

$$PUP \dots UP \quad , \quad (4.20)$$

where each of the P 's can be either P^+ or P^- . The product P^+UP^- , say, describes the scattering of two particles in the Fermi sea to states outside the Fermi sea, as illustrated by figure (4.3). Depending on there being another P^+ or P^- factor, there can then be a scattering to other excited states or to hole states, respectively. Now, the number of hole states is restricted, while the number of states outside the Fermi sea is essentially unlimited. From this simple phase space argument, it is expected that the contribution from terms containing more than one P^- factor is negligible compared to that from terms where all but one of the P 's is P^+ . The significance of making such an approximation is the neglect of hole-hole scattering.

An amplitude Ω^0 and its conjugate Ω^{0+} are now introduced by the equations

$$\Omega^0 = 1 + P^+U\Omega^0 \quad , \quad (4.21a)$$

Figure 4.3

Various scattering processes associated with a pair of electrons initially in the Fermi sea. Process A describes the scattering of the two particles outside the Fermi sea. Process B scatters the two particles to other states outside the Fermi sea. Process C involves scattering of the holes left in the Fermi sea by the electrons.

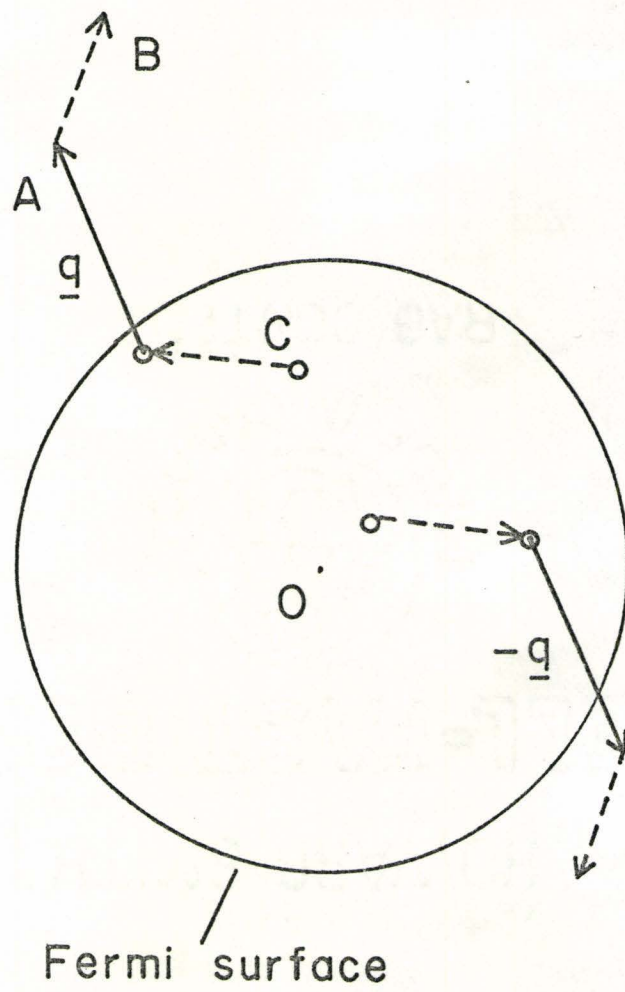


Figure 4.3

$$\Omega^{0\dagger} = 1 + \Omega^{0\dagger} U P^+ \quad . \quad (4.21b)$$

Ignoring hole-hole scattering, as discussed above, means that the product $\Omega^L(P^+ + P^-)$ can be approximated by $\Omega^0 P^- \Omega^{0\dagger}$.

Equation (4.18) can be rewritten as

$$g^L(\underline{q}) = \frac{1}{V} \sum_{\underline{m}\underline{n}} \sum_{\underline{m}'\underline{n}'} \int \frac{d\omega}{2\pi} e^{i\omega 0^+} \Omega_{\underline{m}+\underline{q}, \underline{n}-\underline{q}; \underline{m}', \underline{n}'}^0(\omega) \\ \times p_{\underline{m}', \underline{n}'}^-(\omega) (\Omega^0)_{\underline{m}', \underline{n}'; \underline{m}, \underline{n}}^+(\omega) \quad , \quad (4.22)$$

where $\Omega_{\underline{m}, \underline{n}; \underline{m}', \underline{n}'}^0$, according to equation (4.21a), satisfies the equation

$$\Omega_{\underline{m}, \underline{n}; \underline{m}', \underline{n}'}^0(\omega) = \delta_{\underline{m}, \underline{m}'} \delta_{\underline{n}, \underline{n}'} + p_{\underline{m}, \underline{n}}^+(\omega) \sum_{\underline{q}'} u(\underline{q}'; 0) \\ \times \Omega_{\underline{m}+\underline{q}', \underline{n}-\underline{q}'; \underline{m}', \underline{n}'}^0(\omega) \quad . \quad (4.23)$$

The ω -integration is performed by means of a contour integration to give

$$g^L(\underline{q}) = \frac{1}{V} \sum_{\underline{m}\underline{n}} \sum_{\underline{m}'} \sum_{\substack{\underline{n}' \\ m' < p_F \\ n' < p_F}} \Omega_{\underline{m}, \underline{n}; \underline{m}', \underline{n}'}^0(m'^2 + n'^2) \\ \times \Omega_{\underline{m}+\underline{q}, \underline{n}-\underline{q}; \underline{m}', \underline{n}'}^0(m'^2 + n'^2) \quad . \quad (4.24)$$

The zeroth- and first-order terms in $g^L(q)$ are handled easily, as in section 4.2, so these contributions are subtracted from $g^L(q)$ to leave a quantity which is referred to as $g^{L2}(q)$. It can be derived by keeping one of the Ω^0 factors to zeroth-order and the other to second- and higher-order or by taking both factors down to first-order in u . $g^{L2}(q)$ can be written in terms of a new quantity X as

$$g^{L2}(q) = \frac{1}{V} \sum_{\substack{\tilde{m} \\ m < p_F}} \sum_{\substack{\tilde{n} \\ n < p_F}} [X_{\tilde{m}+q, \tilde{n}-q; \tilde{m}, \tilde{n}}^{(2)} + X_{\tilde{m}-q, \tilde{n}+q; \tilde{m}, \tilde{n}}^{(2)} \\ + \sum_{q'} X_{\tilde{m}+q+q', \tilde{n}-q-q'; \tilde{m}, \tilde{n}} X_{\tilde{m}+q', \tilde{n}-q'; \tilde{m}, \tilde{n}}] , \quad (4.25)$$

where $X_{\tilde{m}+q, \tilde{n}-q; \tilde{m}, \tilde{n}}$ is defined by

$$X_{\tilde{m}+q, \tilde{n}-q; \tilde{m}, \tilde{n}} = \frac{\theta(|\tilde{m}+q| - p_F) \theta(|\tilde{n}-q| - p_F)}{|\tilde{m}+q|^2 + |\tilde{n}-q|^2 - m^2 - n^2} Y_{\tilde{m}+q, \tilde{n}-q; \tilde{m}, \tilde{n}} , \quad (4.26)$$

while $Y_{\tilde{m}+q, \tilde{n}-q; \tilde{m}, \tilde{n}}$ satisfies the integral equation

$$Y_{\tilde{m}+q, \tilde{n}-q; \tilde{m}, \tilde{n}} = \frac{1}{V} u(q; 0) + \frac{1}{V} \sum_{q'} u(q-q'; 0) \\ \times \frac{\theta(|\tilde{m}+q'| - p_F) \theta(|\tilde{n}-q'| - p_F)}{|\tilde{m}+q'|^2 + |\tilde{n}-q'|^2 - m^2 - n^2} \\ \times Y_{\tilde{m}+q', \tilde{n}-q'; \tilde{m}, \tilde{n}} . \quad (4.27)$$

$x_{\tilde{m}+\tilde{q},\tilde{n}-\tilde{q};\tilde{m},\tilde{n}}^{(2)}$ in equation (4.25) is the second- and higher-order part of $x_{\tilde{m}+\tilde{q},\tilde{n}-\tilde{q};\tilde{m},\tilde{n}}$. The first two terms in equation (4.25) are equal.

4.3 Particle-hole Scattering

The Bethe-Goldstone ⁽⁴⁶⁾ equation (4.27) describes the scattering of the ladder diagrams of figure (4.2). The contribution to the scattering amplitude $Y_{\underline{m}+\underline{q}, \underline{n}-\underline{q}; \underline{m}, \underline{n}}$ from these diagrams is described in equation (4.28) as follows: for figure (4.2b),

$$\frac{1}{V} u(\underline{q}) \quad ; \quad (4.28a)$$

for figure (4.2c),

$$\frac{1}{V^2} \sum_{\underline{q}'} \frac{\theta(|\underline{m}+\underline{q}'| - p_F) \theta(|\underline{n}-\underline{q}'| - p_F) u(\underline{q}') u(\underline{q}-\underline{q}')}{|\underline{m}+\underline{q}'|^2 + |\underline{n}-\underline{q}'|^2 - m^2 - n^2} \quad ; \quad (4.28b)$$

for figure (4.2d),

$$\frac{1}{V^3} \sum_{\underline{q}', \underline{q}''} \frac{\theta(|\underline{m}+\underline{q}'| - p_F) \theta(|\underline{n}-\underline{q}'| - p_F)}{|\underline{m}+\underline{q}'|^2 + |\underline{n}-\underline{q}'|^2 - m^2 - n^2} \\ \times \frac{\theta(|\underline{m}+\underline{q}''| - p_F) \theta(|\underline{n}-\underline{q}''| - p_F) u(\underline{q}') u(\underline{q}''-\underline{q}') u(\underline{q}-\underline{q}'')}{|\underline{m}+\underline{q}''|^2 + |\underline{n}-\underline{q}''|^2 - m^2 - n^2} \quad . \quad (4.28c)$$

The ladder approximation ignores hole-hole scattering events, as discussed above. In addition, it fails to account for scattering between a particle and a hole. The theory can easily be extended to include such events by

following the procedure of Kanazawa et al. (70) who included positron-electron hole interactions in a calculation of positron annihilation rates. An additional infinite set of diagrams is introduced in figure (4.4). The contribution of these diagrams to the scattering matrix $Y_{\tilde{m}+\tilde{q}, \tilde{n}-\tilde{q}; \tilde{m}, \tilde{n}}$ is given as follows:

for figure (4.4a),

$$- \frac{1}{v^2} \sum_{\tilde{q}'} \frac{\theta(|\tilde{m}+\tilde{q}| - p_F) \theta(|\tilde{n}-\tilde{q}+\tilde{q}'| - p_F) u(\tilde{q}') u(\tilde{q}-\tilde{q}')}{|\tilde{m}+\tilde{q}|^2 + |\tilde{n}-\tilde{q}+\tilde{q}'|^2 - |\tilde{m}+\tilde{q}'|^2 - n^2} ; \quad (4.29a)$$

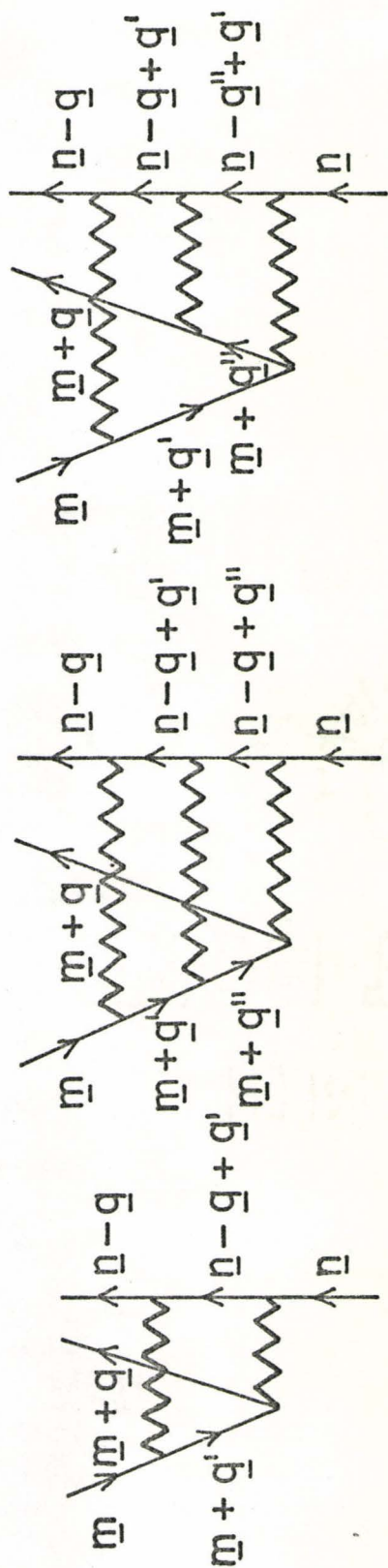
for figure (4.4b),

$$- \frac{1}{v^3} \sum_{\tilde{q}' \tilde{q}''} u(\tilde{q}') u(\tilde{q}'' - \tilde{q}') u(\tilde{q} - \tilde{q}'') \\ \times \frac{\theta(|\tilde{m}+\tilde{q}| - p_F) \theta(|\tilde{n}-\tilde{q}+\tilde{q}'| - p_F) \theta(|\tilde{m}+\tilde{q}| - p_F) \theta(|\tilde{n}-\tilde{q}+\tilde{q}''| - p_F)}{(|\tilde{m}+\tilde{q}|^2 + |\tilde{n}-\tilde{q}+\tilde{q}'|^2 - |\tilde{m}+\tilde{q}'|^2 - n^2) (|\tilde{m}+\tilde{q}''|^2 + |\tilde{n}-\tilde{q}+\tilde{q}''|^2 - |\tilde{m}+\tilde{q}''|^2 - n^2)} ; \quad (4.29b)$$

for figure (4.4c),

$$- \frac{1}{v^3} \sum_{\tilde{q}' \tilde{q}''} u(\tilde{q}') u(\tilde{q}'' - \tilde{q}') u(\tilde{q} - \tilde{q}'') \\ \times \frac{\theta(|\tilde{m}+\tilde{q}''| - p_F) \theta(|\tilde{n}-\tilde{q}''+\tilde{q}'| - p_F) \theta(|\tilde{m}+\tilde{q}| - p_F) \theta(|\tilde{n}-\tilde{q}+\tilde{q}'| - p_F)}{(|\tilde{m}+\tilde{q}''|^2 + |\tilde{n}-\tilde{q}''+\tilde{q}'|^2 - |\tilde{m}+\tilde{q}'|^2 - n^2) (|\tilde{m}+\tilde{q}|^2 + |\tilde{n}-\tilde{q}+\tilde{q}'|^2 - |\tilde{m}+\tilde{q}'|^2 - n^2)} ; \quad (4.29c)$$

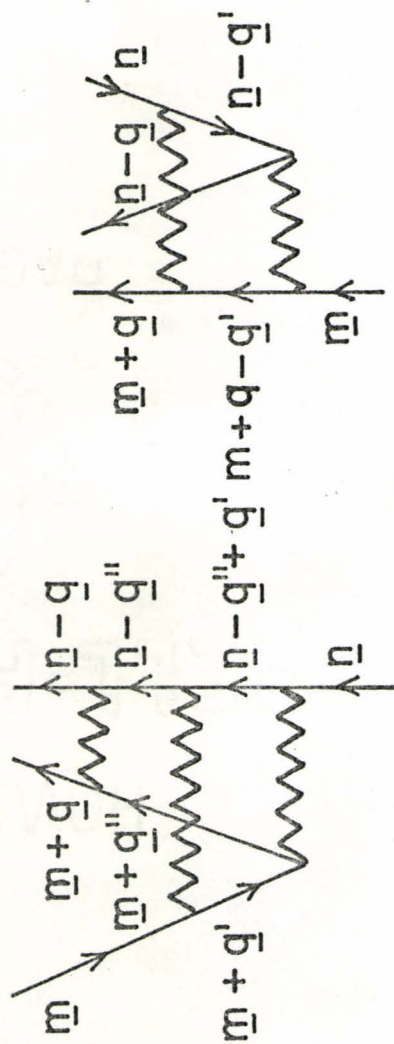
Figure 4.4 Members of an infinite set of diagrams
in the perturbation expansion for the two-
particle Green's function G_{ee} describing
particle-hole scattering.



(a)

(b)

(c)



(d)

(e)

Figure 4.4

for figure (4.4d),

$$\begin{aligned}
 & - \frac{1}{V^3} \sum_{\underline{q}' \underline{q}''} u(\underline{q}') u(\underline{q}'' - \underline{q}') u(\underline{q} - \underline{q}'') \\
 & \frac{\theta(|\underline{m} + \underline{q}''| - p_F) \theta(|\underline{n} - \underline{q}'' + \underline{q}'| - p_F) \theta(|\underline{m} + \underline{q}''| - p_F) \theta(|\underline{n} - \underline{q}''| - p_F)}{(|\underline{m} + \underline{q}''|^2 + |\underline{n} - \underline{q}'' + \underline{q}'|^2 - |\underline{m} + \underline{q}'|^2 - n^2) (|\underline{m} + \underline{q}''|^2 + |\underline{n} - \underline{q}''|^2 - m^2 - n^2)} ; \\
 & \hspace{15em} (4.29d)
 \end{aligned}$$

for figure (4.4e),

$$- \frac{1}{V^2} \sum_{\underline{q}'} \frac{\theta(|\underline{m} + \underline{q} - \underline{q}'| - p_F) \theta(|\underline{n} - \underline{q}| - p_F) u(\underline{q}') u(\underline{q} - \underline{q}')}{|\underline{m} + \underline{q} - \underline{q}'|^2 + |\underline{n} - \underline{q}|^2 - m^2 - |\underline{n} - \underline{q}'|^2} . \quad (4.29e)$$

The Bethe-Goldstone equation can then be rewritten as

$$\begin{aligned}
 Y_{\underline{m} + \underline{q}, \underline{n} - \underline{q}; \underline{m}, \underline{n}} &= \frac{1}{V} u(\underline{q}) \\
 + \frac{1}{V} \sum_{\underline{q}'} & \frac{u(\underline{q} - \underline{q}') \theta(|\underline{m} + \underline{q}'| - p_F) \theta(|\underline{n} - \underline{q}'| - p_F)}{|\underline{m} + \underline{q}'|^2 + |\underline{n} - \underline{q}'|^2 - m^2 - n^2} Y_{\underline{m} + \underline{q}', \underline{n} - \underline{q}'; \underline{m}, \underline{n}} \\
 - \frac{1}{V} \sum_{\underline{q}'} & \frac{u(\underline{q}') \theta(|\underline{m} + \underline{q}| - p_F) \theta(|\underline{n} - \underline{q} + \underline{q}'| - p_F)}{|\underline{m} + \underline{q}|^2 + |\underline{n} - \underline{q} + \underline{q}'|^2 - |\underline{m} + \underline{q}'|^2 - n^2} Y_{\underline{m} + \underline{q}, \underline{n} - \underline{q} + \underline{q}'; \underline{m} + \underline{q}', \underline{n}} \\
 - \frac{1}{V} \sum_{\underline{q}'} & \frac{u(\underline{q}') \theta(|\underline{m} + \underline{q} - \underline{q}'| - p_F) \theta(|\underline{n} - \underline{q}| - p_F)}{|\underline{m} + \underline{q} - \underline{q}'|^2 + |\underline{n} - \underline{q}|^2 - m^2 - |\underline{n} - \underline{q}'|^2} Y_{\underline{m} + \underline{q} - \underline{q}', \underline{n} - \underline{q}; \underline{m}, \underline{n} - \underline{q}'} , \\
 & \hspace{15em} (4.30)
 \end{aligned}$$

where the last two terms are new terms introducing particle-hole interactions into the scattering problem.

4.4 Calculation of Pair Distribution Function

In order to make a calculation, the limit of infinite volume is taken in equations (4.25) and (4.30). The contribution to the p.d.f. from second- and higher-order terms is then written in the form

$$\begin{aligned}
 g^{L2}(\underline{r}) = & \frac{2p_F^6}{(2\pi)^6} \int d^3\tilde{q} e^{i\tilde{q}\cdot\underline{r}} \int_{m < p_F} \int_{n < p_F} d^3\tilde{m} d^3\tilde{n} \\
 & \times [2X_{\tilde{m}+\tilde{q}, \tilde{n}-\tilde{q}; \tilde{m}, \tilde{n}}^{(2)} + \int d^3\tilde{q}' \\
 & \times X_{\tilde{m}+\tilde{q}', \tilde{n}-\tilde{q}'; \tilde{m}, \tilde{n}} X_{\tilde{m}+\tilde{q}+\tilde{q}', \tilde{n}-\tilde{q}-\tilde{q}'; \tilde{m}, \tilde{n}}] \quad , \quad (4.31)
 \end{aligned}$$

where $X_{\tilde{m}+\tilde{q}, \tilde{n}-\tilde{q}; \tilde{m}, \tilde{n}}$ is given in terms of $Y_{\tilde{m}+\tilde{q}, \tilde{n}-\tilde{q}; \tilde{m}, \tilde{n}}$ by equation (4.26) and $Y_{\tilde{m}+\tilde{q}, \tilde{n}-\tilde{q}; \tilde{m}, \tilde{n}}$ satisfies the equation

$$\begin{aligned}
 Y_{\tilde{m}+\tilde{q}, \tilde{n}-\tilde{q}; \tilde{m}, \tilde{n}} = & U(\tilde{q}) \\
 + \int & \frac{d^3\tilde{q}' U(\tilde{q}-\tilde{q}') \theta(|\tilde{m}+\tilde{q}'| - p_F) \theta(|\tilde{n}-\tilde{q}'| - p_F)}{|\tilde{m}+\tilde{q}'|^2 + |\tilde{n}-\tilde{q}'|^2 - m^2 - n^2} Y_{\tilde{m}+\tilde{q}', \tilde{n}-\tilde{q}'; \tilde{m}, \tilde{n}} \\
 - \int & \frac{d^3\tilde{m}' U(\tilde{m}-\tilde{m}') \theta(|\tilde{m}+\tilde{q}| - p_F) \theta(|\tilde{m}' - \tilde{m} + \tilde{n} - \tilde{q}| - p_F)}{|\tilde{m}+\tilde{q}|^2 + |\tilde{m}' - \tilde{m} + \tilde{n} - \tilde{q}|^2 - m'^2 - n^2} Y_{\tilde{m}+\tilde{q}, \tilde{m}' - \tilde{m} + \tilde{n} - \tilde{q}; \tilde{m}', \tilde{n}} \\
 - \int & \frac{d^3\tilde{n}' U(\tilde{n}-\tilde{n}') \theta(|\tilde{n}' - \tilde{n} + \tilde{m} + \tilde{q}| - p_F) \theta(|\tilde{n}-\tilde{q}| - p_F)}{|\tilde{n}' - \tilde{n} + \tilde{m} + \tilde{q}|^2 + |\tilde{n}-\tilde{q}|^2 - m^2 - n'^2} Y_{\tilde{n}' - \tilde{n} + \tilde{m} + \tilde{q}, \tilde{n}-\tilde{q}; \tilde{m}, \tilde{n}'} \quad (4.32)
 \end{aligned}$$

$U(\underline{q})$ now has the form

$$U(\underline{q}) = \alpha / (q^2 + \alpha Q_0(\underline{q})) \quad , \quad (4.33)$$

with

$$Q_0(\underline{q}) = 2\pi \left[1 + \frac{1}{2q} \left(1 - \frac{1}{4} q^2 \right) \ln \left(\frac{q+2}{q-2} \right)^2 \right] \quad . \quad (4.34)$$

All momenta in equations (4.31) through (4.34) are in units of p_F .

In their present form, equations (4.31), (4.26) and (4.32) present a considerable numerical problem. It is noted that in the case where \underline{m} and \underline{n} are both zero vectors, $X_{\underline{m}+\underline{q}, \underline{n}-\underline{q}; \underline{m}, \underline{n}}$ and $Y_{\underline{m}+\underline{q}, \underline{n}-\underline{q}; \underline{m}, \underline{n}}$ depend only on the modulus of \underline{q} . For finite \underline{m} and \underline{n} , the situation is complicated by the presence of vectors $\underline{m}+\underline{q}$ and $\underline{n}-\underline{q}$ but it can be simplified by making the approximation of an average over the angles of \underline{m} and \underline{n} . Such an angle-averaging process was carried out with considerable success by Kahana (25,71) and Carbotte (67) in a similar problem. The angle-averaged quantity $\hat{X}_{\underline{m}+\underline{q}, \underline{n}-\underline{q}; \underline{m}, \underline{n}}$ is then described by

$$\hat{X}_{\underline{m}+\underline{q}, \underline{n}-\underline{q}; \underline{m}, \underline{n}} = \left\langle \frac{\theta(|\underline{m}+\underline{q}| - p_F) \theta(|\underline{n}-\underline{q}| - p_F)}{|\underline{m}+\underline{q}|^2 + |\underline{n}-\underline{q}|^2 - m^2 - n^2} \right\rangle \hat{Y}_{\underline{m}+\underline{q}, \underline{n}-\underline{q}; \underline{m}, \underline{n}} \quad (4.35)$$

On introducing the variables ρ and η by

$$\rho^2 = |m+q|^2 \quad (4.36a)$$

and

$$\eta^2 = |n-q|^2, \quad (4.36b)$$

the first averaged quantity on the right side of equation (4.35), denoted by $1/4 f(m,n,q)$, can be reduced to the form

$$\frac{1}{4} f(m,n,q) = \frac{1}{4mnq^2} \int_{\eta > p_F} d\eta \int_{\rho > p_F} \frac{d\rho}{\rho^2 + \eta^2 - m^2 - n^2}. \quad (4.37)$$

It is shown in Appendix D that the particle-hole contributions in the equation for $\hat{Y}_{\underline{m}+\underline{q}, \underline{n}-\underline{q}; \underline{m}, \underline{n}}$ can be neglected to quite a good approximation. Then, $\hat{Y}_{\underline{m}+\underline{q}, \underline{n}-\underline{q}; \underline{m}, \underline{n}}$ satisfies the equation

$$\begin{aligned} \hat{Y}_{\underline{m}+\underline{q}, \underline{n}-\underline{q}; \underline{m}, \underline{n}} &= U(\underline{q}) + \frac{\pi}{2q} \int_0^\infty dq' q' f(m,n,q') \\ &\times \hat{Y}_{\underline{m}+\underline{q}', \underline{n}-\underline{q}'; \underline{m}, \underline{n}} \int_{|q-q'|}^{|q+q'|} dx x U(x). \quad (4.38) \end{aligned}$$

In this angle-averaged approximation, it is quite a simple matter to the q -angle integration in equation (4.31). $g^{L2}(\underline{r})$ can be written as

$$\begin{aligned}
g^{L2}(r) &= \frac{2p_F^6}{\pi^3 r} \int_0^\infty dq q^2 \sin qr \int_0^1 dn n^2 \int_0^1 dm m^2 \\
&\times [2\hat{X}_{\underline{m}+\underline{q}, \underline{n}-\underline{q}; \underline{m}, \underline{n}}^{(2)} + \int d^3 \underline{q}' \\
&\times \hat{X}_{\underline{m}+\underline{q}', \underline{n}-\underline{q}'; \underline{m}, \underline{n}} \hat{X}_{\underline{m}+\underline{q}+\underline{q}', \underline{n}-\underline{q}-\underline{q}'; \underline{m}, \underline{n}}] \quad (4.39)
\end{aligned}$$

The quantity in square brackets in equation (4.39) can be expressed in terms of $\hat{Y}_{\underline{m}+\underline{q}, \underline{n}-\underline{q}; \underline{m}, \underline{n}}$ as

$$\begin{aligned}
&\frac{\pi}{4} \frac{f(m, n, q)}{q} \int_0^\infty dq' q' f(m, n, q') \\
&\times \hat{Y}_{\underline{m}+\underline{q}', \underline{n}-\underline{q}'; \underline{m}, \underline{n}} \int_{|\underline{q}-\underline{q}'|}^{\underline{q}+\underline{q}'} dx x U(x) \\
&+ \frac{\pi}{8} \int_0^\infty dq' q'^2 f(m, n, q') \hat{Y}_{\underline{m}+\underline{q}', \underline{n}-\underline{q}'; \underline{m}, \underline{n}} \\
&\times \int_1^{-1} d\mu_q f(m, n, |\underline{q}+\underline{q}'|) \hat{Y}_{\underline{m}+\underline{q}+\underline{q}', \underline{n}-\underline{q}-\underline{q}'; \underline{m}, \underline{n}} \quad (4.40)
\end{aligned}$$

In $\hat{X}_{\underline{m}+\underline{q}+\underline{q}', \underline{n}-\underline{q}-\underline{q}'; \underline{m}, \underline{n}}$, \underline{m} and \underline{n} are averaged with respect to the direction of $\underline{q}+\underline{q}'$. On introducing the variable $\underline{x} = \underline{q}+\underline{q}'$, the second part of equation (4.40) reduces to

$$\begin{aligned}
&\frac{\pi}{8q} \int_0^\infty dq' q' f(m, n, q') \hat{Y}_{\underline{m}+\underline{q}', \underline{n}-\underline{q}'; \underline{m}, \underline{n}} \\
&\times \int_{|\underline{q}-\underline{q}'|}^{\underline{q}+\underline{q}'} dx x f(m, n, x) \hat{Y}_{\underline{m}+\underline{x}, \underline{n}-\underline{x}; \underline{m}, \underline{n}} \quad (4.41)
\end{aligned}$$

The integral equation (4.38) for $\hat{Y}_{\tilde{m}+\tilde{q}, \tilde{n}-\tilde{q}, \tilde{m}, \tilde{n}}$ was calculated by introducing a grid of variable size up to 75 points extending from a minimum that satisfies the conditions $m+q>1$ and $n+q>1$ up to 40. This led to a set of inhomogeneous linear equations which were solved by the gauss elimination method. The computation was carried out for electron gas densities corresponding to $\alpha = .1, .2$ and $.3$, in each case for 11 values of m and n between 0 and 1. A 301-point grid between 0 and 40 was introduced for the q -integral in equation (4.39). For a particular density and q -value, the corresponding m -, n -, q '- and x -integrations in equations (4.39), (4.40) and (4.41) were carried out. Finally, the q -integration was performed for 13 values of r between 0 and 2 by means of a program designed to handle an oscillating function. $g_{\uparrow\downarrow}^{(1)}(r)$ was also calculated for the same densities and the same values of r .

The RPA p.d.f. for opposite-spin electrons, $g_{\uparrow\downarrow}^{\text{RPA}}(r)$, is given by

$$g_{\uparrow\downarrow}^{\text{RPA}}(r) = g_{\uparrow\downarrow}^0(r) + g_{\uparrow\downarrow}^{(1)}(r) \quad . \quad (4.42)$$

The effect of including the full set of ladders describing particle-particle interactions is to give the spin-up-spin-down p.d.f.

$$g_{\uparrow\downarrow}(r) = g_{\uparrow\downarrow}^0(r) + g_{\uparrow\downarrow}^{(1)}(r) + g_{\uparrow\downarrow}^{\text{L2}}(r) \quad . \quad (4.43)$$

$g_{\uparrow\downarrow}^{\text{RPA}}(r)$ and $g_{\uparrow\downarrow}(r)$ are plotted in figure (4.5) for $\alpha = .1$, $.2$ and $.3$ over the r -interval between 0 and 2. It can be seen that RPA gives a p.d.f. that is negative at small r over the whole metallic regime. The ladder p.d.f. on the other hand, is slightly negative at small r only for $\alpha = .3$. In fact, its short-range behaviour is quite similar to the spin-up-spin-down p.d.f. calculated by Singwi et al. (20) which is plotted in figure (4.6) for very similar densities corresponding to $r_s = 2, 4$ and 6 . It appears that the set of particle-particle ladder terms in the perturbation expansion accounts for a large part of the short-range correlations between opposite-spin electrons at metallic densities. An extension of the theory to include hole effects in the form of scattering of electrons off holes and holes off holes seems to be an unnecessary complication to the short-range effect considered here.

Figure 4.5 Spin-up-spin-down pair distribution function $g_{\uparrow\downarrow}$ as a function of electron separation r for electron gas densities $\alpha = .1, .2$ and $.3$ ($\alpha = r_s/1.919 \pi^2$). The dashed curves represent the RPA results. The solid curves represent full ladder calculations.

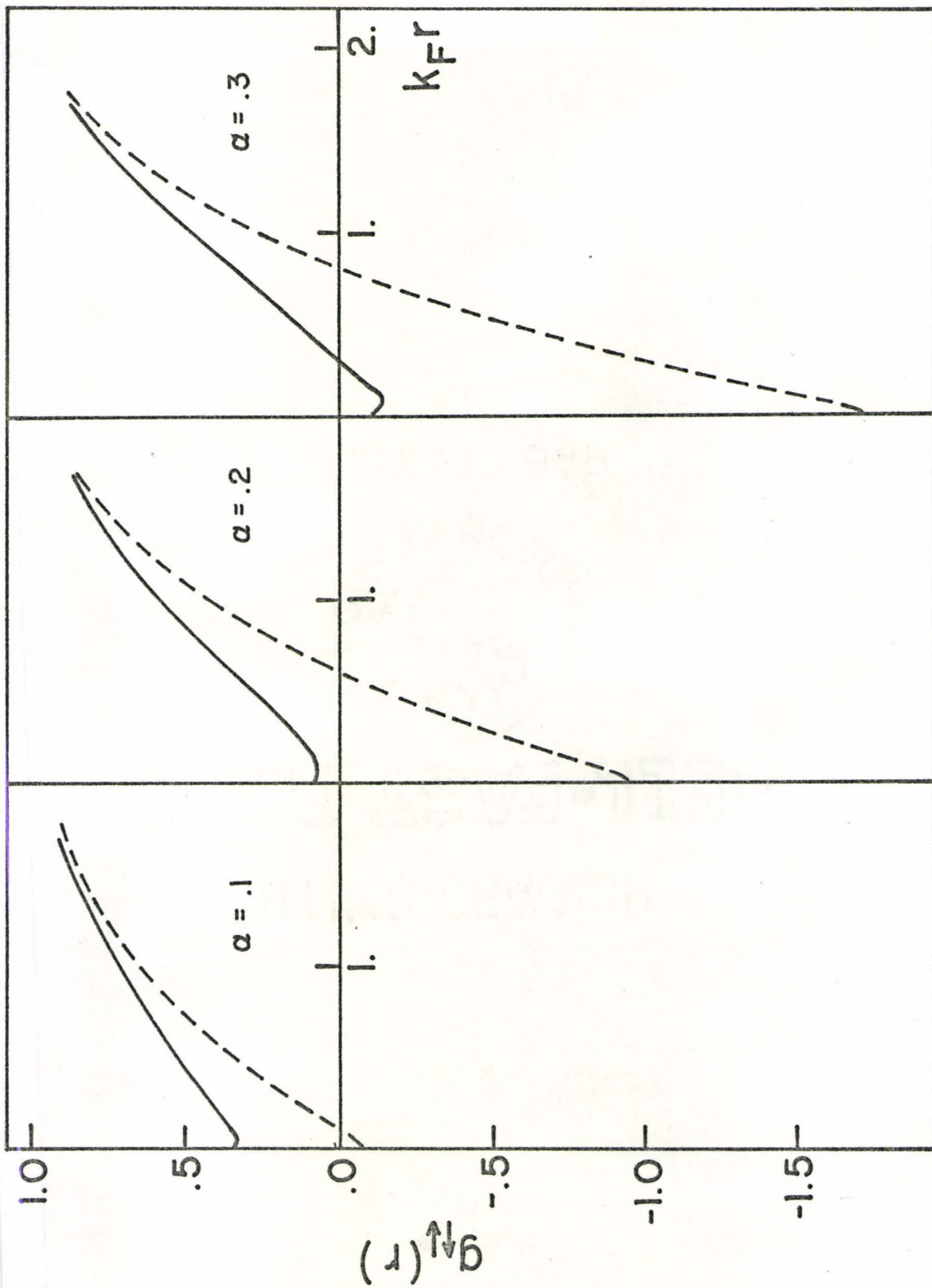


Figure 4.5

Figure 4.6

Spin-up-spin-down p.d.f. as a function
of electron separation r for electron gas den-
sities $r_s = 2, 4$ and 6 (from Singwi et al. (20)).

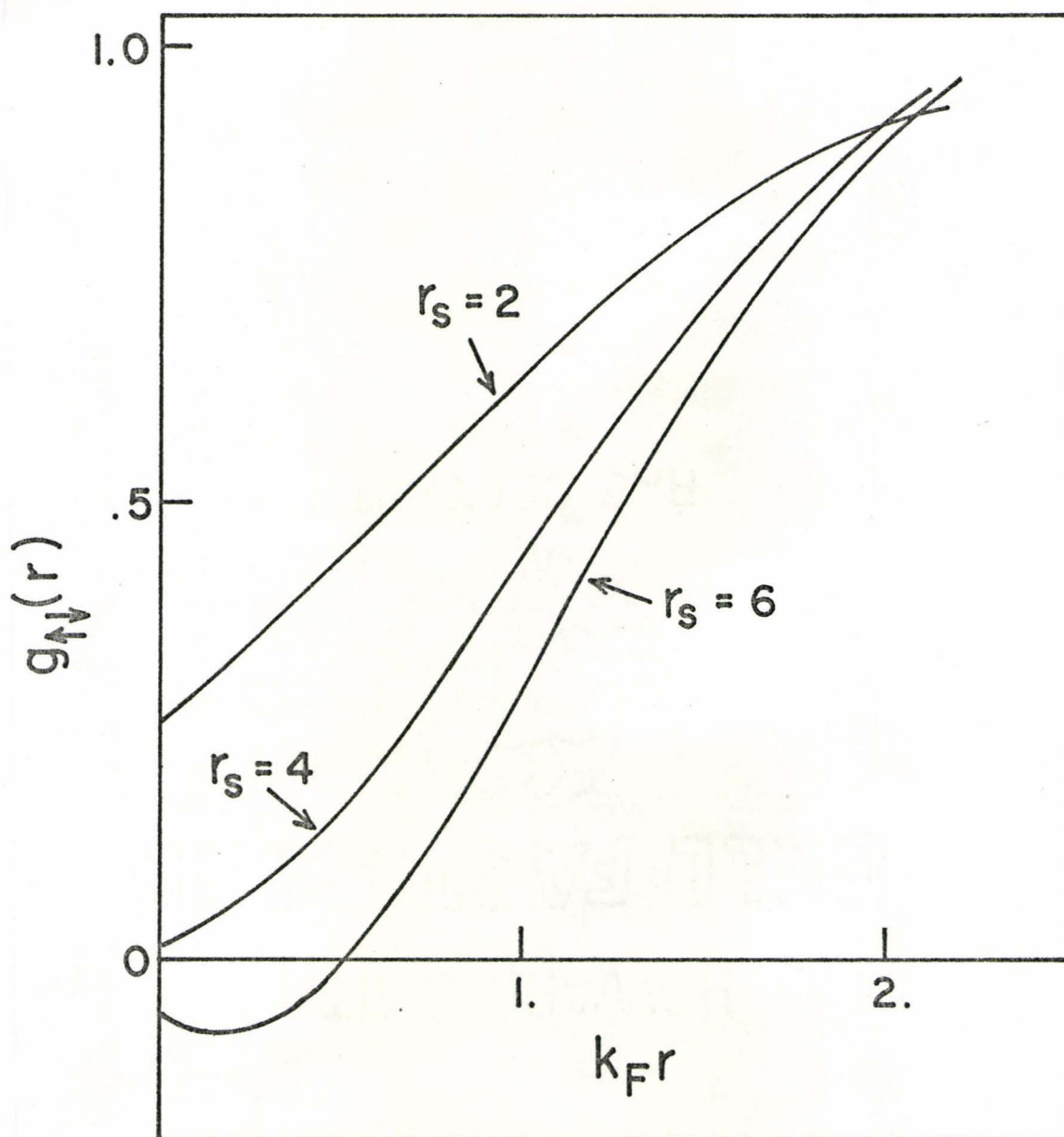


Figure 4.6

CHAPTER V

CONCLUSIONS

5.1 Phonon Smearing of Angular Correlation Data

This thesis has examined three separate and self-contained problems dealing, firstly, with phonon smearing of positron annihilation data at the Fermi momentum, secondly, with the enhancement due to positron-electron correlations of lattice tails in the angular correlation data and thirdly, with correlations between opposite-spin electrons in an electron gas at metallic densities. The Green's function technique was employed in all three problems, with attention being focussed on certain sets of terms in the perturbation expansions of the respective two-particle Green's functions.

In Chapter II the smearing at the cutoff of angular correlation data, which describes the momentum distribution of annihilating electron-positron pairs, was considered. Woll and Carbotte ⁽⁴²⁾ made an estimate of the minimum observable smearing in terms of positron motion through an effective positron temperature, T_{eff} , which they obtained from a Boltzmann equation approach by describing the positron decay in terms of interactions with electrons. The discrepancy between their prediction for T_{eff} and the

experimentally-determined quantity led to a consideration of phonon smearing, described in Chapter II.

The perturbation expansion of the electron-positron Green's function G_{ep} was extended to include phonon effects by introducing positron- and electron-ion interactions and, thus, positron- and electron-phonon interactions, into the Hamiltonian for this many-particle system. The rigid ion model, extended to account for the self-consistent screening of the bare ions, led to a positron-ion form factor that was similar to a pseudopotential form factor for conduction electrons. The weakening of the repulsive ionic potential which tends to exclude the positron from its vicinity was illustrated by the comparison with the screened Coulomb potential in figure (2.10). In the long-wave limit the scattering described by the two potentials is the same, since there it is the shift of the electronic charge, not the details of the ionic potential, that is important. However, such scattering similar to that from a screened impurity is valid only in this limit. The positron sees more of the ions than this simple picture would suggest.

The new terms in the expansion of G_{ep} led to an additional contribution to the partial annihilation rate of equation (2.3) in the form of smearing at the Fermi momentum. A calculation of the smearing from the three lowest-order phonon diagrams of figure (2.6) ignored positron-electron correlations, so that it was compared with thermal smearing

that involved only the unenhanced free-electron momentum distribution. It was found that such phonon smearing was small compared to the smearing that remained unaccounted for by previous theory ⁽⁴²⁾. It should be pointed out that, even with the exclusion of correlations, there remained an infinite number of higher-order phonon diagrams that were neglected. However, it is not expected that the inclusion of these terms would change the qualitative result of the calculation, that phonon effects are too small to explain the smearing at the Fermi cutoff.

Mikeska ⁽⁴⁴⁾ proposed the idea that the smearing and the large minimum positron energies may be explained by the deviation of the positron momentum distribution due to interactions with phonons. He rightly suggested that the whole question of thermalization rates, momentum distributions and smearing would be answered by a proper Boltzmann equation approach. However, it is not obvious that this would result in drastically different conclusions from ours. It would certainly be of considerable use if the experiments measuring the smearing could be repeated with greater accuracy.

5.2 Enhancement of Lattice Tails in $R(p)$ for Simple Metals

In Chapter III the effect of a periodic lattice was included in the formulation of the positron partial annihilation rate through the electron-positron Green's function propagator G_{ep} , firstly, by introducing Bloch states into the zeroth-order Green's functions of the perturbation expansion and secondly, by accounting for it explicitly through electron (positron)-lattice interaction lines. The new diagrams resulting from this latter procedure actually replaced diagrams representing interactions with a uniform positive background usually included in the electron gas to ensure charge neutrality.

The problem that was investigated was the enhancement due to positron-electron correlations of the tails introduced into the annihilation rate by the high electron momentum components that result from the presence of a periodic lattice. The enhancement factor for momenta less than the Fermi momentum has been known, in the case of the electron gas, for some time (25,26). It is essentially a constant factor, with some momentum dependence near the Fermi momentum. The Sommerfeld rate of equation (2.11) and figure (2.1), which reflects the free-electron momentum distribution, is but slightly distorted as a result. The Sommerfeld parabola results from integrating over the area of the p_z -plane subtended by a Fermi sphere at

the origin. A periodic lattice introduces a reciprocal lattice space and corresponding higher momentum components. The p_z -plane then intersects Fermi spheres located at a number of reciprocal lattice points.

A calculation was made in Chapter III of the first-order enhancement, by including lattice interactions explicitly, for a model based on sodium. It assumed a weak interaction, as for sodium, and plane wave states for the positron. This model considered only nearest-neighbour reciprocal lattice points, assuming all other components of the electron-lattice potential to be zero. The resultant first-order enhancement factor of figure (3.10), associated with lattice tails, showed a magnitude and momentum dependence very similar to that of figure (3.9), associated with the dominant central electron gas contribution.

Further correlations are not expected to change the qualitative results of the calculation, any more than they did in the case of an electron gas (25,26). They would, of course, lead to a greater overall enhancement which, on the basis of the first-order calculation, could be expected to be roughly the electron gas enhancement. The greater enhancement in the Fermi surface region, reflecting a higher degree of correlation between electron and positron, would probably become slightly more pronounced as well. Complicated integrations render unlikely any further investigations along that line. In fact, the Monte Carlo technique, which made

possible the present calculation, imposes its own limitations, as illustrated by the error bars in figures (3.9) and (3.10), by depending on a convergence of the results. Nevertheless, the model calculation would seem to indicate that, for metals such as sodium, the angular correlation data, excluding core effects, can be considered to be essentially a constant factor times the uncorrelated contributions, with subtle distortions in the form of a slight bulging of those contributions.

A paper by Fujiwara ⁽⁶¹⁾ introduced a many-body theory which treated the effect of a periodic field on the basis of nearly-free electron theory and included first-order positron-electron correlations. However, it was based on metals whose Fermi surface intersected a zone face and limited its treatment to the immediate vicinity of the zone boundary. At the time of writing of this thesis, the author received a preprint of a further paper by Fujiwara et al. ⁽⁷²⁾, presented in part at the Second International Conference on Positron Annihilation, which extended the treatment to beyond the vicinity of the zone boundary. It was primarily concerned with interband transitions, which become most prominent when the Fermi surface just intersects a zone face.

Fujiwara calculated a first-order enhancement factor for a one-dimensional model that considered only R-L vectors \vec{h} and $-\vec{h}$. For the case where the Fermi momentum lies below the zone boundary, his expression for the first-order intra-band annihilation rate could be derived from equation (B.7)

by reducing it to the same one-dimensional model and approximating the product of coefficients $u_k(g)$, etc. Such a procedure, while obviously useful in obtaining a qualitative understanding of the enhancement for interband transitions is probably not sufficient for a quantitative calculation of the enhancement of lattice tails in simple metals, such as that of Chapter III.

5.3 Correlations in an Electron Gas

In Chapter IV correlations between opposite-spin electrons were examined by a field-theoretic technique as a preliminary step to obtaining a fundamental understanding of the correlations among electrons at metallic densities and, indeed, the dielectric screening function. In particular, certain correlations important in short-range effects were treated in an effort to improve upon the RPA spin-up-spin-down p.d.f. at metallic densities. From the scattering problem presented by a positron or a light negative charge in an electron gas at such densities (25,45), the concept of multiple-scattering through high-order ladder diagrams was introduced into the opposite-spin electron case to account for the fact that at small r the potential between the two particles is not small, as RPA assumes.

Scattering between particles was described in Chapter IV in terms of a Bethe-Goldstone matrix element, denoted by $Y_{\vec{m}+\vec{q}, \vec{n}-\vec{q}; \vec{m}, \vec{n}}$, which had its solution in the integral equation (4.32). The solution was obtained through an angle-averaging approximation with respect to the angles of \vec{m} and \vec{n} . Such an averaging procedure over particle momentum was carried out with justifiable results by Kahana (25,71) and Carbotte (67) in the case of the Bethe-Goldstone function

describing positron-electron scattering. In the case where \tilde{m} and \tilde{n} are zero, the Bethe-Goldstone function does depend only on the magnitude of q and not its direction. A further approximation that was made in order to arrive at the Bethe-Goldstone function was the static approximation for the effective particle-particle interaction. It was made in the same spirit as the angle-averaging, as a first approximation in estimating the effect of multiple scattering on short-range phenomena, specifically, the spin-up-spin-down p.d.f. Particle-hole scattering was considered in addition to the particle-particle ladder diagrams but its contribution was negligible by comparison.

The spin-up-spin-down p.d.f. $g_{\uparrow\downarrow}(r)$ at small r was found to bear a close resemblance to $g_{\uparrow\downarrow}(r)$ as calculated by Singwi et al. (20), who included local-field effects through a semi-classical approach relating a two-particle distribution function to the p.d.f. $g(r)$. This led to an effective field and a dielectric function which included a local-field correction by involving the p.d.f. With $\epsilon(q;\omega)$ a functional of $g(r)$, or more specifically, its Fourier transform, the structure factor $S(q)$, there resulted a system of equations which were then solved self-consistently. It is not clear what the relationship is between the Singwi method and the perturbation-theoretic approach. However, it appears that the set of particle-particle ladders in the perturbation expansion for G_{ep} accounts for a large part of the short-

range correlations between opposite-spin electrons at metallic densities.

The problem of electrons with parallel spin involves the additional local-field effect associated with the exchange hole. It is a far more difficult matter to treat the exchange terms, as evidenced by the approximation Hubbard found necessary for a particular set. Even the handling of the first-order exchange bubble diagram in that set is an imposing task ⁽⁶⁸⁾. Of course, the most satisfactory description of the electron gas would satisfy all of the consistency conditions discussed by Geldart ⁽¹⁶⁾. The significance of the above calculation, however, is one which has been ignored until now, that the important effect of the Coulomb hole at metallic densities is, to a large extent, accounted for by considering multiple scattering through particle-particle ladders.

2

APPENDIX A
POSITRON-PHONON MATRIX ELEMENT

The positron-phonon matrix element describing scattering of the positron is given by

$$M_p(\underline{q}) = - \langle \underline{k} + \underline{q} | \nabla V_p | \underline{k} \rangle , \quad (\text{A.1})$$

where ∇V_p is the gradient of the positron-ion potential and $|\underline{k}\rangle$ represents the set of positron Bloch states. The derivation of this quantity follows a derivation of the electron-phonon matrix element outlined by Ziman ⁽⁷³⁾ which was based on the rigid ion model ⁽⁵⁶⁾, the method of Wigner and Seitz ⁽⁷⁴⁾ and a self-consistent method by Bardeen ⁽⁵⁹⁾ to account for the shift of conduction electrons.

It is assumed that the ionic lattice is surrounded by a uniform negative charge cloud. The usual Wigner-Seitz cell about each ion is replaced by a spherical cell of equal volume in order to simplify the potential seen by a positron. The ionic potential seen by the positron is not just the bare potential, but is rather an effective potential that includes the potential due to the uniform spherical charge distribution. This potential is necessarily zero outside the cell. A positron inside the cell about a particular ion sees the

effective potential due to that ion alone, which is given by

$$w(\underline{r}) = w_{\text{ion}}(\underline{r}) - \left(\frac{3e^2}{2r_0} - \frac{e^2 r^2}{2r_0^3} \right), \quad (\text{A.2})$$

where $w_{\text{ion}}(\underline{r})$ is the bare ion potential and r_0 is the cell radius determined from the lattice constant a by the condition

$$4\pi r_0^3/3 = a^3/2. \quad (\text{A.3})$$

The Schroedinger equation for the positron in a periodic potential $w(\underline{r})$ is

$$[-\nabla^2 + w(\underline{r})]\phi_{\underline{k}}(\underline{r}) = E_{\underline{k}} \phi_{\underline{k}}(\underline{r}), \quad (\text{A.4})$$

where $\phi_{\underline{k}}$ has the Bloch form (2.25). Differentiation of equation (A.4) leads to

$$\begin{aligned} \phi_{\underline{k}}^* (\nabla w) \phi_{\underline{k}} &= \phi_{\underline{k}}^* \nabla^3 \phi_{\underline{k}} + \phi_{\underline{k}}^* (E_{\underline{k}} - w) \nabla \phi_{\underline{k}} \\ &\approx \psi_{\underline{k}}^* \nabla^2 (e^{i\mathbf{k}\cdot\mathbf{r}} \nabla u_{\underline{k}}) - (\nabla^2 \phi_{\underline{k}}^*) e^{i\mathbf{k}\cdot\mathbf{r}} \nabla u_{\underline{k}}, \end{aligned} \quad (\text{A.5})$$

where use was made of the fact that, since phonon energies are small compared to electron energies, $E_{\underline{k}} \approx E_{\underline{k}}$. Integration over the cell volume gives, by Green's theorem,

$$\int \phi_{\underline{k}}^* (\nabla w) \phi_{\underline{k}} d\underline{r} = \int [\phi_{\underline{k}}^* \nabla (e^{i\underline{k} \cdot \underline{r}} \nabla u_{\underline{k}}) - e^{i\underline{k} \cdot \underline{r}} (\nabla u_{\underline{k}}) \phi_{\underline{k}}^*] dS \quad . \quad (\text{A.6})$$

It is assumed that $u_{\underline{k}}(\underline{r})$ can be replaced by $u_0(\underline{r})$, the $\underline{k}=0$ state function. Furthermore, in order to ensure periodicity, the derivative of $u_0(\underline{r})$ must vanish at the cell boundary.

Then,

$$\begin{aligned} \int \phi_{\underline{k}}^* (\nabla w) \phi_{\underline{k}} d\underline{r} &\approx (w(r_0) - E_0) \int \phi_{\underline{k}}^* \phi_{\underline{k}} dS \\ &= (w(r_0) - E_0) \int \nabla(\phi_{\underline{k}}^* \phi_{\underline{k}}) d\underline{r} \quad . \quad (\text{A.7}) \end{aligned}$$

Assuming that the positron is in a plane wave state, equation (A.7) simplifies to

$$\begin{aligned} \int \phi_{\underline{k}}^* (\nabla w) \phi_{\underline{k}} d\underline{r} &\approx (w(r_0) - E_0) \int \nabla(e^{i(\underline{k}-\underline{k}') \cdot \underline{r}}) d\underline{r} \\ &= i(\underline{k}-\underline{k}') (w(r_0) - E_0) G(|\underline{k}-\underline{k}'| r_0) \quad , \quad (\text{A.8}) \end{aligned}$$

where $G(x)$ is given by

$$G(x) = \frac{3}{x^3} (\sin x - x \cos x) \quad . \quad (\text{A.9})$$

Equation (A.8) describes not just the scattering of the positron by the ion itself but also the scattering effect due to the displacement of the uniform spherical charge distribution in the cell. In order to describe the scattering due to the ions alone, it is necessary to subtract the terms

$$- \int_{\text{out}} \phi_{\tilde{k}'}^* \nabla \left(\frac{e^2}{r} \right) \phi_{\tilde{k}} d\tilde{r} - \int_{\text{in}} \phi_{\tilde{k}'}^* \nabla \left(\frac{3e^2}{2r_0} - \frac{e^2 r^2}{2r_0^3} \right) \phi_{\tilde{k}} d\tilde{r} , \quad (\text{A.10})$$

where the integrations refer to regions outside and inside a particular cell. The matrix element describing scattering by the bare ion is then given by

$$M_{\tilde{k}'}(\tilde{k}', \tilde{k}) = \frac{-i}{N} (\tilde{k} - \tilde{k}') G(|\tilde{k} - \tilde{k}'| r_0) (w(r_0) - E_0 - \frac{4\pi n e^2}{|\tilde{k} - \tilde{k}'|^2}) . \quad (\text{A.11})$$

Up until this point, the conduction electrons have been ignored. These occupy the lowest states among the complete set $\psi_{\tilde{k}}$ which are taken to be plane wave states. Scattering which involves the creation or annihilation of a phonon of wavevector \tilde{q} can only connect the conduction electron state $\psi_{\tilde{k}}$ with the states $\psi_{\tilde{k} + \tilde{q} + \tilde{g}}$ and $\psi_{\tilde{k} - \tilde{q} - \tilde{g}}$. The perturbed set of electron states is then determined by first-order perturbation theory to be

$$\Psi_{\tilde{k}} = \psi_{\tilde{k}} + \sum_{\tilde{g}} (a_{\tilde{k}\tilde{g}} \psi_{\tilde{k} + \tilde{q} + \tilde{g}} + b_{\tilde{k}\tilde{g}} \psi_{\tilde{k} - \tilde{q} - \tilde{g}}) , \quad (\text{A.12})$$

where the coefficients $a_{\underline{k}\underline{g}}$ and $b_{\underline{k}\underline{g}}$ are given in terms of the perturbing potential δU by

$$a_{\underline{k}\underline{g}} = \frac{\int e^{-i(\underline{q}+\underline{g}) \cdot \underline{r}} \delta U d\underline{r}}{E_{\underline{k}} - E_{\underline{k}+\underline{q}+\underline{g}}}, \text{ etc.} \quad (\text{A.13})$$

$E_{\underline{k}}$ is the energy of the unperturbed state $\psi_{\underline{k}}$. As a result of the perturbation there is a shift of charge, leading to a new electron density $n(\underline{r})$ given by

$$\begin{aligned} n(\underline{r}) &= \sum_{\underline{k}} \psi_{\underline{k}}^* \psi_{\underline{k}} \\ &= n + \frac{1}{\Omega} \sum_{\underline{k}} \sum_{\underline{g}} [(a_{\underline{k}\underline{g}} + b_{\underline{k}\underline{g}}^*) e^{i(\underline{q}+\underline{g}) \cdot \underline{r}} \\ &\quad + (a_{\underline{k}\underline{g}}^* + b_{\underline{k}\underline{g}}) e^{-i(\underline{q}+\underline{g}) \cdot \underline{r}}] , \end{aligned} \quad (\text{A.14})$$

to first order in the coefficients. The shift from the average density n gives rise to an electrostatic potential energy $U_s(\underline{r})$ determined by Poisson's equation. It is written

$$U_s(\underline{r}) = \sum_{\underline{g}} (U_{s\underline{g}} e^{i(\underline{q}+\underline{g}) \cdot \underline{r}} + U_{s\underline{g}}^* e^{-i(\underline{q}+\underline{g}) \cdot \underline{r}}) , \quad (\text{A.15})$$

where the Fourier coefficients $U_{s\underline{g}}$ and $U_{s\underline{g}}^*$ are given by

$$U_{s\underline{g}} = \frac{4\pi e^2}{\Omega |\underline{q}+\underline{g}|^2} \sum_{\underline{k}} (a_{\underline{k}\underline{g}} + b_{\underline{k}\underline{g}}^*) , \text{ etc.} \quad (\text{A.16})$$

U_s must be included in the perturbing potential, so that the perturbation coefficients of equation (A.13) can be written

$$a_{\tilde{k}\tilde{g}} = \frac{(M_i + U_{sg})}{E_{\tilde{k}} - E_{\tilde{k}+\tilde{g}}} , \text{ etc.} \quad (\text{A.17})$$

The self-consistent total effective scattering matrix $M_p(\underline{q})$ can be determined from equations (A.16) and (A.17) as

$$\begin{aligned} M_p(\underline{q}) &= M_i / \left(1 + \frac{8\pi e^2}{\Omega q^2} \sum_{\tilde{k}} \frac{1}{E_{\tilde{k}+\underline{q}} - E_{\tilde{k}}} \right) \\ &= M_i / \left(1 + \frac{4\pi n e^2}{q^2} f(\underline{q}) \right) . \end{aligned} \quad (\text{A.18})$$

$f(\underline{q})$ is given, as before, by equation (2.35). In terms of a form factor $V_p(\underline{q})$, written

$$V_p(\underline{q}) = G(\underline{q}r_0) \left(\frac{4\pi n e^2}{q^2} + E_0 - w(r_0) \right) / \left(1 + \frac{4\pi n e^2}{q^2} f(\underline{q}) \right) , \quad (\text{A.19})$$

$M_p(\underline{q})$ is given by

$$M_p(\underline{q}) = \frac{-i}{N} \underline{q} V_p(\underline{q}) . \quad (\text{A.20})$$

APPENDIX B

FIRST-ORDER LADDER ANNIHILATION RATE

The contribution to the positron partial annihilation rate from the first-order ladder diagram of figure (3.1b) is given by equation (3.10) as

$$\begin{aligned}
 R(\underline{p}) = & \frac{\lambda}{\Omega} (-i)^2 (-i) \int d^3 \underline{x} d^3 \underline{x}' d^4 z d^4 z' e^{-i \underline{p} \cdot (\underline{x} - \underline{x}')} u(z; z') \\
 & \times G_e^0(\underline{x}; z) G_e^0(z; \underline{x}' t^+) G_p^0(\underline{x}; z') G_p^0(z'; \underline{x}' t^+) \quad . \quad (B.1)
 \end{aligned}$$

It is assumed that the positron can be described by plane wave states so that G_p^0 has the Fourier expansion (2.7), while G_e^0 is expressed in terms of Bloch functions by equation (3.4a). $R(\underline{p})$ can then be expanded in the form

$$\begin{aligned}
R(\underline{p}) = & \frac{\lambda}{\Omega} (-i)^3 \int d^3 \underline{x} d^3 \underline{x}' d^4 z d^4 z' e^{-i \underline{p} \cdot (\underline{x} - \underline{x}')} \\
& \times \sum_{\underline{k} \underline{k}' \underline{q} \underline{K} \underline{K}'} \sum_{\underline{g} \underline{g}' \underline{G} \underline{G}'} \int \frac{d\omega}{2\pi} \frac{d\omega'}{2\pi} \frac{d\varepsilon}{2\pi} \frac{dE}{2\pi} \frac{dE'}{2\pi} \\
& \times e^{i \underline{q} \cdot (\underline{z} - \underline{z}')} e^{i \underline{k} \cdot (\underline{x} - \underline{z})} e^{i \underline{k}' \cdot (\underline{z} - \underline{x}')} \\
& \times e^{i \underline{K} \cdot (\underline{x} - \underline{z}')} e^{i \underline{K}' \cdot (\underline{z}' - \underline{x}')} e^{i \underline{g} \cdot \underline{x}} e^{-i \underline{g}' \cdot \underline{z}} e^{i \underline{G} \cdot \underline{z}} e^{-i \underline{G}' \cdot \underline{x}'} \\
& \times u_{\underline{k}}(\underline{g}) u_{\underline{k}'}^*(\underline{g}') u_{\underline{k}}(\underline{G}) u_{\underline{k}'}^*(\underline{G}') \\
& \times e^{-i \varepsilon (t_z - t_{z'})} e^{-i \omega (t - t_z)} e^{-i \omega' (t_z - t^+)} e^{-i E (t - t_{z'})} \\
& \times e^{-i E' (t_{z'} - t^+)} u(\underline{q}; \varepsilon) \\
& \times G_e^0(\underline{k}; \omega) G_e^0(\underline{k}'; \omega) G_p^0(\underline{K}; E) G_p^0(\underline{K}'; E') \quad . \quad (B.2)
\end{aligned}$$

Integration over the time variables t_z and $t_{z'}$ leads to

$$\delta(\omega - \omega' - \varepsilon) \delta(\varepsilon + E - E') \quad . \quad (B.3)$$

Integration over the space variables leads to the δ -functions

$$\delta(\underline{k} + \underline{g} + \underline{K} - \underline{p}) \delta(\underline{p} - \underline{k}' - \underline{G}' - \underline{K}') \delta(\underline{q} - \underline{k} - \underline{g}' + \underline{k}' + \underline{G}) \delta(\underline{K}' - \underline{K} - \underline{q}) \quad . \quad (B.4)$$

In the limit of infinite volume the δ -function and the Kronecker delta are interchangeable. The sums over $\underline{k}, \underline{k}'$ and \underline{g} and the ω' - and E' -integrations can be performed to give

$$\begin{aligned}
 R(\underline{p}) &= i \frac{\lambda}{\Omega} \sum_{\underline{k}, \underline{k}'} \sum_{\underline{g}, \underline{g}', \underline{G}, \underline{G}'} \\
 &\times u_{\underline{k}}(\underline{g}) u_{\underline{k}}^*(\underline{g}') u_{\underline{k}', (\underline{G})} u_{\underline{k}', (\underline{G}')} u(\underline{k} - \underline{k}' + \underline{g} - \underline{G}'; 0) \\
 &\times \int \frac{d\omega}{2\pi} \frac{d\varepsilon}{2\pi} \frac{dE}{2\pi} e^{i\omega 0^+} e^{iE 0^+} \\
 &\times G_e^0(\underline{k}; \omega) G_e^0(\underline{k}'; \omega - \varepsilon) G_p^0(\underline{p} - \underline{k} - \underline{g}; E) G_p^0(\underline{p} - \underline{k}' - \underline{G}'; E + \varepsilon) \\
 &\times \delta_{\underline{g}, \underline{g}' - \underline{G} + \underline{G}'} \quad , \quad (B.5)
 \end{aligned}$$

where the dynamic effective potential has been replaced by its static limit.

The E -integral can be performed by contour integration in the upper half plane to give

$$\begin{aligned}
 R(\underline{p}) &= \frac{2\lambda}{\Omega} \sum_{\underline{k}, \underline{k}'} \sum_{\underline{g}, \underline{g}', \underline{G}, \underline{G}'} u_{\underline{k}}(\underline{g}) u_{\underline{k}}^*(\underline{g}') u_{\underline{k}', (\underline{G})} u_{\underline{k}', (\underline{G}')} \\
 &\times u(\underline{k} - \underline{k}' + \underline{g} - \underline{G}'; 0) \delta_{\underline{g}, \underline{g}' - \underline{G} + \underline{G}'} \delta_{\underline{p}, \underline{k} + \underline{g}} \\
 &\times \int \frac{d\omega}{2\pi} \frac{d\varepsilon}{2\pi} e^{i\omega 0^+} \frac{G_e^0(\underline{k}; \omega) G_e^0(\underline{k}'; \omega - \varepsilon)}{|\underline{p} - \underline{k}' - \underline{G}'|^2 - \varepsilon - i0^+} \quad . \quad (B.6)
 \end{aligned}$$

Contour integration over ϵ and ω leads to

$$\begin{aligned}
 R(p) = & \frac{2\lambda}{\Omega} \sum_{\tilde{k} < p_F} \sum_{\tilde{k}' > p_F} \sum_{\tilde{g}\tilde{g}'\tilde{G}\tilde{G}'} u_{\tilde{k}}(\tilde{g}) u_{\tilde{k}}^*(\tilde{g}') u_{\tilde{k}'}(\tilde{G}) u_{\tilde{k}'}^*(\tilde{G}') \\
 & \times \frac{u(\tilde{k}-\tilde{k}'+\tilde{g}-\tilde{G}'; 0) \delta_{\tilde{g}, \tilde{g}'-\tilde{G}+\tilde{G}'} \delta_{\tilde{p}, \tilde{k}+\tilde{g}}}{E_{\tilde{k}'} - E_{\tilde{k}} + |\tilde{k}-\tilde{k}'+\tilde{g}-\tilde{G}'|^2}, \quad (B.7)
 \end{aligned}$$

where \tilde{p} has been explicitly replaced by $\tilde{k}+\tilde{g}$ in the energy denominator.

APPENDIX C
PROPAGATOR EQUATIONS

The perturbation series for a Green's function propagator is obtained by deriving the equation of motion for the propagator and then solving the equation by making a perturbation expansion in powers of the potential. The positron Green's function propagator G_p is expressed in terms of the positron field operator $\phi(x)$ as

$$\begin{aligned} G_p(x;x') &= i \langle T(\phi(x)\phi^\dagger(x')) \rangle \\ &= i \langle \theta(t-t')\phi(x)\phi^\dagger(x') - \theta(t'-t)\phi^\dagger(x')\phi(x) \rangle. \end{aligned} \tag{C.1}$$

Now, operators such as $\phi(x)$ and the electron operator $\psi(x)$ obey Fermi statistics. In particular they satisfy the anticommutation rules

$$\{\phi(\underline{x}t), \phi^\dagger(\underline{x}'t)\} = \delta^3(\underline{x}-\underline{x}') \quad , \tag{C.2a}$$

$$\{\phi(\underline{x}t), \phi(\underline{x}'t)\} = 0 \quad . \tag{C.2b}$$

Furthermore, a positron operator anticommutes with an electron operator. Differentiating equation (C.1) with respect

to the time variable t gives

$$\begin{aligned}
 i \frac{\partial}{\partial t} G_p(x; x') &= i^2 \langle T(\frac{\partial}{\partial t} \phi(x) \phi^\dagger(x')) \rangle \\
 &\quad - \delta(t-t') \langle \{\phi(x), \phi^\dagger(x')\} \rangle_{t'=t} \\
 &= i^2 \langle T(\frac{\partial}{\partial t} \phi(x) \phi^\dagger(x')) \rangle - \delta^4(x-x') \quad .
 \end{aligned}
 \tag{C.3}$$

The equation of motion for the positron field variable $\phi(x)$ is

$$i \frac{\partial}{\partial t} \phi(x) = [\phi(x), H] \quad , \tag{C.4}$$

where H is the Hamiltonian for the positron-electron system immersed in a crystal lattice given by equation (3.1). It follows that

$$\begin{aligned}
 i \frac{\partial}{\partial t} \phi(\underline{x}t) &= H_p(x) \phi(\underline{x}t) + \int d^3z v(\underline{x}; \underline{z}) \\
 &\quad \times [\phi^\dagger(\underline{z}t) \phi(\underline{z}t) - \psi^\dagger(\underline{z}t) \psi(\underline{z}t)] \phi(\underline{x}t) \quad (C.5)
 \end{aligned}$$

from the anticommutator rules discussed above. Substituting this result into equation (C.3) gives

$$\begin{aligned}
i \frac{\partial}{\partial t} G_p(\underline{x}; \underline{x}') &= H_p(\underline{x}) G_p(\underline{x}; \underline{x}') - \delta^4(\underline{x} - \underline{x}') + i \int d^3 \underline{z} v(\underline{x}; \underline{z}) \\
&\times [\langle T(\phi^\dagger(\underline{z}t^+) \phi(\underline{z}t) \phi(\underline{x}) \phi^\dagger(\underline{x}')) \rangle \\
&- \langle T(\psi^\dagger(\underline{z}t^+) \psi(\underline{z}t) \phi(\underline{x}) \phi^\dagger(\underline{x}')) \rangle] \quad , \quad (C.6)
\end{aligned}$$

which can be written in the form

$$\begin{aligned}
(-i \frac{\partial}{\partial t} + H_p(\underline{x})) G_p(\underline{x}; \underline{x}') &= \delta^4(\underline{x} - \underline{x}') - i \int d^3 \underline{z} v(\underline{x}; \underline{z}) \\
&\times [G_{pp}(\underline{z}t, \underline{x}; \underline{z}t^+, \underline{x}') \\
&- G_{ep}(\underline{z}t, \underline{x}; \underline{z}t^+, \underline{x}')] \quad . \quad (C.7)
\end{aligned}$$

An equivalent equation is obtained for the electron Green's function propagator G_e by replacing "p" ("e") by "e" ("p").

In a similar fashion it is possible to derive the equation of motion for the general n-particle Green's function defined as

$$\begin{aligned}
&G_{p_1 p_2 \dots p_n}(\underline{x}_1, \dots, \underline{x}_n; \underline{x}'_1, \dots, \underline{x}'_n) \\
&= i^n \langle T(\phi_{p_1}(\underline{x}_1) \dots \phi_{p_n}(\underline{x}_n) \phi_{p_n}^\dagger(\underline{x}'_n) \dots \phi_{p_1}^\dagger(\underline{x}'_1)) \rangle \quad , \quad (C.8)
\end{aligned}$$

where ϕ_{p_i} refers to a positron (electron) operator if p_i is "p" ("e"). Then

$$\begin{aligned}
 & \frac{\partial}{\partial t_1} [T(\phi_{p_1}(x_1) \dots \phi_{p_n}(x_n) \phi_{p_n}^\dagger(x'_n) \dots \phi_{p_1}^\dagger(x'_1))] \\
 = & T[\frac{\partial}{\partial t_1} (\phi_{p_1}(x_1) \dots \phi_{p_n}(x_n) \phi_{p_n}^\dagger(x'_n) \dots \phi_{p_1}^\dagger(x'_1))] \\
 & + \sum_{j=1}^n (-1)^{j+1} \delta^4(x_1 - x'_j) T(\phi_{p_2}(x_2) \dots \phi_{p_n}(x_n) \phi_{p_n}^\dagger(x'_n) \dots \\
 & \dots \phi_{p_{j+1}}^\dagger(x'_{j+1}) \phi_{p_{j-1}}^\dagger(x'_{j-1}) \dots \phi_{p_1}^\dagger(x'_1)) \quad . \quad (C.9)
 \end{aligned}$$

In the last term the sum is over the primed positron (electron) coordinates if p_1 is a positron (electron) index. From the equation of motion (C.5) for the field operator, equation (C.9) can be rewritten, on taking expectation values, as

$$\begin{aligned}
 & (-i \frac{\partial}{\partial t_1} + H_{p_1}(x_1)) G_{p_1 \dots p_n}(x_1, \dots, x_n; x'_1, \dots, x'_n) \\
 = & -i \int d^3 z v(x_1; z) [G_{p_1 p_1 p_2 \dots p_n}(z t_1, x_1, \dots, x_n; z t_1^+, x'_1, \dots, x'_n) \\
 & - G_{p_1 p_1 p_2 \dots p_n}(z t_1, x_1, \dots, x_n; z t_1^+, x'_1, \dots, x'_n)] + \sum_{j=1}^n (-1)^{j+1} \delta^4(x_1 - x'_j) G_{p_1 p_2 \dots p_n}(x_2, \dots, x_n; x'_1, \dots, x'_{j-1} x'_{j+1}, \dots, x'_n), \quad (C.10)
 \end{aligned}$$

where p_1' stands for "p" ("e") if p_1 refers to "e" ("p"). The quantity $G_{p_1 p_2 \dots p_n} (x_2, \dots, x_n; x_1', \dots, x_{j-1}', x_{j+1}', \dots, x_n')$ stands for

$$i^{n-1} \langle T (\phi_{p_2} (x_2) \dots \phi_{p_n} (x_n) \phi_{p_n}^\dagger (x_n') \dots \dots \phi_{p_{j+1}}^\dagger (x_{j+1}') \phi_{p_{j-1}}^\dagger (x_{j-1}') \dots \phi_{p_1}^\dagger (x_1')) \rangle . \quad (C.11)$$

In the absence of interactions in equation (C.7), the equation of motion for the free-particle propagator has the conjugate equation

$$(i \frac{\partial}{\partial t} - \nabla_{\underline{x}}^2) G_{p_1}^0 (x_1; x) = \delta^4 (x_1 - x) , \quad (C.12)$$

where the symbol $\nabla_{\underline{x}}^2$ indicates the Laplacian with respect to the variable \underline{x} . The variable x_1 in equation (C.10) is changed for convenience to x and the equation is multiplied on the right by $G_{p_1}^0 (x_1; x)$. Equation (C.12) is multiplied on the left by $G_{p_1 \dots p_n} (x, x_2, \dots, x_n; x_1', \dots, x_n')$ and the result is subtracted from the first quantity. Integration over the 4-vector x then leads to the equation

$$\begin{aligned}
& G_{p_1 \dots p_n}(x_1, \dots, x_n; x'_1, \dots, x'_n) \\
= & \sum_{j=1}^n (-1)^{j+1} G_{p_1}^0(x_1; x'_j) \\
& \times G_{p_1 \dots p_n}(x_2, x_3, \dots, x_n; x'_1, \dots, x'_{j-1}, x'_{j+1}, \dots, x'_n) \\
& - i \int d^4 x d^3 z \tilde{v}(x; z) G_{p_1}^0(x_1; x) \\
& \times [G_{p_1 p_1 p_2 \dots p_n}(z^t, x, x_2, \dots, x_n; z^t, x'_1, \dots, x'_n) \\
& - G_{p_1 p_1 p_2 \dots p_n}(z^t, x, x_2, \dots, x_n; z^t, x'_1, \dots, x'_n)] \\
& - \int d^4 x G_{p_1}^0(x_1; x) V_{p_1}(x) G_{p_1 \dots p_n}(x, x_2, \dots, x_n; x'_1, \dots, x'_n) \quad , \\
& \hspace{20em} (C.13)
\end{aligned}$$

which follows from the fact that

$$\begin{aligned}
& \int d^4 x [G_{p_1}^0(x_1; x) (-i \frac{\partial}{\partial t} - \nabla_x^2) G_{p_1 \dots p_n}(x, x_2, \dots, x_n; x'_1, \dots, x'_n) \\
& - G_{p_1 \dots p_n}(x, x_2, \dots, x_n; x'_1, \dots, x'_n) (i \frac{\partial}{\partial t} - \nabla_x^2) G_{p_1}^0(x_1; x)] \\
& \hspace{20em} (C.14)
\end{aligned}$$

can be shown to vanish by integration by parts. The positron propagator then satisfies the integral equation

$$\begin{aligned}
G_p(x_1; x'_1) &= G_p^0(x_1; x'_1) - i \int d^4x d^3z v(\underline{x}; \underline{z}) G_p^0(x_1; x) \\
&\quad \times [G_{pp}(\underline{z}t, x; \underline{z}t^+, x'_1) - G_{ep}(\underline{z}t, x; \underline{z}t^+, x'_1)] \\
&\quad - \int d^4x G_p^0(x_1; x) V_p(x) G_p(x; x'_1) \quad , \quad (C.15)
\end{aligned}$$

and there is a similar equation for the electron propagator G_e . The two-particle electron-positron propagator G_{ep} is described by the equation

$$\begin{aligned}
G_{ep}(x_1, x_2; x'_1, x'_2) &= G_e^0(x_1; x'_1) G_p(x_2; x'_2) \\
&\quad - i \int d^4x d^3z v(\underline{x}; \underline{z}) G_e^0(x_1; x) \\
&\quad \times [G_{eep}(\underline{z}t, x, x_2; \underline{z}t^+, x'_1, x'_2) \\
&\quad - G_{pep}(\underline{z}t, x, x_2; \underline{z}t^+, x'_1, x'_2)] \\
&\quad - \int d^4x G_e^0(x_1; x) V_e(x) \\
&\quad \times G_{ep}(x, x_2; x'_1, x'_2) \quad . \quad (C.16)
\end{aligned}$$

It can be expanded as a perturbation series in powers of v . The only difference from the case of an electron gas is the presence of additional terms in the expansion involving the positron (electron)-lattice interaction $V_p(e)$ which do not completely cancel against the bubble diagrams.

APPENDIX D

BETHE-GOLDSTONE EQUATION

The amplitude $X_{\underline{m}+\underline{q}, \underline{n}-\underline{q}; \underline{m}, \underline{n}}$ described by equations (4.26) and (4.32) can also be written in the form

$$\begin{aligned}
 X_{\underline{m}+\underline{q}, \underline{n}-\underline{q}; \underline{m}, \underline{n}} &= \frac{\theta(|\underline{m}+\underline{q}|-p_F)\theta(|\underline{n}-\underline{q}|-p_F)}{|\underline{m}+\underline{q}|^2+|\underline{n}-\underline{q}|^2-m^2-n^2} [U(\underline{q}) \\
 &+ \int d^3\underline{q}' U(\underline{q}-\underline{q}') X_{\underline{m}+\underline{q}', \underline{n}-\underline{q}'; \underline{m}, \underline{n}} \\
 &- \int d^3\underline{m}' U(\underline{m}-\underline{m}') X_{\underline{m}+\underline{q}, \underline{m}'-\underline{m}+\underline{n}-\underline{q}; \underline{m}', \underline{n}} \\
 &- \int d^3\underline{n}' U(\underline{n}-\underline{n}') X_{\underline{n}', -\underline{n}+\underline{m}+\underline{q}, \underline{n}-\underline{q}; \underline{m}, \underline{n}'}] .
 \end{aligned}
 \tag{D.1}$$

$X_{\underline{m}+\underline{q}, \underline{n}-\underline{q}; \underline{m}, \underline{n}}$ is approximated by a quantity $\hat{X}_{\underline{m}+\underline{q}, \underline{n}-\underline{q}; \underline{m}, \underline{n}'}$ obtained by averaging over the angles of \underline{m} and \underline{n} . In taking the average of equation (D.1), the quantities $\hat{X}_{\underline{m}+\underline{q}, \underline{m}'-\underline{m}+\underline{n}-\underline{q}; \underline{m}', \underline{n}}$ and $\hat{X}_{\underline{n}', -\underline{n}+\underline{m}+\underline{q}, \underline{n}-\underline{q}; \underline{m}, \underline{n}'}$ in the last two integrals are approximated by $\hat{X}_{\underline{m}+\underline{q}, \underline{n}-\underline{q}; \underline{m}, \underline{n}}$ which can be removed from the \underline{m}' - and \underline{n}' -integrations. The approximation is equivalent to replacing \underline{m}' by \underline{m} and \underline{n}' by \underline{n} , respectively, in these quantities. There results the integral equation

$$\begin{aligned}
\hat{X}_{\underline{m}+\underline{q}, \underline{n}-\underline{q}; \underline{m}, \underline{n}} &= \frac{1}{4} f(m, n, q) [U(\underline{q}) \\
&+ \int d^3 \underline{q}' U(\underline{q}-\underline{q}') \hat{X}_{\underline{m}+\underline{q}', \underline{n}-\underline{q}'; \underline{m}, \underline{n}} \\
&- \hat{X}_{\underline{m}+\underline{q}, \underline{n}-\underline{q}; \underline{m}, \underline{n}} \int d^3 \underline{m}' U(\underline{m}-\underline{m}') \\
&- \hat{X}_{\underline{m}+\underline{q}, \underline{n}-\underline{q}; \underline{m}, \underline{n}} \int d^3 \underline{n}' U(\underline{n}-\underline{n}')] \quad . \quad (D.2)
\end{aligned}$$

Returning to the averaged Bethe-Goldstone quantity $\hat{Y}_{\underline{m}+\underline{q}, \underline{n}-\underline{q}; \underline{m}, \underline{n}}$ through the equation (4.35), written alternatively as

$$\hat{X}_{\underline{m}+\underline{q}, \underline{n}-\underline{q}; \underline{m}, \underline{n}} = \frac{1}{4} f(m, n, q) \hat{Y}_{\underline{m}+\underline{q}, \underline{n}-\underline{q}; \underline{m}, \underline{n}} \quad , \quad (D.3)$$

$\hat{Y}_{\underline{m}+\underline{q}, \underline{n}-\underline{q}; \underline{m}, \underline{n}}$ can be shown to satisfy the equation

$$\begin{aligned}
\hat{Y}_{\underline{m}+\underline{q}, \underline{n}-\underline{q}; \underline{m}, \underline{n}} &= U(\underline{q}) + \frac{\pi}{2q} \int_0^\infty dq' q' f(m, n, q') \\
&\times \hat{Y}_{\underline{m}+\underline{q}', \underline{n}-\underline{q}'; \underline{m}, \underline{n}} \int_{|q-q'|}^{q+q'} dx x U(x) \\
&- \frac{\pi}{2} \frac{f(m, n, q)}{m} \hat{Y}_{\underline{m}+\underline{q}, \underline{n}-\underline{q}; \underline{m}, \underline{n}} \\
&\times \int_0^1 dm' m' \int_{|m-m'|}^{m+m'} dx x U(x)
\end{aligned}$$

$$\begin{aligned}
& - \frac{\pi}{2} \frac{f(m, n, q)}{n} \hat{Y}_{\tilde{m}+\tilde{q}, \tilde{n}-\tilde{q}; \tilde{m}, \tilde{n}} \\
& \times \int_0^1 dn' n' \int_{|n-n'|}^{n+n'} dx x U(x) \quad . \quad (D.4)
\end{aligned}$$

The quantity $\hat{Y}_{\tilde{m}+\tilde{q}, \tilde{n}-\tilde{q}; \tilde{m}, \tilde{n}}$ was determined from equation (D.4) for 11 values of m and n between 0 and 1 for $\alpha = .2$. It was also obtained in an approximation which involved omitting the last two terms (hole contributions) in equation (D.4). The respective integral equations were solved by introducing a grid of variable size up to 75 points extending from a minimum which satisfied the conditions $m+q>1$ and $n+q>1$ up to a maximum of 40. The resultant set of inhomogeneous linear equations was solved by gauss elimination.

$\hat{Y}_{\tilde{m}+\tilde{q}, \tilde{n}-\tilde{q}; \tilde{m}, \tilde{n}}$'s for the two approximations are plotted in figure (D.1) for several values of m and n . It can be seen that particle-hole contributions can be neglected to a good approximation. $\hat{Y}_{\tilde{m}+\tilde{q}, \tilde{n}-\tilde{q}; \tilde{m}, \tilde{n}}$ is then given by the simpler equation

$$\begin{aligned}
\hat{Y}_{\tilde{m}+\tilde{q}, \tilde{n}-\tilde{q}; \tilde{m}, \tilde{n}} &= U(\tilde{q}) + \frac{\pi}{2\tilde{q}} \int_0^1 dq' q' f(m, n, q') \\
&\times \hat{Y}_{\tilde{m}+\tilde{q}', \tilde{n}-\tilde{q}'; \tilde{m}, \tilde{n}} \int_{|q-q'|}^{q+q'} dx x U(x) \quad . \quad (D.5)
\end{aligned}$$

Figure D.1

Ratio of the Bethe-Goldstone matrix
element $Y_{m+q,n-q;m,n}$ which includes particle-
hole interactions to that involving just particle-
particle scattering as a function of q for various
values of m and n for density parameter $\alpha = .2$.

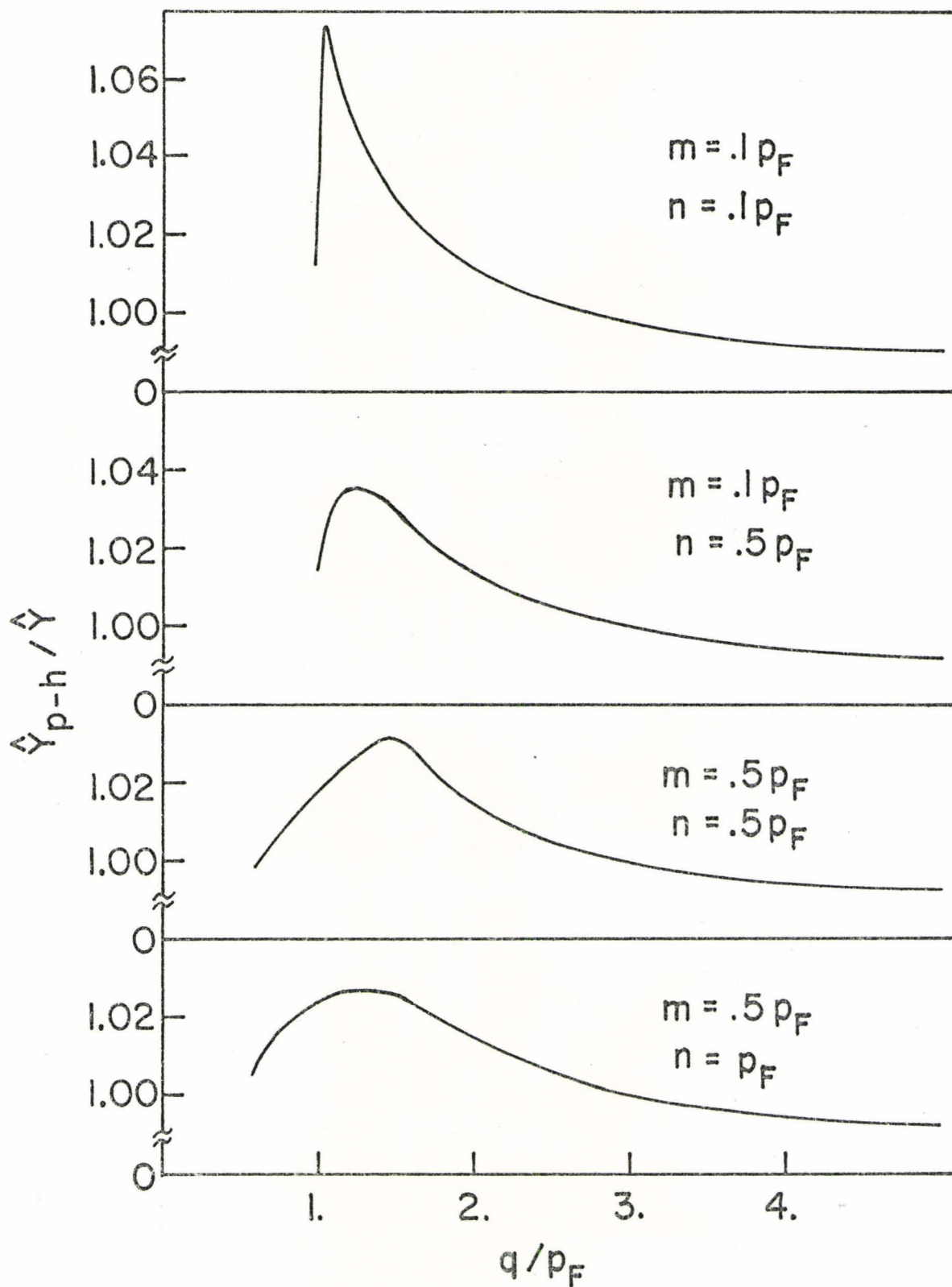


Figure D.1

REFERENCES

1. A. Sommerfeld, Z. Physik 47, 1 (1928).
2. V. Fock, Z. Physik 61, 126 (1930).
3. D. Pines, in Advances in Solid State Physics, edited by F. Seitz and D. Turnbull (Academic Press, New York, 1955), Vol. I.
4. E. P. Wigner, Phys. Rev. 46, 1002 (1934); Trans. Faraday Soc. 34, 678 (1938).
5. D. Pines and D. Bohm, Phys. Rev. 85, 338 (1952).
6. D. Bohm and D. Pines, Phys. Rev. 92, 609 (1953).
7. M. Gell-Mann and K. A. Brueckner, Phys. Rev. 106, 364 (1957).
8. R. P. Feynman, Phys. Rev. 76, 769 (1949).
9. A. J. Glick and R. A. Ferrell, Ann. Phys. (N.Y.) 11, 359 (1960).
10. L. Hedin, Phys. Rev. 139, A796 (1965).
11. P. Nozieres and D. Pines, Phys. Rev. 111, 442 (1958).
12. J. Hubbard, Proc. Roy. Soc. (London), A243, 336 (1958).
13. V. Heine and L. M. Falicov, Advances in Physics 37, 57 (1961).
14. T. M. Rice, Ann. Phys. 31, 100 (1965).
15. D. J. W. Geldart and S. H. Vosko, Can. J. Phys. 44, 2137 (1966).

16. D. J. W. Geldart, *Can. J. Phys.* 45, 3139 (1967).
17. K. S. Singwi, M. P. Tosi and A. Sjölander, *Nuovo Cimento* 54, B160 (1968).
18. K. S. Singwi, M. P. Tosi, R. H. Land and A. Sjölander, *Phys. Rev.* 176, 589 (1968).
19. K. S. Singwi, A. Sjölander, M. P. Tosi and R. H. Land, *Solid State Commun.* 7, 1503 (1969).
20. K. S. Singwi, A. Sjölander, M. P. Tosi and R. H. Land, *Phys. Rev.* B1, 1044 (1970).
21. S. deBenedetti, C. E. Cowan, W. R. Konneker and H. Primakoff, *Phys. Rev.* 77, 205 (1950).
22. G. E. Lee-Whiting, *Phys. Rev.* 97, 1157 (1955).
23. R. A. Ferrell, *Rev. Mod. Phys.* 28, 308 (1956).
24. A. T. Stewart, *Can. J. Phys.* 35, 168 (1957).
25. S. Kahana, *Phys. Rev.* 129, 1622 (1963).
26. J. P. Carbotte and S. Kahana, *Phys. Rev.* 139, A213 (1965).
27. A. Klein and R. E. Prange, *Phys. Rev.* 112, 1008 (1958).
28. A. Klein, in Lectures on the Many-Body Problem, edited by E. R. Caianello (Academic Press, London, 1962).
29. R. E. Bell and M. H. Jorgensen, *Can. J. Phys.* 38, 652 (1960).
30. J. H. Terrell, H. L. Weisberg and S. Berko, in Positron Annihilation, edited by A. T. Stewart and F. Roellig (Academic Press, New York, 1967).
31. E. Daniel, *J. Phys. Chem. Solids* 6, 205 (1958).

32. S. Berko and J. S. Plaskett, Phys. Rev. 112, 1877 (1958).
33. J. P. Carbotte and A. Salvadori, Phys. Rev. 162, 290 (1967).
34. A. G. Gould and R. N. West, in Proceedings of the Second International Conference on Positron Annihilation, (unpublished).
35. D. Stroud and H. Ehrenreich, Phys. Rev. 171, 399 (1968).
36. N. K. Dave, B. T. A. McKee, A. T. Stewart, M. J. Stott and W. Triftsthäuser, in Proceedings of the Second International Conference on Positron Annihilation, (unpublished).
37. J. P. Carbotte, Ph.D. Thesis, McGill University, Montreal, Canada, (unpublished) (1963).
38. S. M. Kim, Ph.D. Thesis, University of North Carolina, Chapel Hill, U.S.A., (unpublished) (1967).
39. A. T. Stewart, J. B. Shand and S. M. Kim, Proc. Phys. Soc. 88, 1001 (1966).
40. S. M. Kim, A. T. Stewart and J. P. Carbotte, Phys. Rev. Letters 18, 385 (1967).
41. J. P. Carbotte and H. L. Arora, Can. J. Phys. 45, 387 (1967).
42. E. J. Woll, Jr. and J. P. Carbotte, Phys. Rev. 164, 985 (1967).
43. A. Perkins and J. P. Carbotte, Phys. Rev. B1, 101 (1970).

44. H. Mikeska, Z. Physik 232, 159 (1970).
45. J. P. Carbotte, Phys. Rev. Letters 18, 837 (1967).
46. H. A. Bethe and J. Goldstone, Proc. Roy. Soc. (London) A238, 551 (1957).
47. G. Wick, Phys. Rev. 80, 268 (1950).
48. S. Tomanaga, Progr. Theoret. Phys. (Kyoto) 1, 27 (1946).
49. F. J. Dyson, Phys. Rev. 75, 486 (1949).
50. D. R. Hamann, Phys. Rev. 146, 277 (1966).
51. B. Bergersen and E. Pajanne, Phys. Rev. 186, 375 (1969).
52. B. Bergersen and E. Pajanne, Phys. Rev. B3, 1588 (1971).
53. A. T. Stewart and J. B. Shand, Phys. Rev. Letters 16, 261 (1966).
54. J. R. Schrieffer, Theory of Superconductivity, (W. A. Benjamin, Inc., New York, 1964).
55. B. B. J. Hede and J. P. Carbotte, Can. J. Phys. 48, 2661 (1970).
56. L. Nordheim, Ann. Physics 9, 607 (1931).
57. N. W. Ashcroft, Phys. Letters 23, 48 (1966).
58. J. Lindhard, Kgl. Videnskab. Selskab, Mat. Fys. Medd. 28, No. 8 (1954).
59. J. Bardeen, Phys. Rev. 52, 688 (1937).
60. B. Hayman and J. P. Carbotte, (private communication).
61. K. Fujiwara, J. Phys. Soc. Japan 29, 1479 (1970).
62. J. Callaway, Phys. Rev. 123, 1255 (1961).
63. B. B. J. Hede and J. P. Carbotte, J. Phys. Chem. Solids 33, 727 (1972).

64. N. P. Buslenko, D. I. Golenko, Yu. A. Shreider, I. M. Sobol' and V. G. Sragovich, The Monte Carlo Method, edited by Yu. A. Shreider (Pergamon Press, Oxford, 1966).
65. J. J. Donaghy and A. T. Stewart, Phys. Rev. 164, 396 (1967).
66. D. Pines, Elementary Excitations in Solids, (W. A. Benjamin, Inc., New York, 1963).
67. J. P. Carbotte, Phys. Rev. 155, 197 (1967).
68. S. Ueda, Progr. Theoret. Phys. 26, 45 (1961).
69. B. B. J. Hede and J. P. Carbotte, (accepted for publication in Canadian Journal of Physics).
70. H. Kanazawa, Y. Ohtsuki and S. Yanagawa, Progr. Theoret. Phys. (Kyoto) 33, 1010 (1965).
71. S. Kahana, Phys. Rev. 117, 123 (1960).
72. K. Fujiwara, T. Hyodo and J. Ohyama, in Proceedings of the Second International Conference on Positron Annihilation, (unpublished).
73. J. M. Ziman, Electrons and Phonons, (Clarendon Press, Oxford, 1960).
74. E. P. Wigner and F. Seitz, Phys. Rev. 43, 804 (1933).